Summer 1996

A Progressive Damage Methodology for Residual Strength Predictions of Center-Crack Tension Composite Panels

Timothy William Coats
Old Dominion University

A PROGRESSIVE DAMAGE METHODOLOGY FOR RESIDUAL STRENGTH PREDICTIONS OF CENTER-CRACK TENSION COMPOSITE PANELS

A Dissertation
by
TIMOTHY WILLIAM COATS

submitted to the Office of Graduate Studies
Old Dominion University
in partial fulfillment of the requirements for the degree of

DOCTOR OF PHILOSOPHY

ENGINEERING MECHANICS

August 1996

Approved By:

R. Prabhakaran (Co-Chairman)

C.E. Harris (Co-Chairman)

Y. Mikata (Member)

S. Cupschalk (Member)

ABSTRACT

A PROGRESSIVE DAMAGE METHODOLOGY FOR RESIDUAL STRENGTH PREDICTIONS OF CENTER-CRACK TENSION COMPOSITE PANELS.

Timothy William Coats
Old Dominion University, 1996

Co-Chairs of Advisory Committee: Dr. R.Prabhakaran
Dr. C.E. Harris

An investigation of translaminate fracture and a progressive damage methodology was conducted to evaluate and develop residual strength prediction capability for laminated composites with through penetration notches. This is relevant to the damage tolerance of an aircraft fuselage that might suffer an in-flight accident such as an uncontained engine failure. An experimental characterization of several composite materials systems revealed an R-curve type of behavior. Fractographic examinations led to the postulate that this crack growth resistance could be due to fiber bridging, defined here as fractured fibers of one ply bridged by intact fibers of an adjacent ply.

The progressive damage methodology is currently capable of predicting the initiation and growth of matrix cracks and fiber fracture. Using two different fiber failure criteria, residual strength was predicted for different size panel widths and notch lengths. A ply discount fiber failure criterion yielded extemely conservative results while an elastic-perfectly plastic fiber failure criterion showed that the fiber bridging concept is valid for predicting residual strength for tensile dominated failure loads. Furthermore, the R-curves predicted by the model using the elastic-perfectly plastic fiber failure criterion compared very well with the experimental R-curves.

ACKNOWLEDGEMENTS

I would like to thank my advisor, Dr. R. Prabhakaran, for allowing and encouraging me to focus all my efforts and time on this research. The very generous financial support was provided by the Mechanics of Materials Branch (MEMB) at the NASA Langley Research Center. For this, I owe a very special and sincere thank-you to Dr. Charles E. Harris. I also want to thank Dr. Harris for providing me the opportunities I've had to learn and grow as a researcher in the field of fracture of composite materials. The use of the facilities at the MEMB is also much appreciated. Many thanks to all those in MEMB who contributed their time and efforts to expand my knowledge, especially Mr. C.C. (Buddy) Poe and Dr. C.E. Harris. I thank everyone in MEMB for making this a pleasurable and unforgettable experience. A special thank-you to Susanne Walts, graphics illustrator, for her time, patience, and professional hard work. Thank-you again Dr. Prabhakaran and Dr. Harris, for helping me accomplish so great a task.

NOMENCLATURE

a	Characteristic Half Crack Length
a_o	Initial Half Crack Length (Before Damage)
cod	Crack Opening Displacement
da	Crack Extension Length
E_x	Young's Modulus
l,L	Length
Q_{11}	Ply Level Reduced Modulus
Q_{12}	Ply Level Reduced Modulus
Q_c	General Fracture Toughness Parameter
Q_c/ε_{tuf}	General Fracture Toughness Ratio
S	Applied Stress
S_{ult}	Ultimate Strength
S_x^{cr}	Longitudinal Critical Strength
w	Width
α_1	Fiber Fracture Internal State Variable
α_2	Mode II matrix Cracking Internal State Variable
$d\alpha^M_{L_{11}}$	Change in the Fiber Fracture Internal State Variable
$d\alpha^M_{L_{22}}$	Change in the Mode II matrix Cracking Internal State Variable
β	Monotonic Damage Growth Parameter for Matrix Cracking
Δa	Effective Crack Growth
ε_{22}	Transverse Tensile Strain
ε_{22crit}	Critical Transverse Tensile Strain

ε_{11}	Longitudinal Tensile Strain
ε_{11crit}	Critical Longitudinal Tensile Strain
ε_c	Critical Strain of Laminate
ε_{tuf}	Ultimate Strain of the Fibers
γ	Monotonic Damage Growth Parameter for Fiber Fracture
σ_1	Longitudinal Ply Stress

TABLE OF CONTENTS

TABLE OF CONTENTS CONT'D

LIST OF TABLES

LIST OF FIGURES

LIST OF FIGURES CONT'D

LIST OF FIGURES CONT'D

LIST OF FIGURES CONT'D

LIST OF FIGURES CONT'D

CHAPTER I
INTRODUCTION

Industrial Applications and Problems

Damage tolerance has recently been the underlying issue driving much of the research in aircraft structure design. Consider, for example, any modern civilian aircraft with a large number of accumulated flight hours. For such an aircraft the flaws in a particular component may become critical before detection. Such a component will have to be designed to a safe life because it is not damage tolerant. The structural component will have to be overhauled or replaced before the aircraft completes a certain number of flight hours. A damage tolerant design insures detectable damage before catastrophic failure. Damage tolerance is the attribute of a structural component such as the fuselage or wing that allows the aircraft to survive an in-flight accident such as an uncontained fan blade or engine failure, or an impact with a foreign object such as a bird.

A familiar incident that occurred in 1988 that escalated damage tolerance research was the inflight structural failure of a particular Airlines flight [1, 2], Figure 1. The upper fuselage ripped open and a large section of the skin peeled away. The cause for this failure has been identified as a flaw in the rivet design. The stress concentrations at the knife edges of the rivet holes caused the formation of small fatigue cracks. Since these cracks occurred between the skins of the lap splice joints, they were virtually undetectable. To insure that this didn't occur with any of the other 737's, doublers were inserted using a hot bond adhesive between the riveted joints. Activities to insure the safe operation of the aging aircraft fleet includes increased maintenance and inspections, repair and

modifications, new advanced inspection technology to locate visually undetectable fatigue cracks, and research to design damage tolerant materials and structures.

Damage tolerance studies have discovered similarities between metals and fiber-reinforced composites as well as some obvious differences. Unlike homogeneous metals, composite materials are made of multiple constituents. Therefore, the modes and types of failure are more complex. While the matrix material in the composite may have similarities to metal in terms of modes of crack opening, composites have fiber fractures and delaminations which affect the redistribution of load. This leads to the conclusion that the toughening mechanisms are different in composites and metals. Toughening mechanisms are physical phenomena responsible for crack growth resistance. Crack-tip plasticity, for example, is a dominant toughening mechanism in metals. The toughening mechanisms in composites are due to micro-cracking. Even though the toughening mechanisms are fundamentally different for metals and composites, the result for both materials is the elimination of the stress singularity and the effect on load redistribution.

Currently, much research is being done to characterize the damage tolerance of various composite aircraft structures. For example, critical issues surrounding the advanced composite fuselage, Figure 2, are the catalysts for many research programs. Consider the crown region of a composite fuselage. Hoop and longitudinal stresses in the crown section are caused by cabin pressure while additional longitudinal stresses are due to the empennage forces on the aircraft during flight. If the fuselage suffers a through penetration by some foreign object, the "flaw" or "notch" would reduce the residual strength of the structure. Residual strength prediction capability for curved stiffened composite structures such as a composite fuselage does not yet exist. To develop a progressive damage methodology capable of accurate residual strength predictions for a damaged composite fuselage, accurate damage modelling of a much smaller scale must be accomplished first.

As a first step, the behavior of center-crack tension composite laminate panels with through penetration notches has been studied. The center-crack tension composite

laminate, Figure 3, simulates a small region in the crown portion of the fuselage and assumes the through penetration occurs perpendicular to either the hoop stresses or the longitudinal stresses. In addition to disregarding the curvature of the fuselage, it narrows in on the notch-tip region and assumes the through penetration occurred away from all stiffeners. The following literature survey will briefly describe others' contributions in the area of damage tolerance and residual strength of composite structures.

Literature Survey

Many fracture models are being developed to model damage and predict residual strength. Whitney and Nuismer (WN) [3,4] developed the "point-stress" and the "average-stress" failure criteria. Both criteria assume fracture occurs when the stress at some characteristic distance from the crack tip equals the unnotched strength. Pipes, Wetherhold, and Gillespie (PWG) proposed a fracture model to predict the notched strength of composite laminates [5]. In this model they claim the characteristic distance used in the WN model is not a material constant. Finally, the inherent flaw model developed by Waddoups, Eisenmann, and Kaminski [6] is an applied classical LEFM model which utilizes a characteristic distance and unnotched laminate strength to predict the notched laminate strength.

A thorough study of the fracture toughness and residual strength of various fibrous composites was done by Poe [7-11]. Poe found in his investigations of brittle laminated composites that linear elastic fracture mechanics (LEFM) could be used to determine the fracture toughness of a notched composite panel without loading it to failure. Harris and Morris [12-16] conducted a thorough investigation of translaminate fracture in notched composite laminates. The influence of stacking sequence is documented as well as the role of delamination in thick notched composite laminates. Many observations were made concerning fiber fracture, delamination, matrix cracking, and the influence of laminate

thickness. Damage was documented using x-ray radiography, and in some cases, specimen deply techniques were used. Some successful strength predictions were made using LEFM, including Poe's general fracture toughness parameter. Harris [17] also conducted an investigation into the use of crack-tip opening displacement with a Dugdale-type model to predict notched laminate strength. Similar investigations by Poe et al. [18] provides more deplied laminates revealing the ply-by-ply fiber damage.

Poe et al. [19] continued with damage tolerance studies by considering the crack growth resistance of large fuselage panels with through penetrations that represent discrete source damage. Crack growth resistance was plotted using the fracture data from various tests and residual strength predictions were made using LEFM. Poe found that LEFM predictions were too conservative, but crack growth resistance curves (R-curves) determined from strengths of unstiffened sheets made reasonably accurate predictions. Further discussion of the general fracture toughness parameter is included. Orange [20] presents a method by which the crack growth resistance is estimated from residual strength data for notched laminates. Information from simple test results can seemingly then be used to estimate the failure loads of more complicated structures of the same material and thickness. Schwalbe [21] provides an investigation into crack-tip opening displacement and crack growth resistance. R-curve methodolgy is explained in detail and driving force predictions are made reasonably well.

The characterization of damaged notched composite laminates has led to numerous damage growth models. Aronsson and Bäcklund [22] used a damage zone model to predict strength and load vs. displacement behavior. Damage is represented by a Dugdale/Barenblatt cohesive zone where the cohesive stresses decrease linearly with an increase in crack opening. Chang et al. [23] used the progressive damage analysis developed by Chang [24] to predict damage growth and failure of an open-hole tension composite specimen. The failure analysis consisted of property degradation models and failure criteria for matrix cracking as well as fiber and fiber-matrix shearing failure. The

Allen-Harris model [25-29] is a continuum damage model which utilizes kinematics based volume averaged damage variables to represent matrix crack growth and fiber fracture. This model has a mode I matrix crack growth law for fatigue as well as monotonic tension. As of now, Delamination and Mode II matrix crack growth is modeled empirically. Recent works extending from this model can be found in the literature [30-35]. An experimental verification of its ability to predict stiffness loss was documented by Coats [33,34] and its ability to predict residual strength was documented by Lo et al. [35]. Unfortunately, none of the mentioned models provide a means to predict delamination initiation and growth and the resulting stress redistribution. There is, however, much work being done in that area.

Ko et al. [36] predicts delamination initiation load and location by averaging the stress over the characteristic length in conjuction with the Hashin-Rotem criterion [37,38]. This research was applicable to balanced symmetric laminates containing a hole. Eason and Ochoa [39] incorporated a shear deformable theory, to predict out-of-plane shear and normal stress, into a finite element formulation for a plate with an open hole loaded in-plane. This allowed for the approximation of interlaminar stress, and as a result, the prediction of delamination initiation and growth. A technique for calculating strain-energy-release rate, G, for delamination around an open hole is developed by O'Brien and Raju [40]. The location of delamination around the hole boundary was successfully predicted for quasi-isotropic laminates. Lagace and Saeger [41] developed a methodology for predicting delamination initiation at holes in composite laminates. They used the interlaminar stress state in conjunction with a mechanics of materials failure criterion to compute the delamination initiation load.

All of the previous mentioned works were investigations or modelling with the goal to arrive at a prediction methodology that will predict the residual strength of notched composite laminates by taking into account all of the failure mechanisms. There are certain mechanisms that will redistribute the load at or around a notch. This load redistribution can cause a reduction in stress concentration and an increase in strength. Such mechanisms

must be accounted for if accurate residual strength predictions are required. For example, axial splits at a notch are a means of load redistribution and therefore reduce the stress concentrations at the notch. The axial splits, therefore, are known as a toughening mechanism. The key is to identify toughening mechanisms and incorporate them into the modelling.

The toughening issue will be discussed thoroughly in Chapter II and Chapter III. Chapter II, Experimental Characterization, will discuss in detail the experimental procedures and the experimental verification of crack growth resistance. Since toughening mechanisms are responsible for crack growth resistance, experimental evidence and a postulate concerning toughening mechanisms is discussed. The Progressive Damage Analysis, Chapter III, addresses the issue of modelling the damage. The mechanics for matrix cracking and fiber fracture are discussed as well as the mathematical framework for the progressive damage model - the Allen/Harris non-linear constitutive model. The progressive damage analysis scheme consists of a damage-dependent finite element analysis implemented into the NASA Computational Structural Mechanics Testbed (COMET). Accounting for the gradual load redistribution effects of toughening is discussed in this chapter and analytical results are presented.

Objectives and Approach

Since fibers are the major load bearing component in most composites, then predicting residual strength of a center-notched composite laminate would require a knowledge of fiber fracture as well as matrix crack growth. Therefore, the research herein takes an in-depth look at the failure mechanisms involved in translaminate fracture of center-crack tension composite panels. Furthermore, fiber bridging in the sense of intact fibers of one ply of a laminate bridging the fractured fibers in an adjacent ply is considered as a possible explanation for crack growth resistance as stable tearing occurs from the notch-tip.

The objective of this study is to develop a progressive damage methodology capable of predicting residual strength of composite structures. The approach is as follows:

- Experimental characterization of failure mechanisms by the following methods:

  (a) x-ray radiography

  (b) ply-level fractography

  (c) R-curve behavior

- Theoretical postulate resulting from the experimental study: a fiber bridging effect is present and is a mechanism of crack growth resistance.
- Develop fiber fracture failure criteria and implement them into the Allen-Harris progressive damage model.
- Utilize a damage dependent finite element code where the damage is modeled using the Allen-Harris model [25-29].

  (a) mesh refinement study.

  (b) residual strength predictions using a ply discount and an elastic-perfectly plastic monotonic damage growth law.

  (c) compare the two damage growth laws to illustrate the bridging effects in the elastic-perfectly plastic growth law.

  (d) R-curve predictions.

CHAPTER II
EXPERIMENTAL CHARACTERIZATION

This Chapter will provide a detailed description of the experimental study. Discussed first will be the experimental procedure, i.e. specimen preparation, test setup, and loading. The next discussion will be on specimen deply techniques and R-curves to illustrate crack growth resistance. Finally, fiber bridging will be introduced as a possible toughening mechanism.

Experimental Procedure

Material and Specimen Configuration

Through-penetration of an aircraft fuselage is simulated on a small scale using the center-crack tension (cct) specimen, Figure 3. Five configuration groups were tested; 1" unnotched coupons for collecting unnotched material properties, 4" wide and 12" wide specimens where the 4" wide specimens had 1/2" notches ($2a_o$=1/2", w=4", L=18") and 1" notches ($2a_o$=1", w=4", L=18"), the 12" wide specimens had a 3" notch ($2a_o$=3", w=12", L=34"), and the 36" wide panels had 9" notches ($2a_o$=9", w=36", L=90"). Each configuration group consisted of the materials AS4/8553-40, AS4/938, and AS4/3501-6. The AS4/3501-6 was manufactured using a tape pre-preg while the others were made from the tow-placement technique. The AS4/938 specimens had two different tow spacings. All of the test materials with their test identification name, material identification, dimensions, and manufacturing techniques are summarized in Table 1. The layups used were $[\mp 45/0/90/\mp 30/\bar{0}]_s$ for the center-crack tension specimens and its transverse

$[\pm 45/45/90/0/\pm 60/\bar{90}]_s$ was used for some of the unnotched coupons as well. The specimens were fabricated by Boeing and shipped to NASA Langley Research Center for testing. The laminate stacking sequences are for fuselage structures designed by Boeing.

Specimen Preparation

Each specimen was strain gaged according to Figures 4-7c. The 1" unnotched coupons and the 4"wide panels were monotonically loaded to failure in a 50 kip servo-hydraulic testing machine. The 12" and 36" wide panels had anti-buckling guide plates attached just above and below the notch. They were loaded to failure in a 100 kip and 500 kip servo-hydraulic testing machine, respectively. The strain gages were all wired to a Vishay Measurements Group System 4000 data acquisition unit. The system 4000 also collected the applied load from the load cell and the center-crack opening displacement from the ring gage secured in the center of the notch.

Loading and Data Collection

As the panels were being loaded, the discrete source damage (fiber fracture, delamination, and matrix cracking local to the notch tip) was frequently audible. Periodically, as damage progressed with increasing load, a zinc-iodide dye penetrant was applied to the notch and edge of the specimen. X-ray radiographs were taken of the right and left notch-tip regions. The damage absorbed the zinc-iodide dye penetrant and the damage is accurately represented in the x-ray radiograph as a blackened or shaded region, Figure 8. Lamina material properties were obtained from the literature and are provided in Table 2. The laminate properties including failure loads are given in Tables 3 thru 8. The accuracy of the lamina material properties is somewhat questionable since the lamina material properties were obtained from various references and it was nearly impossible to find a complete and consistent set of data. Lamina properties for AS4/3501-6 were taken from an ASTM STP [42] and the other properties were taken from Boeing test data [43].

Some of the panels were not loaded to catastrophic failure. Instead, x-rays were taken periodically up to a percentage of the ultimate failure load. The specimen was then taken out of the grips and the area surrounding the notch tip was deplied. Implications and conclusions about crack growth resistance from the x-ray radiographs and specimen deply techniques are discussed in the following paragraphs.

Verification of Crack Growth Resistance

There are a number of ways to verify crack growth resistance. To do this, an understanding of what crack growth resistance means is necessary. Crack growth resistance is simply a resistance to crack propagation. A damage tolerant material has a high resistance to crack growth and the physics of this resistance can be illustrated in x-ray radiographs of the notch-tip damage, fractographs of deplied specimens, and R-curves.

X-Ray Radiography

Typical damage tolerance as might be seen in a composite fuselage can be illustrated in an x-ray radiograph of a center-crack tension panel, Figure 8. Notice in this figure the amount of damage accumulation, or the damage tolerated. The left and right notch tip damage is shown. What looks like a "tear" in the panel is fiber fracture, and the shading surrounding it is local delamination. The lines extending from the notch tip and through the fractured region are matrix cracks in the off-axis plies. The key issue here is the amount of crack growth before catastrophic failure. This x-ray radiograph is evidence of crack growth resistance in the composite fuselage because the panel is still sustaining the very load that created such damage. Notice that in Figure 8 the damage seen is only at 89.6% of failure when this x-ray radiograph was taken. This is an indication of a damage tolerant structure.

A series of x-ray radiographs from various size panels are provided in Figures 9-11b to illustrate crack growth resistance. It was deemed unnecessary to provide the x-ray radiographs for every specimen since damage initiation and growth occurred similarly for all of the specimens anyway. Notice the loads at which these x-ray radiographs were taken. Crack growth resistance is what keeps the fiber fracture from traversing the entire width of the laminate. The mechanism of such resistance will be discussed later in this chapter in Isolation of Toughening Mechanisms. The point here is that because the x-ray radiograph shows such extreme damage at only a percentage of ultimate failure, crack growth resistance exists.

Fractography of Ply Level Damage

A few specimens were chosen to be loaded only up to a percentage of ultimate failure. Then the notch-tip damage region was isolated and pyrolized in an oven at 850°F until the neat resin had burned away (about four hours). The individual plies were separated and examined using a JEOL JSM-6400 scanning electron microscope. Fiber fracture is clearly visible in these plies, Figures 12a-c. The zinc iodide stain produced from the x-ray procedure is a reliable indication of local delamination. A schematic of the fiber fracture and local delamination is provided in Figure 13 to aid the eye in locating and quantifying the ply damage. The dark patches drawn on the schematics at the notch-tips represent local delamination and fiber fracture is represented by the "free-hand" drawn lines. Dimensions are given for most of the delaminations and the fiber fracture is dimensioned as *da*. Schematic representations of more fractographs are provided in Figures A-1 to A-3 of Appendix A. The schematics illustrate the evidence of crack growth resistance as well as the fractographs. It is not necessary to show all of the fractographs and schematics because they are repetitive illustrations of the various patterns and magnitudes of fiber fracture in each ply. Therefore, the conclusion that crack growth resistance is clearly evident is the same for all of the fractographic examinations.

R-Curve Behavior

During the monotonic loading of these panels, the applied load and the crack opening displacement (cod) at the center of the notch was recorded and used to produce load/cod plots, Figures 14-16. Discontinuities, or *jumps*, exist at various places along the load/cod plot where the fiber fracture was audible during loading. At these discontinuities the specimen was unloaded to take an x-ray and are labeled A, B, C, etc., on the load/cod plot. The corresponding x-ray radiographs are given in the plots to illustrate the amount of damage at each discontinuity. A closed form elasticity solution [44] for determing the characteristic half crack length, a, for a quasi-isotropic material under plane stress is

$$COD = \frac{4 \bullet S \bullet a}{E_x} \tag{1}$$

where E_x is the longitudinal modulus, S is the applied stress, and a is the characteristic half crack length. Given that $\Delta a = a - a_o$, and after some algebraic manipulation,

$$\Delta a = a_o \left\{ \left[\frac{COD \bullet E_x}{4S} \right]_i^{-1} \left[\frac{COD \bullet E_x}{4S} \right] - 1 \right\} \tag{2}$$

is the elasticity solution for effective crack growth and is shown in the figures as well. The initial half crack length is a_o, and the subscript *i* indicates the initial load/cod slope up to the point of separation between the load/cod curve and its initial slope. The load/cod plots illustrate the use of this closed form solution.

A plot of fracture toughness as a function of effective crack growth is called a crack growth resistance curve (R-curve). The fracture toughness, in terms of the general fracture toughness ratio, of large notched composite laminates is given in Figure 17 [19]. The general fracture toughness ratio, Q_c/ε_{tuf}, was developed by Poe [7-11] using linear elastic fracture mechanics (LEFM) where Q_c is the general fracture toughness parameter and ε_{tuf} is the tensile failing strain of the fibers. Q_c is independent of laminate orientation and was derived on the basis of fiber failure in the principal load-carrying laminae. Q_c is

proportional to the critical value of the mode I stress intensity factor (S.I.F.) and the constant of proportionality depends only on the elastic constants of the laminate. Poe showed that the ratio Q_c/ε_{tuf} was a constant for all brittle epoxy composite laminates regardless of layup. Therefore, a single value of Q_c/ε_{tuf} could be used to predict the fracture toughness of these fibrous composite laminates from only the elastic constants and ε_{tuf}. Experimental data [7-10] indicated Q_c/ε_{tuf} is reasonably constant, 0.3 $\sqrt{in}$, except for instances where extensive delamination or 0^o ply splitting occurred.

A couple of the laminates in Figure 17 exhibited significantly higher fracture toughness than Poe's prediction. Furthermore, the crack growth resistance evident in Figure 18 [19] portrays a much higher fracture toughness than Poe's previous investigations. This is due to toughening mechanisms not accounted for in the constant general fracture toughness parameter. The various toughening mechanisms affect crack growth resistance and thus affect the shape of the R-curve and the value of the fracture toughness.

The effective crack growth calculated from the load/cod plots mentioned above and the corresponding applied stress is used in Poe's general fracture toughness solution [7-11]

$$Q_c = \frac{S}{E_x}\left[\pi(a+\Delta a)\sec\frac{\pi(a+\Delta a)}{W}\right]^{1/2}(\zeta) \qquad (3)$$

to generate crack growth resistance curves (R-curves) in Figures 19-21. An x-ray radiograph for one of the specimens in each graph is supplied to illustrate the extent of the notch tip damage. The dashed line noted as *previous work* is the constant Q_c/ε_{tuf} determined in Poe's previous investigations [7-11] and is placed in the figures to illustrate that the fracture toughness of some notched composite laminates is not accurately predicted by the constant ratio.

The R-curves are experimental verification of crack growth resistance because they illustrate the continuing load carrying capability with increasing discrete source damage. From the three experimental verification techniques, x-ray radiography, scanning electron

microscope fractography, and R-curve behavior, we can state that these center-crack tension panels were damage tolerant since much of the damage was detectable long before catastrophic failure. The crack growth resistance was due to a dominant toughening mechanism and these toughening mechanisms need to be accounted for in a progressive damage analysis if accurate residual strength predictions are to be obtained.

Isolation of Toughening Mechanisms

Ample evidence of crack growth resistance was presented in the previous sections. Materials that are damage tolerant resist crack growth because of one or more existing toughening mechanisms. It has been proposed and accepted by many researchers that fiber bridging, intact fibers bridging the wake of a matrix crack, is a dominant toughening mechanism in many materials. Fibers bridging matrix cracks is not a likely or realistic toughening mechanism for the center-crack tension panels investigated in this study. However, we may postulate that fiber bridging in the sense of intact fibers of one ply bridging the fractured fibers of another ply is a dominant toughening mechanism by which load is redistributed. It is obvious from the x-ray radiographs in Figures 9-11 and in the ply fractographs in Figures 12a-c that this type of fiber bridging is an existent physical phenomenon in the center-crack tension composite panels. Throughout the remainder of this study, this type of bridging will be referred to as ply bridging. (Appendix B provides a discussion on fiber bridging and ply bridging, including a literature survey of fiber bridging). The next step involves applying the load redistribution effect of the ply bridging in a progressive damage analysis so that it will be possible to predict residual strengths of the center-crack tension panels within an acceptable level of accuracy.

CHAPTER III
PROGRESSIVE DAMAGE ANALYSIS

Fiber fracture criteria were developed and implemented into an existing progressive damage model framework, the Allen-Harris model [25-29]. The progressive damage model was implemented into a multi-purpose finite element code [35] and a residual strength prediction capability was developed. This progressive damage methodology is damage dependent and can therefore model the damage development at and around the notch-tip. It is also independent of laminate stacking sequence, and the finite element analysis makes it possible to analyze any geometrical configuration.

A Progressive Damage Model

The Allen-Harris Model

The damage model of Allen and Harris [25-29] was originally developed to model the behavior of microcrack damage in brittle epoxy systems and has recently been extended to toughened polymer systems. The model predicts the growth of intraply matrix cracks for monotonic tensile loadings and for tension-tension fatigue, the associated ply level damage-dependent stress and strain states, and the residual strength of laminates with geometric discontinuities. The model also accounts for the effects of delaminations but uses an empirical relationship that requires the user to supply an estimate of the delamination area. The empirical relationship must be used because the model currently does not calculate free edge interlaminar stresses. (The mathematical formulation of the model may be found in the literature [29] and will not be reproduced herein.) The model uses internal state

variables (ISV) to represent the local deformation effects of the various modes of damage. Loading history dependence is modelled by ISV damage growth laws. The progression of damage is predicted by an iterative and incremental procedure outlined in the flowchart shown in Figure 22. This entire progressive failure analysis scheme has been implemented into the finite element formulation in the NASA Computational Mechanics Testbed (COMET) [35] computer code. The first block of Figure 22 is a description of the information needed as model input. A FORTRAN code consisting of the damage dependent constitutive model and a damage growth law for matrix cracking was incorporated into a classical lamination theory analysis to produce effective lamina and laminate properties for unnotched laminates. The program is called FLAMSTR (Fatigue LAMinate STRess) [32] and makes up the first constitutive module. The fourth block is a damage dependent finite element analysis code [35] from which the second constitutive module performs a ply level elemental stress analysis and simulates damage growth via damage growth laws for each element. The damage growth calculations, block six, are used to update the damage state, block seven, for the notched laminates. Note that for unnotched laminates, only the first constitutive module is needed to update the damage state.

The material property descriptions required for the model include standard ply stiffness and strength data determined in the usual manner. In addition, the tension-tension fatigue matrix crack growth law must be determined from test data obtained from the $[0/90_2/0]_s$ laminate. Under tension-tension fatigue, matrix cracks accumulate in the 90 degree layers and, therefore, the effects of mode I matrix crack growth is isolated. The mode II matrix crack growth law can be obtained from fatigue tests of the $[45/-45]_s$ laminate which isolates the 45 degree plies in pure shear. (The mode II growth law is not currently implemented into the finite element code.) A procedure [33] has been developed for determining the ISV (damage parameters) from the test data obtained from these two laminates.

Quasi-Static Loads and Damage Modelling

Recall that the model uses internal state variables to represent the local deformation effects of the various modes of damage. For instance, the ISV representing mode I matrix cracking is α^{M}_{L22}. When the material is subjected to quasi-static (monotonic) loads, the rate of change of the internal state variable, α^{M}_{L22}, is of the form

$$d\alpha^{M}_{L22} = \begin{cases} \beta d(\varepsilon_{22}-\varepsilon_{22crit}) & \text{if } \varepsilon_{22} > \varepsilon_{22crit}; \\ 0 & \text{if } \varepsilon_{22} < \varepsilon_{22crit} \end{cases} \tag{4}$$

where ε_{22crit} is the critical tensile failure strain and β is a factor that describes the load carrying capability of the material after the critical tensile strain has been reached. A similar relationship is used to describe the tensile failure of the reinforcing fibers. The internal state variable for this mode of damage is α^{M}_{L11} and its rate of change is of the form

$$d\alpha^{M}_{L11} = \begin{cases} \gamma d(\varepsilon_{11}-\varepsilon_{11crit}) & \text{if } \varepsilon_{11} > \varepsilon_{11crit}; \\ 0 & \text{if } \varepsilon_{11} < \varepsilon_{11crit} \end{cases} \tag{5}$$

where ε_{11crit} is the tensile fiber fracture strain and γ is a factor describing the residual load carrying capability of the material after fiber fracture has occurred. The numerical details of 0^{o} ply fiber fracture as they appear in the finite element code are as follows. The longitudinal 0^{o} ply stress (ignoring thermal strains) is written as

$$\sigma_1 = Q_{11}\left[\varepsilon_1 - \alpha_1^{new}\right] + Q_{12}\left[\varepsilon_2 - \alpha_2^{new}\right] \tag{6}$$

where σ_1 is the longitudinal 0^{o} ply stress, Q_{11} and Q_{12} are the ply level reduced moduli, ε_1 and ε_2 are the 0^{o} ply longitudinal and transverse strains, respectively, and α_1^{new} and α_2^{new} represent the updated 0^{o} ply local deformation effects of fiber fracture and matrix cracking, respectively. The change in the ISV representing the effects due to tensile fiber fracture is

$$d\alpha_1 = \frac{Q_{11}\left(\varepsilon_1 - \alpha_1^{old}\right) + Q_{12}\left(\varepsilon_2 - \alpha_2^{old}\right) - \gamma S^{y}_{x}}{Q_{11}} \tag{7}$$

where S_x^y is the lamina longitudinal critical strength. The ISVs are updated by

$$\alpha_1^{new} = \alpha_1^{old} + d\alpha_1 \tag{8}$$

and then equation (8) is substituted into equation (6). The result of this substitution is

$$\sigma_1 = Q_{11}\left[\varepsilon_1 - \left\{ \alpha_1^{old} + d\alpha_1 \right\}\right] + Q_{12}\left[\varepsilon_2 - \alpha_2^{new}\right] \tag{9}$$

which is further modified by substituting equation (7) into equation (9) to obtain

$$\sigma_1 = Q_{11}\left[\varepsilon_1-\alpha_1^{old} - \left\{\varepsilon_1-\alpha_1^{old} + \frac{Q_{12}}{Q_{11}}(\varepsilon_2-\alpha_2) - \frac{\gamma S_x^y}{Q_{11}}\right\}\right] + Q_{12}(\varepsilon_2-\alpha_2) \tag{10}$$

and

$$\sigma_1 = \gamma S_x^y \tag{11}$$

is the result of obvious cancellations. Notice that if γ=0, the monotonic failure criterion results in a ply discount type of behavior. If γ=1, elastic-perfectly plastic behavior is obtained. A computer algorithm has been written for this computational scheme and implemented into a finite element analysis code.

Finite Element Analysis

Model Configuration and Mesh Refinement

A previous mesh refinement study showed that the analytical solutions for residual strength converges very well for open-hole laminates. (The open-hole mesh refinement study is documented in Appendix C). In the analysis of the center-crack tension panels, an initial mesh refinement study revealed that a very fine mesh in the notch region severely under-predicted the failing load, and a course mesh resulted in a failure load much higher

than the experimental values. The fine mesh analysis revealed out-of-plane displacements and in-plane rotations were occurring at and around the notch-tip on the order of 10^{-1}. The course mesh results showed no such in-plane rotations or out-of-plane displacements more than on the order of 10^{-14}. It was decided that these rotations and displacements must be an indication of localized buckling.

The reliability in the experimental and analytical strain field correlation was previously demonstrated by the stiffness loss predictions for the open-hole laminates [34]. Therefore, a comparison of the model predicted buckling effect to the experimental strain gage data was observed to confirm the existence of localized buckling. Typical notch-tip stress/strain behavior for the center-crack tension panels, Figure 23, is an obvious illustration of localized buckling. This demonstrates that the experimental stress/strain behavior correlates well with the analytical displacements and rotations to conclude that localized buckling is indeed occurring at and around the notch-tip of the center-crack tension panels. This is a reasonable conclusion since localized buckling in center-crack panels under tensile loadings is a well known phenomenon. Sawicki et al. [45] documented this phenomenon in their photoelastic investigations of center-crack tension panels.

The mesh refinement study also addressed the issue of choosing an optimum mesh that provides the best results. The model averages the kinematic effect of damage over the entire element. This averaging procedure results in a length scale which is an important consideration in mesh generation. Since the progressive damage model represents damage with volume averaged quantities that are averaged over the entire element, an element too large may not represent the effects of the stress singularity and results in an over-prediction of strength. If the element area relative to the notch size and the material constituents is small, that element size approaches the micro scale. An element too small may cause the averaging process to exaggerate the effects of the stress singularity and result in an under-prediction of strength. This is similar to the Whitney/Nuismer point stress or average stress criteria [3,4]. Based on experimental data, there seems to be a characteristic distance

which determines the proper element size. This phenomenon is also not unique to composites. There has already been much discussion on this topic relating to crack-tip plasticity in metals and dates back at least as far as the investigations by Chan et. al. [46].

The finite element model configuration is a quarter panel mesh of a center-crack tension panel with a 0.02" notch, Figures 24-27. These meshes have an element size and spacing at the notch-tip which resulted from the combined mesh refinement and localized buckling study. The meshes were constructed so as to allow the existence of localized buckling and obtain reasonable analytical solutions. All of the nodes on the y-axis midplane from the notch tip to the panel's edge are constrained in the x-direction, the nodes on the x-axis midplane are constrained in the y-direction, and all the nodes are constrained in out of plane rotation. The loading is applied in the x-direction.

Analytical Predictions

Residual strength predictions have been made for center-crack tension laminates loaded in monotonic tension. R-curves for the center-crack panels were predicted and all predictions were compared with experimental data. These results will be discussed in the next two sections.

Residual Strength Predictions

The progressive damage model computed residual strengths using two different failure criteria (monotonic damage growth laws). The first law, a ply discount criterion, was achieved by setting the monotonic growth law parameter, γ, to zero (γ=0). Recall from equation (11) that when fiber fracture occurred, if γ=0, the load carrying capability of a ply within an element would be eliminated. This criterion does not account for any toughening mechanisms and is therefore extremely conservative. The second law, achieved with γ=1, is an elastic-perfectly plastic criterion. The longitudinal ply stress can only be as high as the ply critical strength of the ply at or after fiber fracture in this case. This criterion

accounts for load redistribution and is more likely to represent some of the toughening mechanisms seen in the experiments such as ply bridging.

The 0^o ply longitudinal stresses were plotted along the transverse distance from the notch-tip for the AS4/938 panel with the 3" notch. The plots for both failure criteria are plotted together prior to any damage in Figure 28 to demonstrate that for no damage, the stress calculations are consistent and the failure criteria has no effect prior to damage. Ply discount is illustrated in Figure 29 by the portion of the plot that shows a ply stress value of zero psi. Fracture in the 0^o plies has occurred in the elements at a transverse distance away from the notch-tip at almost 0.9". Along this distance the load carrying capability of the fractured plies has reduced to zero. The load carrying capability plateaus at the ply critical strength for the γ=1 case in Figure 30. There are load cycles when the notch-tip stresses reach negative values for both cases γ=0 and γ=1. This is due to the extreme displacements and rotations occurring at the notch-tip. The change in the internal state variables is not as drastic as the strains in this region and as fracture progresses away from the notch, the notch-tip strains decrease, the internal state variables do not decrease, and the resulting stress is negative. This is a numerical artifact in the code that will be corrected in the near future. This does not affect the residual strength results.

The residual strength predictions for γ=0 and γ=1 are illustrated in Figures 31-33 where the model predictions are compared to the experimental averages. The error bars represent the experimental minimums and maximums when available. The experimental values were given in Tables 4-8 and the values represented in Figures 31-33 are given in Tables 9-11.

The predictions were reasonable considering the model depends on accurate material properties. The lamina material properties used in this investigation were not experimentally measured from a sample of the material tested. The literature was searched for a consistent set of material properties for AS4/3501-6 and the only complete set found was in a journal article [42]. The other properties came from data documentation by Boeing [43].

A lamina material properties sensitivity study revealed that a change in only one property could have a noticeable affect on the analytical solution. In Tables 12 and 13, three analytical studies were performed. The first analytical column provides the actual chosen properties for this study and the resulting solution is listed at the bottom of the table. The second and third analytical columns each have a property in italic and bold faced font. These values were the only change for that analysis and the resulting solutions are given at the bottom of the tables. The experimental column has the experimental minimum and maximum residual strength. Notice that for AS4/8553-40, a 1.5% increase in E_{11} results in a 1.8% increase in strength. Furthermore, an 11.5% increase in critical strain results in a 4.7% increase in residual strength. For AS4/3501-6, a 10% decrease in E_{22} had no effect as expected, and a 10% decrease in G_{12} resulted in a 4.7% decrease in residual strength. No attempt was made herein to match the experimental results by selecting material properties that "optimized" the predictions.

The residual strength predictions are not only sensitive to the lamina material properties but to the fiber fracture failure criteria as well. The decision to choose γ=1 (elastic-perfectly plastic) and γ=0 (ply discount) was not a random thought or an attempt to find a criterion that would match experimental results. The school of thought here was to have two extremes that would allow a study of the toughening mechanism caused by the ply bridging without any other phenomenological influences that would fit the analytical solutions to the experimental data. Both of the failure criteria allow load redistribution through ply bridging. Unlike the elastic-perfectly plastic criterion, the ply discount method does not allow a fractured ply in a given element to carry any load. The load redistribution is sudden and the adjacent plies fail very quickly after the first ply failure. This is why the ply discount method is said not to have any toughening mechanisms even though load redistribution is occurring.

If the ply discount method was able to predict the residual strengths of the center-crack tension panels within ±10%, there would be no need for this progressive damage model or a fiber fracture failure criterion that accounts for the toughening effects observed in the experiments. The model, utilizing the elastic-perfectly plastic fiber fracture failure criterion, made predictions that fell within ±10% of the experimental averages in most cases. Most of these predictions fell within or very near the experimental data scatter. Considering that the material properties may vary ±10% depending on where and how they are obtained, the residual strength predictions are about as good as they can get with the exceptions of perhaps the 1" notch of the AS4/8553-40 and the 9" notch of the AS4/3501-6. It was believed that the failure load of the 9" notch AS4/3501-6 was much lower than it should have been given the lamina material properties of this material. The lamina material properties for the AS4/8553-40 was found in a NASA Contractor Report [43]. The properties was for a material with a fiber volume fraction of about 53% and the actual material tested in this study had a fiber volume fraction of 58%. The rule of mixtures was applied to obtain the lamina material properties used in the model, and there is obviously compounding errors due to that step as well.

These results show that the model has reached a level of maturity where it can be used to model fiber and matrix damage progression and predict the residual strength of notched composite laminates. This study was key in developing the model to this level of maturity. The predicted R-curves will demonstrate this further and conclude the analytical results of this investigation.

R-Curve Behavior

The R-curves are plotted in Figures 34-45 using the elastic-perfectly plastic monotonic damage growth law. These figures show model generated R-curves compared to the experimental R-curves. The effective crack growth, Δa, is calculated using the closed form solution in equation (2). R-curves were generated using actual Δa measurements from the

x-ray radiographs in Appendix D. However, due to the subjectivity of measuring the damage from an x-ray radiograph, the closed form solution approach in Figures 34-45 will be the center of discussion in this section.

Notice in these figures that the general shape of the model generated R-curve is similar to the experimental R-curves except for the initial data points. These initial points of fracture are critical because they determine the slope and curvature of the initial portion of the curve. The R-curves reveal that the predicted initial fiber fracture occurs at a higher fracture toughness than the experimental data. However, as loading continued, an under-prediction of residual strength was manifested in a lower fracture toughness in the model generated R-curves. Likewise, the model generated R-curve revealed a higher fracture toughness than the experimental fracture toughness where the residual strengths were over-predicted. There was one exception in Figure 46 where it would seem only panel G2TAPEA failed at a higher load than the model prediction, when in fact panel F1TAPEA had a higher residual strength as well. The problem with modelling the initial fiber fracture at a higher fracture toughness is evident here and is a characteristic of the monotonic damage growth law, lamina material properties, and the critical failing strains used in the model.

CHAPTER IV
CONCLUDING REMARKS

An experimental investigation of translaminate fracture was conducted and a residual strength prediction capability was developed using a progressive damage methodology. An experimental characterization of several composite materials systems revealed an R-curve type of behavior. Fractographic examinations led to the postulate that this crack growth resistance could be due to ply bridging, defined in this study as fractured fibers of one ply bridged by intact fibers of an adjacent ply. The Allen-Harris model was used in a finite element code to model the matrix cracking and fiber fracture that results from the notch-tip stresses in center-crack tension composites. Two fiber failure criteria were used to model the progression of fiber fracture. The first criterion is essentially the classical ply discount method because as fiber fracture occurred in a particular ply for any given element, that ply in the given element would no longer have any load carrying capability. Therefore, this criterion did not allow for any toughening effects. The other fiber failure criterion is an elastic-perfectly plastic fiber failure growth law. As a ply fractures in an element, this fiber failure criterion allows for a more gradual load redistribution and the load carrying capability of that ply in the element is constrained to the lamina longitudinal failure strain. These criteria were chosen as two extremes to compare the results and obtain an understanding of the ply bridging effect in the elastic-perfectly plastic criterion. Perhaps a criterion somewhere in between that is more representative of strain softening [47] would provide more accurate results.

Residual strength was predicted using both of the fiber failure criteria. The elastic-perfectly plastic criterion resulted in predictions within $\pm$ 10% of the experimental

averages in most cases. Furthermore, because the elastic-perfectly plastic criterion is more representative of the toughening mechanisms observed in the experiments, the ply bridging concept was shown to be valid for predicting residual strength for tensile dominated failure loads. Predictions of the R-curve type of behavior were made as well. These predictions were relatively consistent with the residual strength predictions in that under-predicted residual strengths also resulted in under-predicted R-curves.

This investigation was only a small step in the efforts to develop a progressive damage methodology to predict residual strengths of composite aircraft structures. For this particular model, not all of the mechanisms of damage have been included. Delamination initiation and growth still needs to be incorporated into this model as well as compression damage mechanisms. All of these mechanisms contribute to the failure process as well as load redistribution. It is difficult to say, for instance, whether or not the residual strength predictions will decrease if the mechanism of delamination is introduced into the modelling. One thought is that delamination would weaken the laminate causing a reduction in the residual strength. However, local delamination at or around a notch could relieve the high stress concentration and thus increase the residual strength.

REFERENCES

[1] Newman, J.C. and Harris, C.E.,"Fracture Mechanics Research at NASA Related to the Aging Commercial Transport Fleet," NASA CP 3160, 1991 International Conference on Aging Aircraft and Structural Airworthiness, 1991, pp. 75-91.

[2] National Transportation Saftey Board, "Aloha Airlines, Flight 243 Boeing 737-200, N73711, Near Maui, Hawaii, April 28, 1988," Government Accession No. PB89-910404.

[3] Whitney, J.M. and Nuismer, R.J.,"Stress Fracture Criteria for Laminated Composites Containing Stress Concentrations," *J. Composite Materials*, Vol. 8, pp. 253-265, 1974.

[4] Nuismer, R.J. and Whitney, J.M.,"Uniaxial Failure of Composite Laminates Containing Stress Concentrations," *Fracture Mechanics of Composites, ASTM STP 593, American Society of Testing and Materials*, pp. 117-142, 1975.

[5] Pipes, R.B., Wetherhold, R.C., and Gillespie, J.W. Jr.,"Macroscopic Fracture of Fibrous Composites," *Materials Science and Engineering*, Vol. 45, pp. 247-253, 1980.

[6] Waddoups, M.E., Eisenmann, J.R., and Kaminski, B.E.,"Macroscopic Fracture Mechanics of Advanced Composite Materials," *J. Composite Materials*, Vol. 5, pp. 446-454, 1971.

[7] Poe, C.C., Jr.," Strain Intensity Factor Approach for Predicting the Strength of Continuously Reinforced Metal Matrix Composites," *Metal Matrix Composites: Testing, Analysis, and Failure Modes, ASTM STP 1032*, W.S. Johnson, Ed., American Society for Testing and Materials, Philadelphia, 1989, pp. 173-193.

[8] Poe, C.C., Jr., "A Unifying Strain Criterion for Fracture of Fibrous Composite Laminates," *Engineering Fracture Mechanics*, Vol. 17, No. 2, pp. 153-171, 1983.

[9] Poe, C.C., Jr., "A Parametric Study of Fracture Toughness of Fibrous Composite Materials," *J. of Offshore Mechanics and Arctic Engineering*, Vol. 111, August 1989, pp. 161-169.

[10] Poe, C.C., Jr. and Sova, J.A. "Fracture Toughness of Boron/Aluminum Laminates with Various Proportions of 0° and 45°Plies," *NASA Technical Paper 1707*, Nov. 1980.

[11] Poe, C.C., Jr. and Sova, J.A. "Fracture Toughness of Fibrous Composite Materials," *NASA Technical Paper 2370,* Nov. 1984.

[12] Harris, C.E. and Morris, D.H., "A Fractographic Investigation of the Influence of Stacking Sequence on the Strength of Notched Laminated Composites," *Fractography of Modern Engineering Materials: Composites and Metals, ASTM STP 948*, J.E. Masters and J.J. Au, Eds., American Society for Testing and Materials, Philadelphia, 1987, pp.131-153.

[13] Harris, C.E. and Morris, D.H., "Translaminate Fracture of Notched Graphite/ Epoxy Laminates," *Fracture Mechanics: Twenty-Third Symposium, ASTM STP 1189*, Ravinder Chona, Ed.,, American Society for Testing and Materials, Philadelphia, 1993, pp. 751-774.

[14] Harris, C.E. and Morris, D.H., "Role of Delamination and Damage Development on the Strength of Thick Notched Laminates," Delamination and Debonding of Materials, ASTM STP 876, W.S. Johnson, Ed., American Society for Testing and Materials, Philadelphia, 1985, pp. 424-447.

[15] Harris, C.E. and Morris, D.H., "A Damage Tolerant Design Parameter for Graphite/Epoxy Laminated Composites," *J. of Composites Technology & Research*, Vol. 7, No. 3, Fall 1985, pp. 77-81.

[16] Harris, C.E. and Morris, D.H., "Fracture Behavior of Thick, Laminated Graphite/Epoxy Composites," *NASA Contractor Report 3784*, March 1984.

[17] Harris, C.E. and Morris, D.H.,"On the Use of Crack-Tip-Opening Displacement to Predict the Fracture Strength of Notched Graphite/Epoxy Laminates," *Experimental Mechanics*, Vol. 25, No. 2, June 1985.

[18] Poe, C.C., Jr., Harris, C.E., and Morris, D.H., "Surface Crack Analysis Applied to Impact Damage in a Thick Graphite/Epoxy Composite," *Surface-Crack Growth: Models, Experiments, and Structures, ASTM STP 1060*, W.G. Reuter, J.H. Underwood, and J.C. Newman, Jr., Eds., American Society for Testing and Materials, Philadelphia, 1990, pp. 194-212.

[19] Poe, C.C., Jr., Harris, C.E., Coats, T.W., and Walker, T.H., "Tension Strength with Discrete Source Damage," *Proceedings of the Fifth NASA/DOD Advanced Composites Technology Conference*, Seattle, Washington, Aug. 1994.

[20] Orange, T.W., "Estimating the R-Curve from Residual Strength Data," *NASA TM 87182*, Feb. 1986.

[21] Schwalbe, K.H., "The Prediction of Failure Situations Using the CTOD Concept Based on the Engineering Treatment Model (ETM)," *The Crack Tip Opening Displacement in Elastic-Plastic Fracture Mechanics, Proceedings of the Workshop on the CTOD Methodology GKSS-Forschungszentrum Geesthacht*, GmbH, Geesthacht, Germany, April 23-25, 1985.

[22] Aronsson, C-G and Bäcklund, J., "Damage Mechanics Analysis of Matrix Effects in Notched Laminates," *Composite Materials: Fatigue and Fracture, ASTM STP 907*, H.T. Hahn, Ed., American Society for Testing and Materials, Philadelphia, 1986, pp. 134-157.

[23] Chang, K-Y, Sheng, L., and Chang, F-K, "Damage Tolerance of Laminated Composites Containing an Open Hole and Subjected to Tensile Loadings," J. of Composite Materials, Vol. 25, March 1991, pp. 274-301.

[24] Chang, Fu-Kuo and Chang, Kuo-Yen, "A Progressive Damage Model for Laminated Composites Containing Stress Concentrations," *J. of Composite Materials*, Vol. 21, Sept. 1987, pp. 834-855.

[25] Allen, D.H., Groves, S.E., and Harris, C.E., "A Cumulative Damage Model for Continuous Fiber Composite Laminates with Matrix Cracking and Interply Delamination," *Composite Materials: Testing and Design (8th Conference), ASTM STP 972*, J.D. Whitcomb, Ed., American Society for Testing and Materials, Philadelphia, 1988, pp. 57-80.

[26] Allen, D.H., Harris, C.E., Groves, S.E., "A Thermomechanical Constitutive Theory for Elastic Composites with Distributed Damage-I. Theoretical Development," *Int. J. Solids Structures*, Vol. 23, No. 9, 1987, pp. 1301-1318.

[27] Allen, D.H., Harris, C.E., Groves, S.E., "A Thermomechanical Constitutive Theory for Elastic Composites with Distributed Damage-II. Application to Matrix Cracking in Laminated Composites," *Int. J. Solids Structures*, Vol. 23, No. 9, 1987, pp. 1319-1338.

[28] Lee, J.W., Allen, D.H., Harris, C.E., "Internal State Variable Approach for Predicting Stiffness Reductions in Fibrous Laminated Composites with Matrix Cracks," *J. of Composite Materials*, Vol. 23, Dec. 1989, pp. 1273-1291.

[29] Harris, C.E. and Allen, D.H., "A Continuum Damage Model of Fatigue-Induced Damage in Laminated Composites," *SAMPE Journal*, July/August 1988, pp. 43-51.

[30] Lo, D.C., Allen, D.H., and Harris, C.E.; "A Continuum Model for Damage Evolution in Laminated Composites," *Inelastic Deformation of Composite Materials*, G.J. Dvorak, ed., Springer -Verlag, 1990, pp. 549-561.

[31] Lo, D.C., Allen, D.H., and Buie, K.D., "Damage Prediction in Laminated Composites with Continuum Damage Mechanics," *Serv. Durability Constr. Mater. Eng. Congr., Part I*, 1990, pp. 164-173.

[32] Lo, D.C., Allen, D.H., and Harris, C.E., "A Procedure for Utilization of a Damage-Dependent Constitutive Model for Laminated Composites," *NASA Technical Memorandum 104219*, NASA LaRC, February 1992.

[33] Coats, T.W., "Experimental Verification of a Progressive Damage Model for Composite Laminates Based on Continuum Damage Mechanics," M.S. Thesis, NASA Contractor Report 195020, Dec. 1994.

[34] Coats, T.W., "Experimental Verification of a Progressive Damage Model for IM7/5260 Laminates Subjected to Tension-Tension Fatigue," *J. of Composite Materials*, Vol. 29, No. 3, 1995, pp. 280-305.

[35] Lo, D.C., Coats, T.W., Harris, C.E., and Allen, D.H., "Progressive Damage Analysis of Laminated Composite (PDALC) (A Computational Model Implemented in the NASA COMET Finite Element Code)," *NASA Technical Memorandum* 4724, NASA LARC, August 1996.

[36] Ko, C-C, Lin, C-C, and Chin, H., "Prediction for Delamination Initiation Around Holes in Symmetric Laminates," *Composite Structures*, Vol. 22, 1992, pp. 187-191.

[37] Hashin, Z. and Rotem, A., "A Fatigue Failure Criterion for Fiber Reinforced Materials," *J. of Composite Materials*, Vol. 7, 1973, pp. 448-464.

[38] Hashin, Z., "Failure Criterion for Unidirectional Fiber Composites," *J. of Applied Mechanics*, Vol. 47, 1980, pp. 329-335.

[39] Eason, T.G. and Ochoa, O.O., "Incorporation of a Shear Deformable Element Into ABAQUS to Model Composite Structures," *AIAA -94-1452-CP, AIAA/ASME/ASCE/AHS/ASC Structures, Structural Dynamics, and Materials Conference*, 35th, Hilton Head, SC, Apr 1994.

[40] O'Brien, T.K. and Raju, I.S., "Strain-Energy-Release Rate Analysis of Delamination Around an Open Hole in Composite Laminates," *AIAA -84-0961, AIAA/ASME/ASCE/AHS Structures, Structural Dynamics, and Materials Conference*, 25th, Palm Springs, Ca, May 1984.

[41] Lagace, P.A. and Saeger, K.J., "Methodology for Prediction of Delamination Initiation at Holes in Composite Laminates," *AIAA -90-1019-CP, AIAA/ASME/ASCE/AHS/ASC Structures, Structural Dynamics, and Materials Conference*, 31st, Long Beach, Ca, 1990.

[42] Lagace, P.A., Bhat, N.V., and Gundogdu, A., "Response of Notched Graphite/Epoxy and Graphite/Peek Systems," *Composite Materials: Fatigue and Fracture*, Fourth Volume, ASTM STP 1156, W.W. Stinchcomb and N.E. Ashbaugh, Eds., American Society for Testing and Materials, Philadelphia, 1993, pp. 55-71.

[43] Scholz, D.B., Dost, E.F., and Flynn, B.W., "Advanced Technology Composite Fuselage - Materials and Processes," NASA Contractor Report 4731, 1995.

[44] Tada, H., Paris, P.C., and Irwin, G.R., "The Stress Analysis of Cracks Handbook", Del Research Corp., St. Louis, Mo., 1973.

[45] Sawicki, A.J., Graves, M.J., and Lagace, P.A., "Failure of Graphite/Epoxy Panels with Stiffened Strips," *Composite Materials: Fatigue and Fracture*, Fourth Volume, ASTM STP 1156, W.W. Stinchcomb and N.E. Ashbaugh, Eds., American Society for Testing and Materials, Philadelphia, 1993, pp. 5-34.

[46] Chan, S.K., and Tuba, I.S., and Wilson, W.K., "On the Finite Element Method in Linear Fracture Mechanics," *Engineering Fracture Mechanics*, Vo. 2, 1970, pp. 1-17.

[47] Walker, T.H., Ilcewics, L.B., Pollard, D.R., and Poe, C.C.,"Tension Fracture of Laminates for Transport Fuselage - Part 2: Large Notches," *Third NASA Adv. Composites Tech. Conf.*, Vol. 1, Part 2, NASA CP - 3178, pp. 727-758.

Table 1 Summary of Experimental Test Matrix

Material	Specimen Names	Layup	Thickness (t), inches	Width (w), inches	Lenght (l), inches	Notch Length ($2a_o$), inches
AS4/8553-40	A10-A13	(a)	0.103	1	11	unnotched
(Panel AK1)	A6-A9	(b)	0.103	1	11	unnotched
[c]tow-placed	A3-A5,B2-B6	(a)	0.103	4	18	0.5 and 1.0
	A1,A2,B1	(a)	0.110	12	34	3.0
	AK1	(a)	0.102	36	90	9.0
AS4/938	C10-C13	(a)	0.093	1	11	unnotched
(Panel AK5A)	C6-C9	(b)	0.091	1	11	unnotched
[d]tow-placed	C3-C5,D2-D6	(a)	0.093	4	18	0.5 and 1.0
	C1,C2,D1	(a)	0.095	12	34	3.0
	AK5A	(a)	0.085	36	90	9.0
AS4/938	E10-E13	(a)	0.093	1	11	unnotched
(Panel AK5B)	E6-E9	(b)	0.091	1	11	unnotched
[e]tow-placed	E3-E5,F2-F6	(a)	0.091	4	18	0.5 and 1.0
	E1,E2,F1	(a)	0.090	12	34	3.0
	AK5B	(a)	0.084	36	90	9.0
AS4/3501-6	G12-G18	(a)	0.093	1	11	unnotched
(Panel TAPEA)	G6-G11	(b)	0.093	1	11	unnotched
Tape Prepreg	G3-G5,H2-H6	(a)	0.093	4	18	0.5 and 1.0
	G1,G2,H1	(a)	0.093	12	34	3.0
	TAPEA	(a)	0.084	36	90	9.0

a $[\bar{+}45/0/90/\bar{+}30/\bar{0}]_s$

b $[^{+}45/90/0/^{+}60/\bar{90}]_s$

c 0.015" $\pm$ 0.015" gaps with stacked bands

d 0.025" $\pm$ 0.015" gaps with stacked bands

e 0.015" $\pm$ 0.015" gaps with offset bands

Table 2 Lamina Material Properties

Material	E_{11} (Msi)	E_{22} (Msi)	G_{12} (Msi)	ν_f (%)	ν_{12}	$\varepsilon_{\sigma}^{90}$ (%)	ε_{σ}^{0} (%)
[a]AS4/8553-40	19.7	1.31	0.65	58.2	0.34	0.87	1.56
[a]AS4/938	19.6	1.36	0.72	57.2	0.32	0.50	1.48
[b]AS4/3501-6	20.0	1.36	0.87	60.3	0.28	0.50	1.50

a Reference [43]

b Reference [42]

Table 3 Data From 1" Wide Unnotched $[\pm 45/0/90/\pm 30/\bar{0}]_S$ Laminates

Panel	Failure Load (kips)	Failure Stress (ksi)	Failure Strain (με)	Longitudinal Modulus (Msi)	Shear Modulus (Msi)	Poisson's Ratio
[a]AK1 (3 tests)	10.900	106	14000	7.720	2.575	0.499
	11.500	111	14000	7.990	2.650	0.507
	11.156	108	13550	8.005	2.560	0.470
[b]AK5A (3 tests)	7.045	75.226	9500	7.799	2.819	0.410
	7.489	80.917	10100	8.028	2.819	0.424
	7.051	75.291	9500	8.270	2.939	0.407
[c]AK5B (3 tests)	7.488	80.270	10000	7.908	2.731	0.448
	7.699	82.379	10500	8.217	2.841	0.446
	7.817	83.470	10500	7.897	2.701	0.462
[d]TAPEA (3 tests)	8.324	89.412	10600	8.567	2.881	0.487
	7.961	85.511	10300	8.369	2.820	0.484
	8.341	89.593	10700	8.445	2.809	0.503

a AS4/8553-40 tow placed (0.015" $\pm$ 0.015" gaps with stacked bands)

b AS4/938 tow placed (0.025" $\pm$ 0.015" gaps with stacked bands)

c AS4/938 tow placed (0.015" $\pm$ 0.015" gaps with offset bands)

d AS4/3501-6 tape prepreg

Table 4 Data From 1" Wide Unnotched $[\pm 45/90/0/\pm 60/\bar{90}]_S$ Laminates

Panel	Failure Load (kips)	Failure Stress (ksi)	Failure Strain (με)	Longitudinal Modulus (Msi)	Shear Modulus (Msi)	Poisson's Ratio
[a]AK1 (2 tests)	6.66 6.13	64.6 59.5	0.015 0.014	4.34 4.77	1.69 1.86	0.281 0.279
[b]AK5A (3 tests)	4.85 4.39 4.88	52.4 47.0 52.8	0.012 0.012 0.013	5.02 4.52 5.07	1.99 1.76 2.02	0.259 0.282 0.257
[c]AK5B (2 tests)	4.77 4.98	50.5 53.2	0.012 0.013	4.86 4.73	1.93 1.88	0.257 0.262
[d]TAPEA	N/A	N/A	N/A	N/A	N/A	N/A

a AS4/8553-40 tow placed (0.015" $\pm$ 0.015" gaps with stacked bands)

b AS4/938 tow placed (0.025" $\pm$ 0.015" gaps with stacked bands)

c AS4/938 tow placed (0.015" $\pm$ 0.015" gaps with offset bands)

d AS4/3501-6 tape prepreg

Table 5 Data From 4" Wide Notched $[\pm 45/0/90/\pm 30/\bar{0}]_s$ Panels ($2a_o$=1/2")

Panel	Failure Load (kips)	Failure Stress (ksi)	Failure Strain (με)	Longitudinal Modulus (Msi)	Width (in.)	Thickness (in.)	Q_o/ε_{tuf} $\sqrt{in}$
[a]AK1	23.3	56.6	7183	7.980	4.005	0.103	0.4198
(3 tests)	24.6	59.6	7617	7.907	4.005	0.103	0.4104
	20.5	49.6	6421	7.577	4.005	0.103	0.4461
[b]AK5A	20.3	58.6	6782	8.669	3.843	0.093	0.2975
(3 tests)	20.7	56.3	6544	8.622	4.003	0.092	0.2925
	20.8	57.1	6855	8.409	4.002	0.093	0.3183
[c]AK5B	19.9	56.9	6636	8.393	3.844	0.093	0.3104
(3 tests)	19.3	53.5	6381	8.443	4.005	0.093	0.2916
	18.8	51.7	6237	8.327	4.002	0.093	0.2850
[d]TAPEA	17.7	47.2	5535	8.480	4.020	0.093	0.2714
(2 tests)	20.0	54.0	6226	8.713	4.020	0.093	0.2944

a AS4/8553-40 tow placed (0.015" $\pm$ 0.015" gaps with stacked bands)

b AS4/938 tow placed (0.025" $\pm$ 0.015" gaps with stacked bands)

c AS4/938 tow placed (0.015" $\pm$ 0.015" gaps with offset bands)

d AS4/3501-6 tape prepreg

Table 6 Data From 4" Wide Notched $[\pm 45/0/90/\pm 30/\bar{0}]_s$ Panels ($2a_o$=1")

Panel	Failure Load (kips)	Failure Stress (ksi)	Failure Strain (με)	Longitudinal Modulus (Msi)	Width (in.)	Thickness (in.)	Q_o/ε_{tuf} $\sqrt{in}$
[a]AK1 (3 tests)	19.4	47.2	5972	8.051	4.005	0.103	0.4124
	17.4	42.3	5341	7.878	4.005	0.103	0.4172
	16.3	39.4	5026	7.773	4.005	0.103	0.3182
[b]AK5A (3 tests)	13.5	37.7	4775	7.913	3.845	0.093	0.2885
	14.5	40.5	5019	8.084	3.843	0.093	0.3254
	16.7	44.8	5313	8.472	4.004	0.093	0.4210
[c]AK5B (2 tests)	15.9	44.2	5264	8.317	4.005	0.090	0.3429
	14.6	41.2	4942	8.336	3.843	0.092	0.3155
[d]TAPEA (2 tests)	13.3	35.5	4180	8.471	4.023	0.093	0.2805
	13.8	36.9	4311	8.532	4.024	0.093	0.2740

a AS4/8553-40 tow placed (0.015" ± 0.015" gaps with stacked bands)

b AS4/938 tow placed (0.025" ± 0.015" gaps with stacked bands)

c AS4/938 tow placed (0.015" ± 0.015" gaps with offset bands)

d AS4/3501-6 tape prepreg

Table 7 Data From 12" Wide Notched $[\mp 45/0/90/\mp 30/\bar{0}]_S$ Panels ($2a_o$=3")

Panel	Failure Load (kips)	Failure Stress (ksi)	Failure Strain (με)	Longitudinal Modulus (Msi)	Width (in.)	Thickness (in.)	Q_d/ε_{tuf} $\sqrt{in}$
[a]AK1	31.3	24.1	3023	7.843	11.8	0.110	0.3070
(3 tests)	28.6	22.0	2999	7.283	11.8	0.110	0.3316
	29.6	23.5	2854	9.139	12.0	0.105	0.2748
[b]AK5A	34.9	30.6	3536	8.508	12.0	0.095	0.3977
(3 tests)	30.2	26.5	3374	7.876	12.0	0.095	0.3675
	31.0	27.2	3131	8.921	12.0	0.095	0.3491
[c]AK5B	29.5	27.3	3299	8.188	12.0	0.090	0.3728
(3 tests)	30.8	28.5	3213	8.664	12.0	0.090	0.3484
	29.9	27.7	3159	8.518	12.0	0.090	0.3636
[d]TAPEA	30.7	27.5	2931	9.367	12.0	0.093	0.5544
(2 tests)	32.9	29.5	3164	8.609	12.0	0.093	0.3935

a AS4/8553-40 tow placed (0.015" $\pm$ 0.015" gaps with stacked bands)

b AS4/938 tow placed (0.025" $\pm$ 0.015" gaps with stacked bands)

c AS4/938 tow placed (0.015" $\pm$ 0.015" gaps with offset bands)

d AS4/3501-6 tape prepreg

Table 8 Data From 36" Wide Notched $[\mp 45/0/90/\mp 30/\bar{0}]_S$ Panels ($2a_o$=9")

Panel	Failure Load (kips)	Failure Stress (ksi)	Failure Strain (με)	Longitudinal Modulus (Msi)	Width (in.)	Thickness (in.)	Q_o/ε_{tuf} $\sqrt{in}$
[a]AK1 (1 test)	62.8	17.1	1990	8.49	36.0	0.102	0.3440
[b]AK5A (1 test)	70.7	23.1	2320	9.92	36.0	0.085	0.4020
[c]AK5B (1 test)	60.3	19.9	2050	9.66	36.0	0.084	0.3540
[d]TAPEA (1 test)	51.2	15.7	1650	9.45	36.0	0.084	0.2840

a AS4/8553-40 tow placed (0.015" $\pm$ 0.015" gaps with stacked bands)

b AS4/938 tow placed (0.025" $\pm$ 0.015" gaps with stacked bands)

c AS4/938 tow placed (0.015" $\pm$ 0.015" gaps with offset bands)

d AS4/3501-6 tape prepreg

Table 9 AS4/8553-40: Experimental and Predicted Failure Loads

Notch Size (in.)	Experimental Low/High (kips)	Experimental Average. (lb)	Model Solution (lb) (γ=0)	% Difference (γ=0)	Model Solution (lb) (γ=1)	% Difference (γ=1)
1/2	20.5/24.6	22,787	16,576	-27.3	19,048	-16.4
1	16.3/19.4	17,711	11,312	-36.1	14,096	-20.4
3	28.6/31.3	29,845	21,400	-28.3	27,552	-7.7
9	N/A	62,800	49,752	-20.8	70,920	+12.9

Table 10 AS4/938: Experimental and Predicted Failure Loads

Notch Size (in.)	Experimental Low/High (kips)	Experimental Average. (lb)	Model Solution (lb) (γ=0)	% Difference (γ=0)	Model Solution (lb) (γ=1)	% Difference (γ=1)
1/2	18.8/20.8	19,972	15,896	-20.4	18,104	-9.4
1	13.5/16.7	15,066	11,672	-22.5	13,496	-10.4
3	29.5/34.9	31,067	20,688	-33.4	26,880	-13.5
9	60.3/70.7	65,500	46,080	-29.6	68,112	+4.0

Table 11 AS4/3501-6: Experimental and Predicted Failure Loads

Notch Size (in.)	Experimental Low/High (kips)	Experimental Average. (lb)	Model Solution (lb) (γ=0)	% Difference (γ=0)	Model Solution (lb) (γ=1)	% Difference (γ=1)
1/2	17.7/20.0	18,812	16,736	-11.0	20,176	+7.3
1	13.3/13.8	13,545	11,984	-11.5	14,928	+10.2
3	30.7/32.9	31,842	19,584	-38.5	29,568	-7.1
9	N/A	51,200	49,824	-2.7	72,360	+41.3

Table 12 - AS4/8553-40 Material Property Sensitivity Study

Properties	Analytical	Analytical	Analytical	Experimental
E_{11}	19.7 Msi	***20.0 Msi***	19.7 Msi	n/a
E_{22}	1.31 Msi	1.31 Msi	1.31 Msi	n/a
G_{12}	0.65 Msi	0.65 Msi	0.65 Msi	n/a
ν_{12}	0.34	0.34	0.34	n/a
ε_{cr}^{90}	0.87%	0.87%	0.87%	n/a
ε_{cr}^{0}	1.56%	1.56%	***1.74%***	n/a
Solution	27.6 kips -7.7% Exp.Avg.	28.1 kips -5.8% Exp. Avg.	28.9 kips -3.3% Exp. Avg.	28.6/31.3 kips

Table 13 - AS4/3501-6 Material Property Sensitivity Study

Properties	Analytical	Analytical	Analytical	Experimental
E_{11}	20.0 Msi	20.0 Msi	20.0 Msi	n/a
E_{22}	1.36 Msi	1.36 Msi	***1.22 Msi***	n/a
G_{12}	0.87 Msi	***0.78 Msi***	0.87 Msi	n/a
ν_{12}	0.28	0.28	0.28	n/a
ε_{cr}^{90}	0.5%	0.5%	0.5%	n/a
ε_{cr}^{0}	1.5%	1.5%	1.5%	n/a
Solution	29.6 kips -7.1% Exp. Avg.	28.2 kips -11% Exp. Avg.	29.6 kips -7.1% Exp. Avg.	30.7/32.9 kips

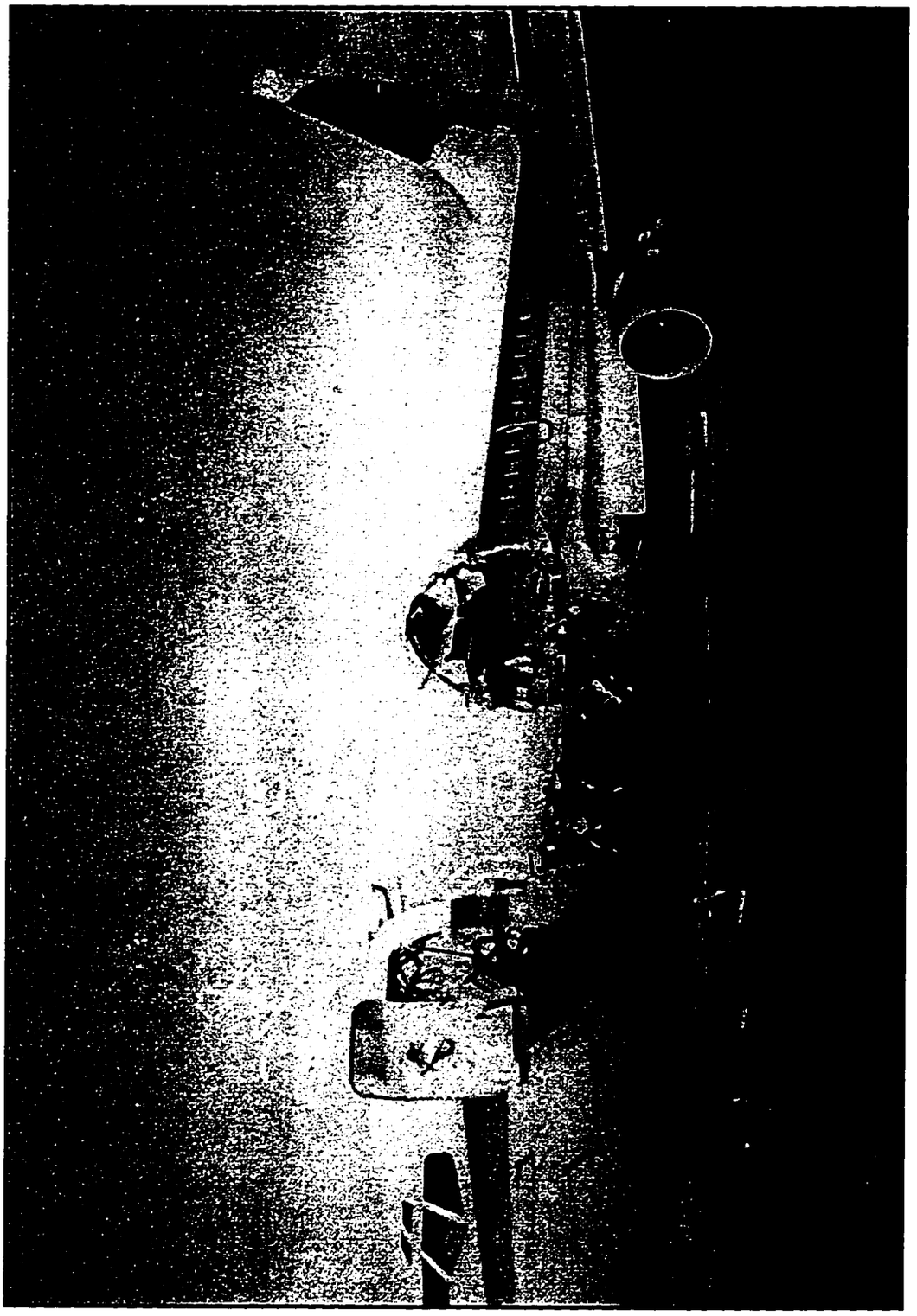

Figure 1 - In-Flight Structural Failure.

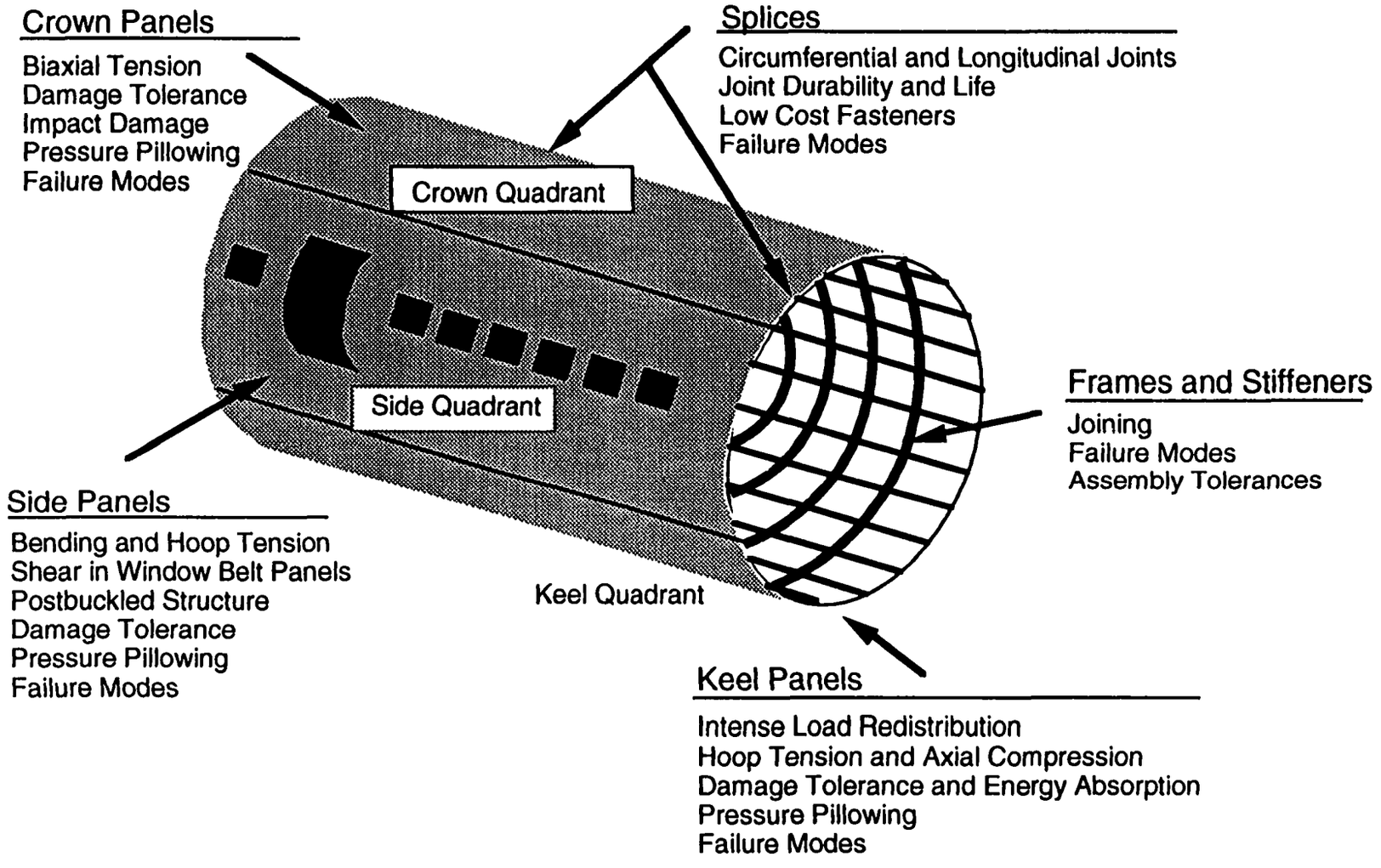

Figure 2 - Fuselage Critical Technology Issues.

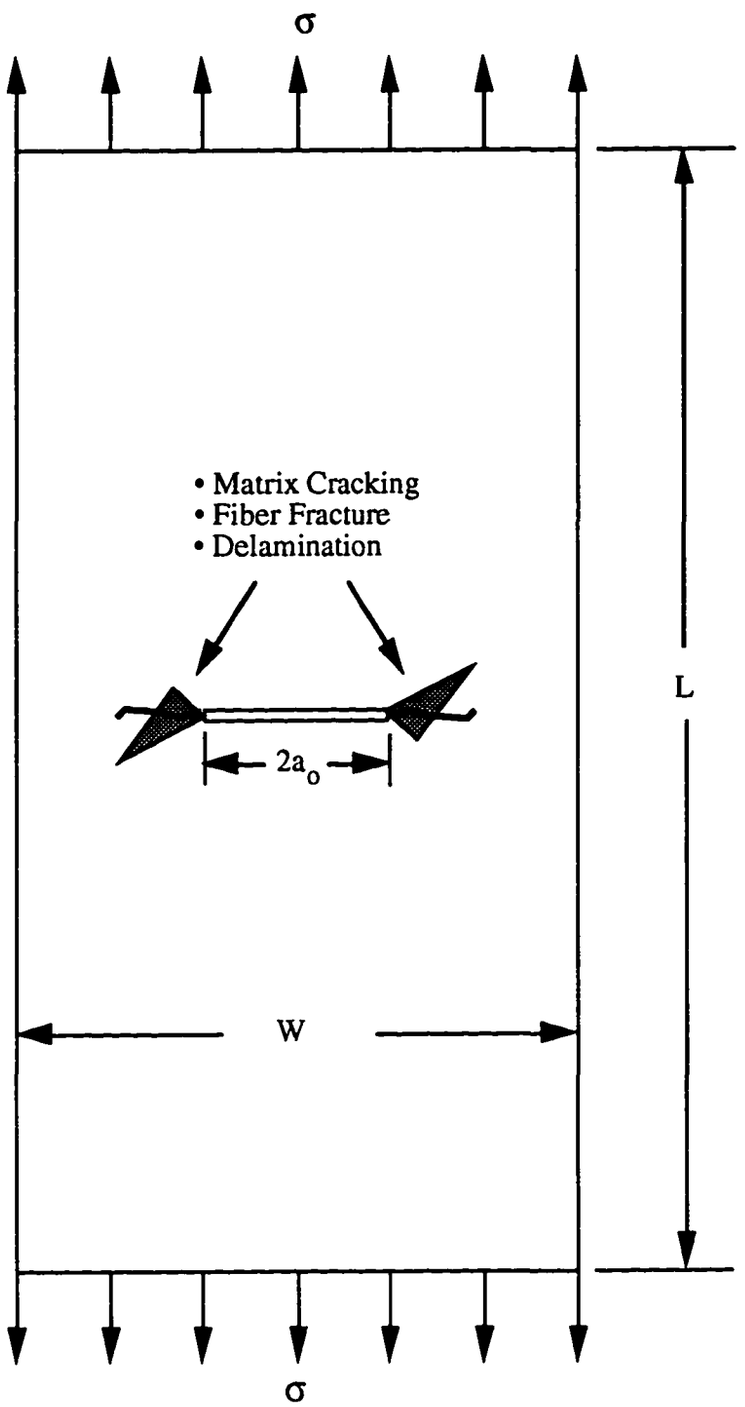

Figure 3 - Center-Crack Tension Panel.

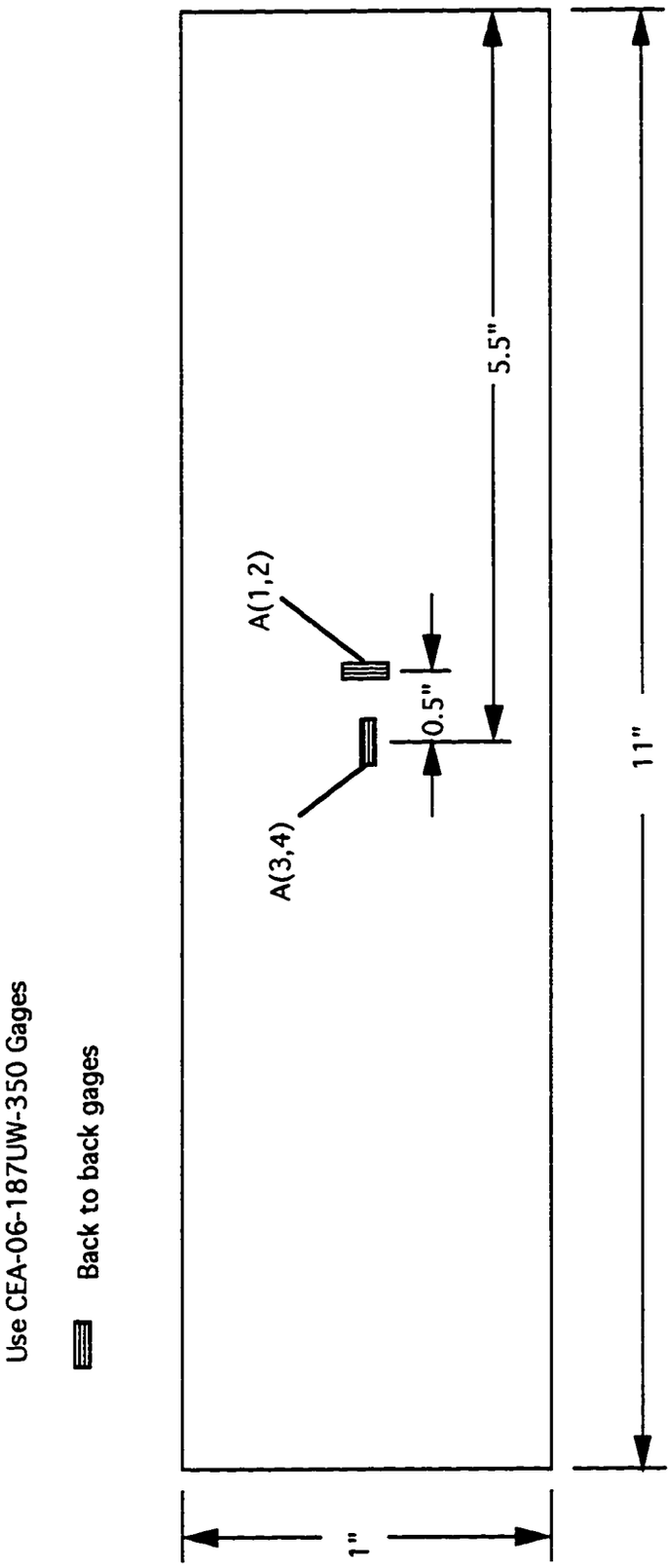

Figure 4 - Strain Gage Schematic for a 1" Wide Unnotched Panel.

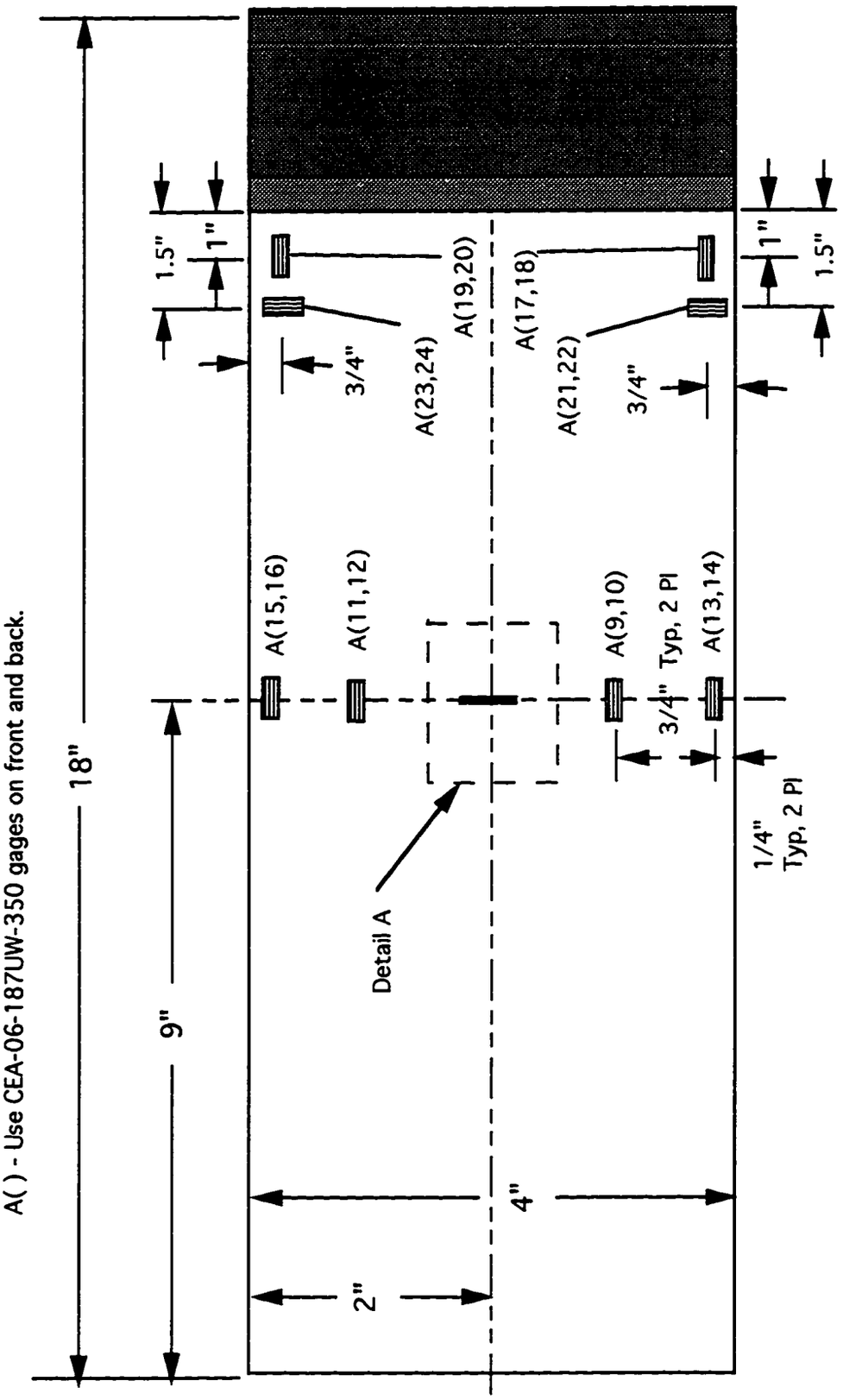

Figure 5a - Strain Gage Schematic for a 4" Wide Notched Panel.

B( ) - Use EA-06-070LC-350 single gages on front and back. Write the gage number in parentheses next to the gage.

C( ) - Use EA-06-070LC-350 single gages on front side only. Write the gage number in parentheses next to the gage.

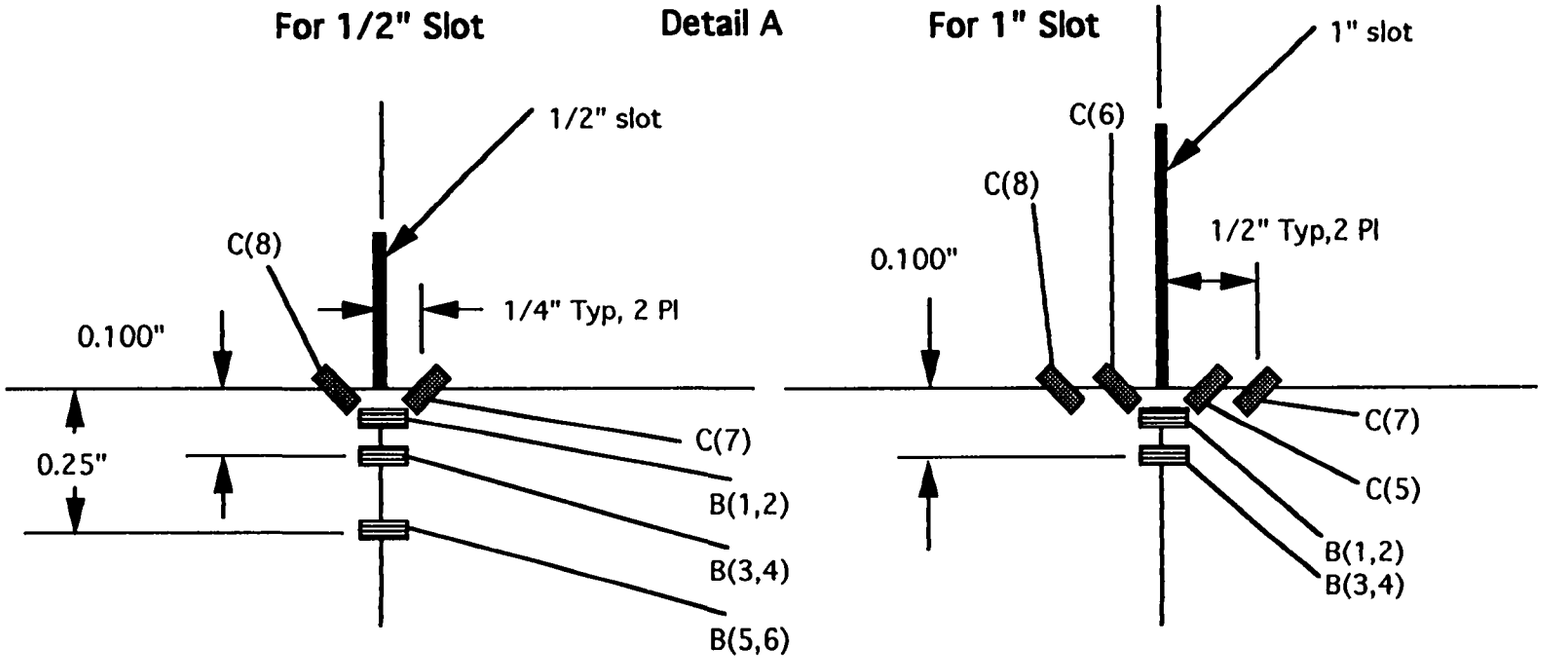

Figure 5b - Strain Gage Schematic at the Notch for the 4" Wide Panel.

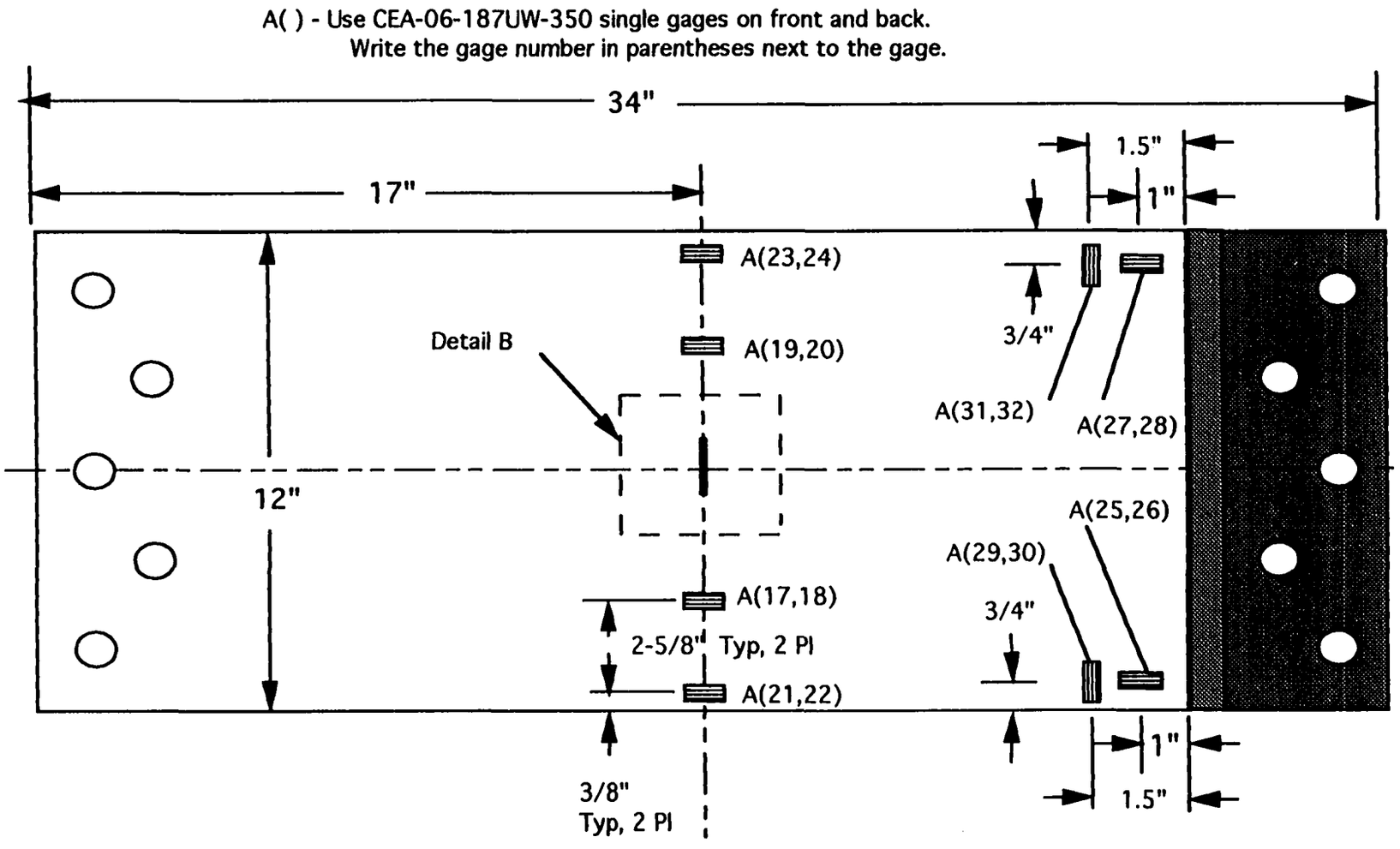

Figure 6a - Strain Gage Schematic for a 12" Wide Notched Panel.

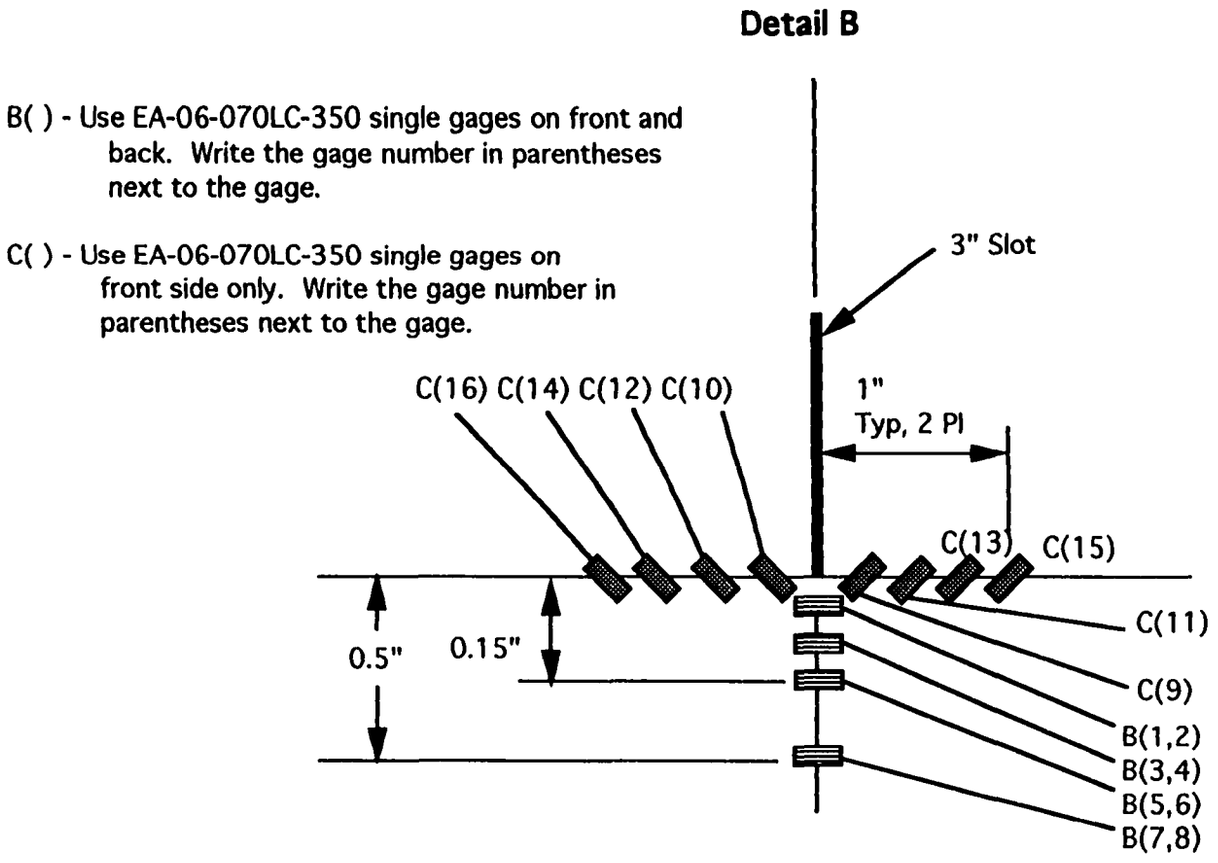

Figure 6b - Strain Gage Schematic at the Notch for the 12" Wide Panel.

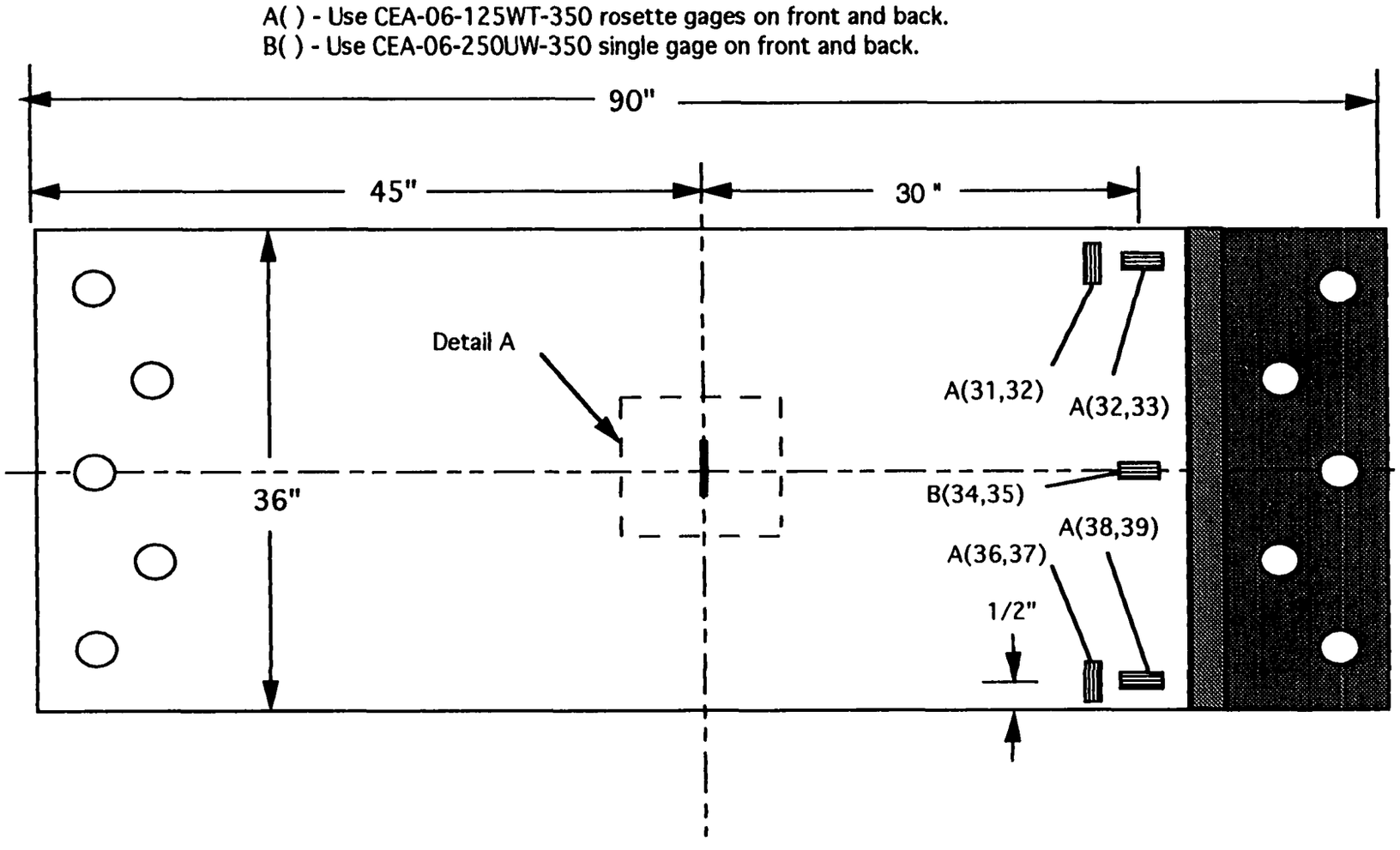

Figure 7a - Strain Gage Schematic for a 36" Wide Notched Panel.

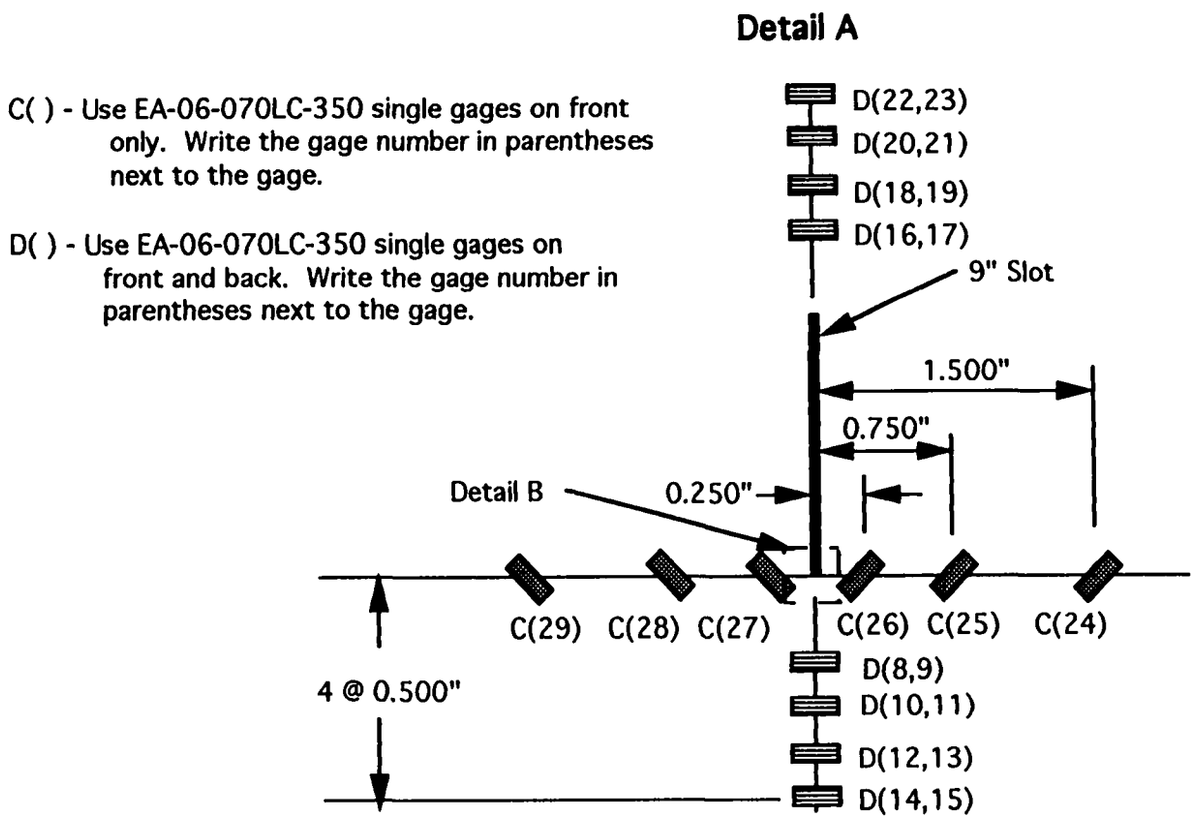

Figure 7b - Strain Gage Schematic at the Notch for the 36" Wide Panel.

Detail B

E( ) - Use C-891113-C single gages on front and back. Write the gage number in parentheses next to the gage.

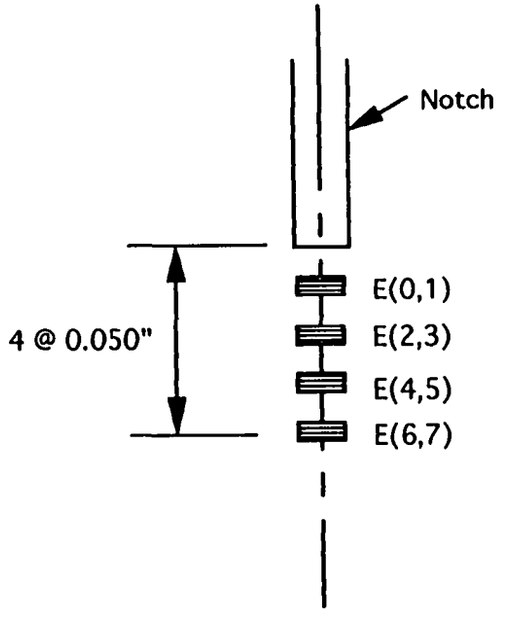

Figure 7c - Strain Gage Schematic at the Notch for the 36" Wide Panel.

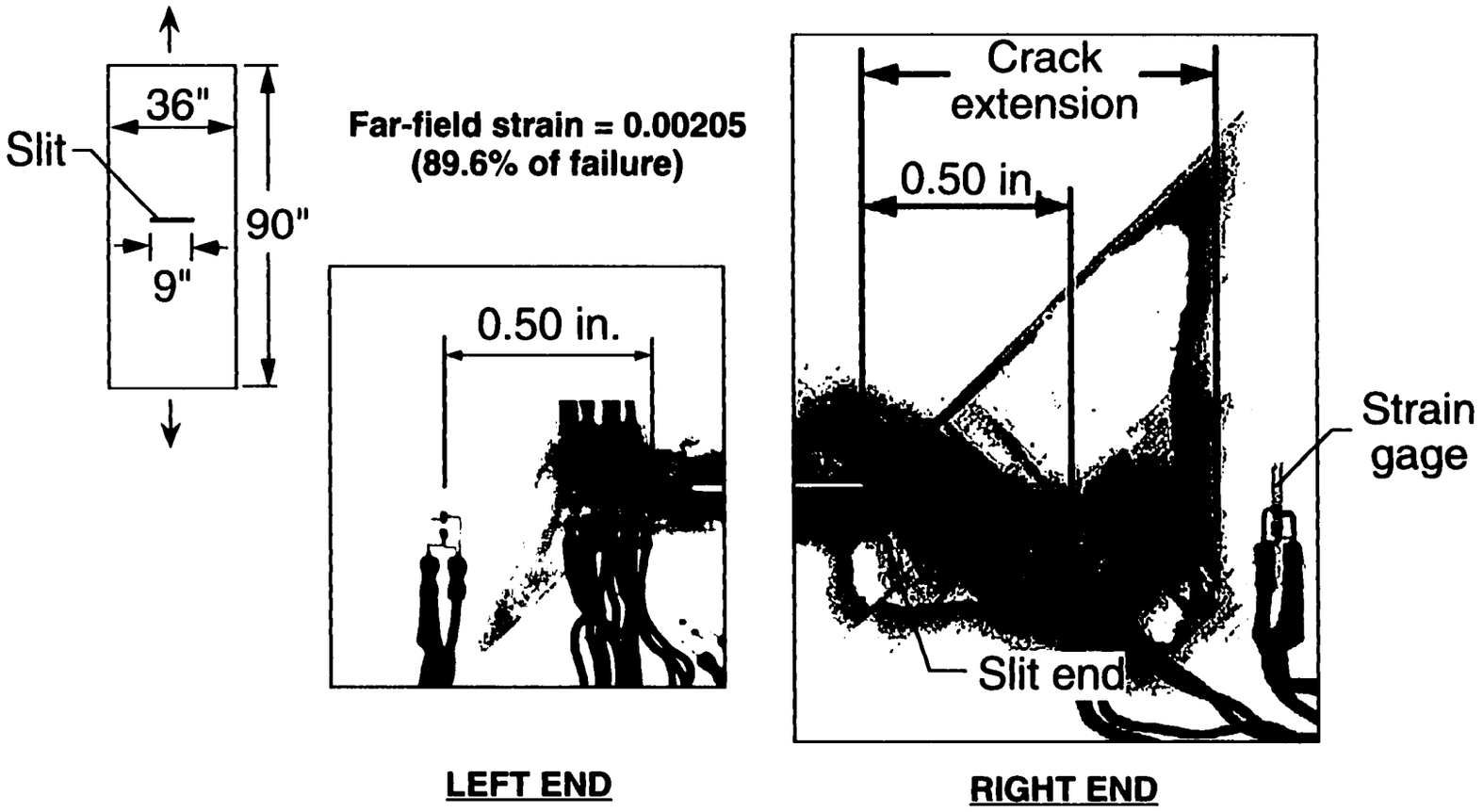

Figure 8 - Typical Crack-Tip Damage Due to Hoop Stresses in an AS4/938 Crown Quadrant of a Fuselage Laminate.

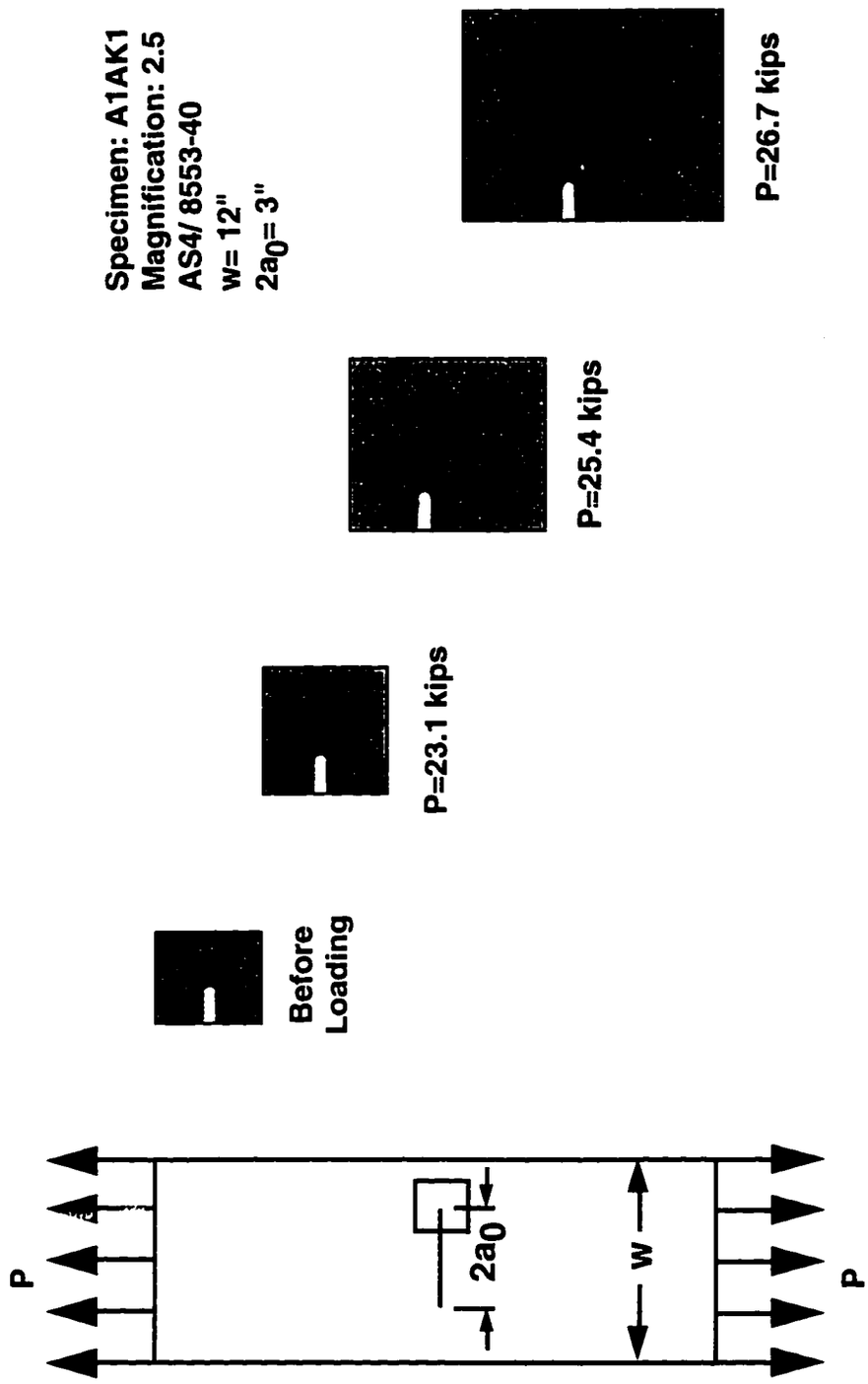

Figure 9 - X-Ray Radiographs of the Right Notch Tip Damage for the AS4/8553-40 Panels.

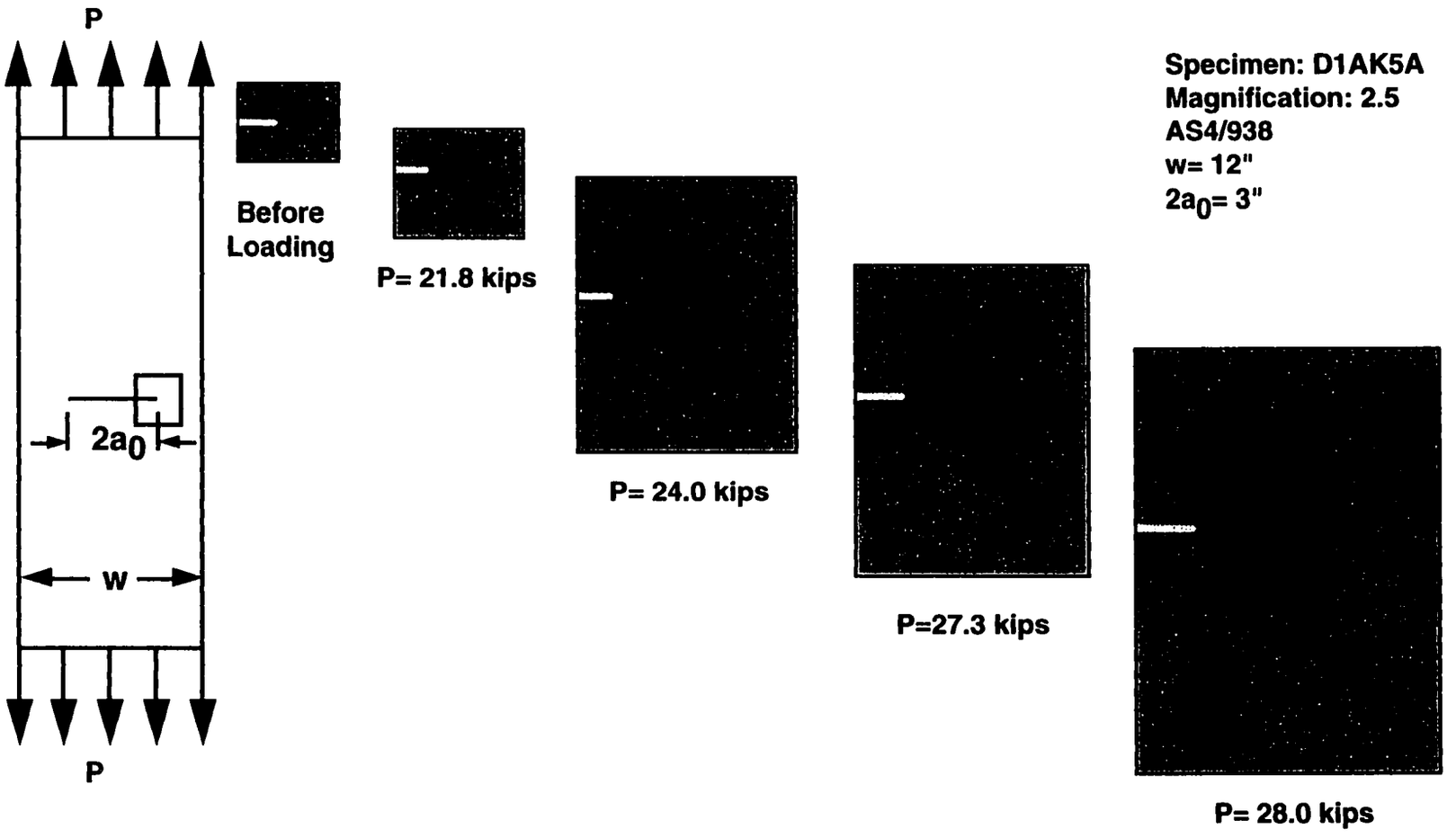

Figure 10a - X-Ray Radiographs of the Right Notch Tip Damage for the AS4/938 Panels.

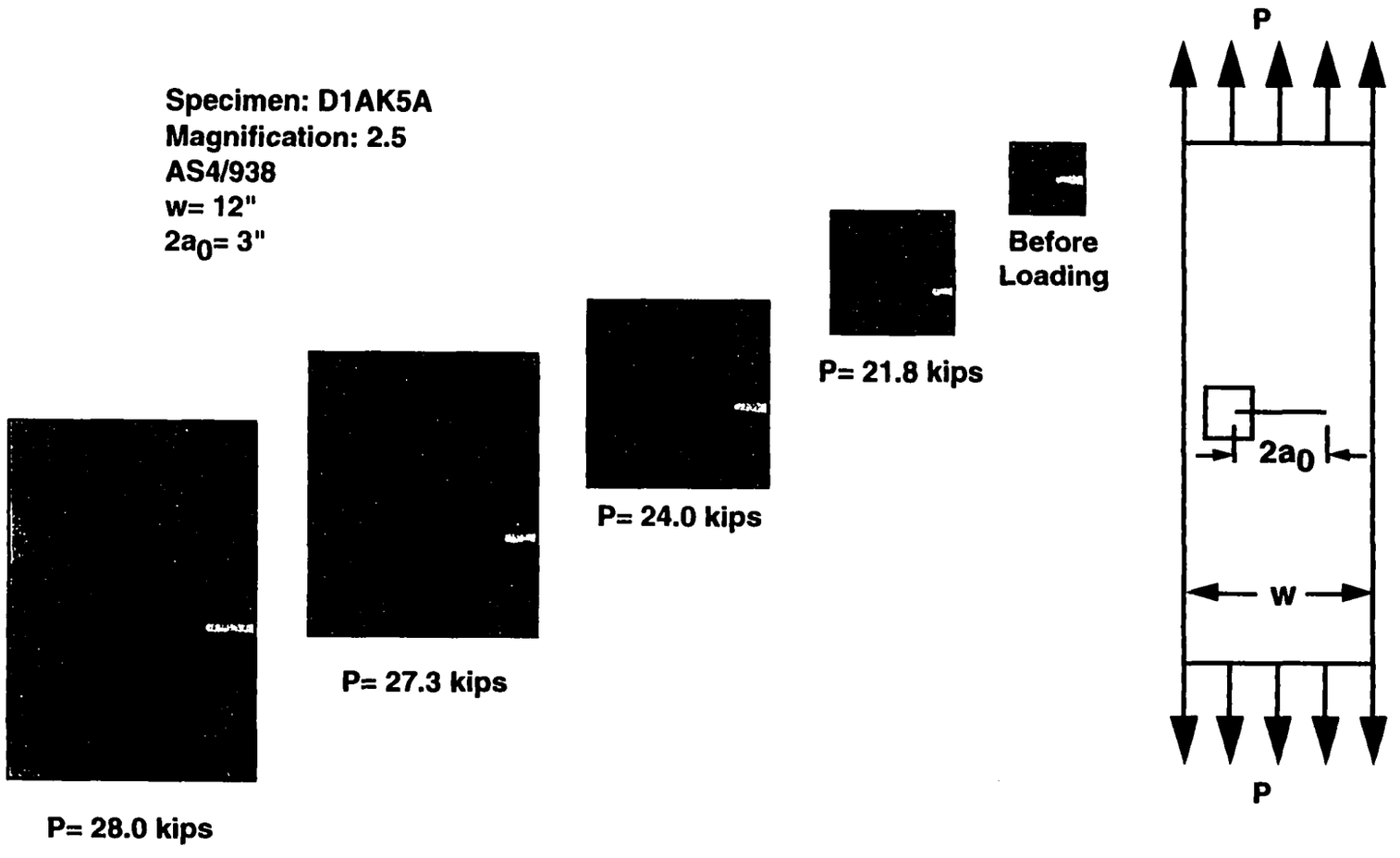

Figure 10b - X-Ray Radiographs of the Left Notch Tip Damage for the AS4/938 Panels.

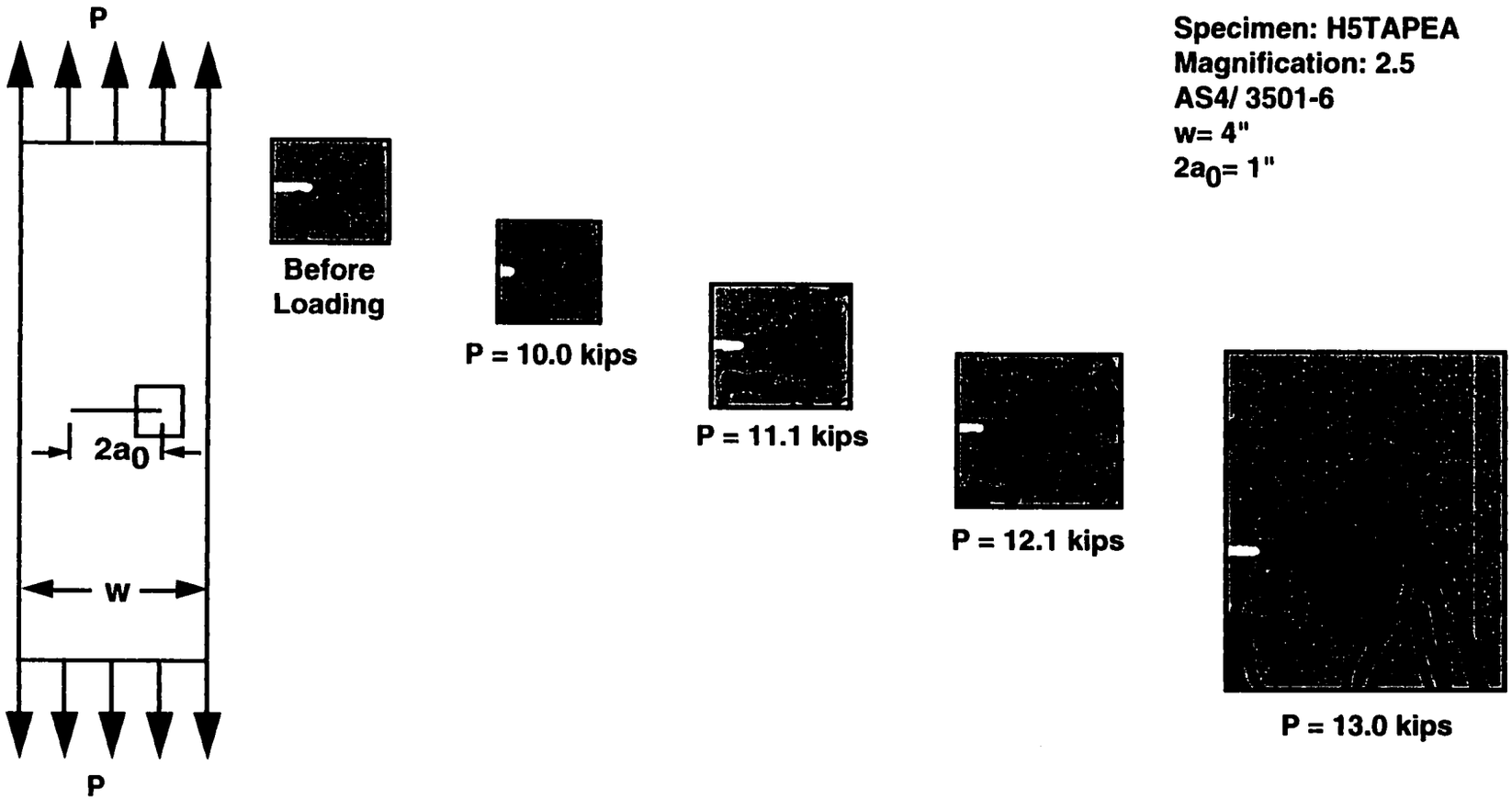

Figure 11a - X-Ray Radiographs of the Right Notch Tip Damage for the AS4/3501-6 Panels.

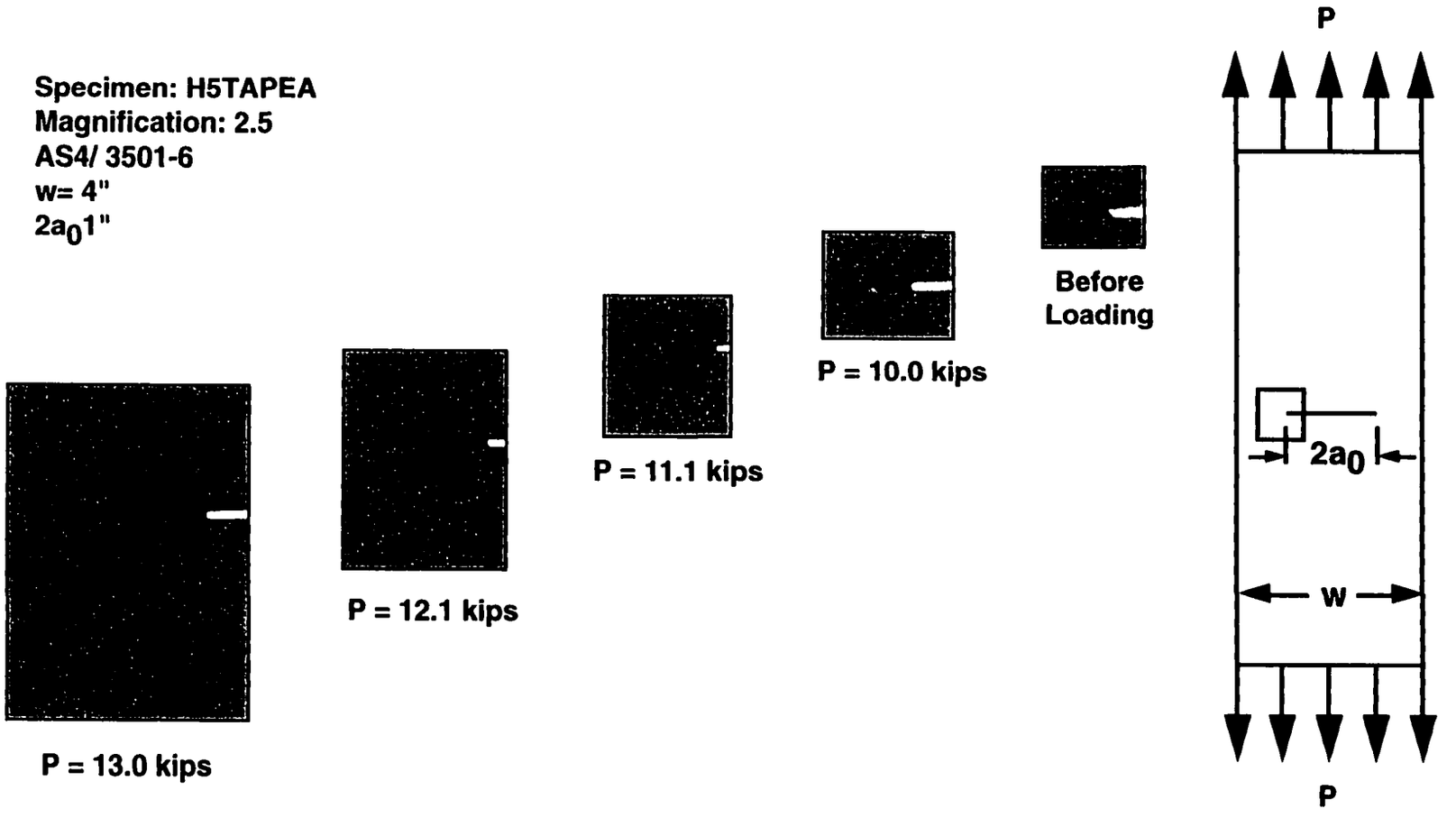

Figure 11b - X-Ray Radiographs of the Left Notch Tip Damage for the AS4/938 Panels.

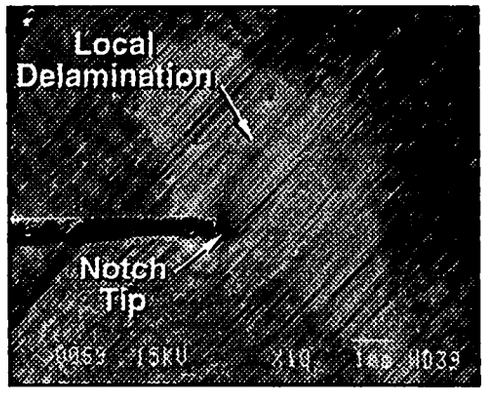

1st 45° ply, -45/45 Interface

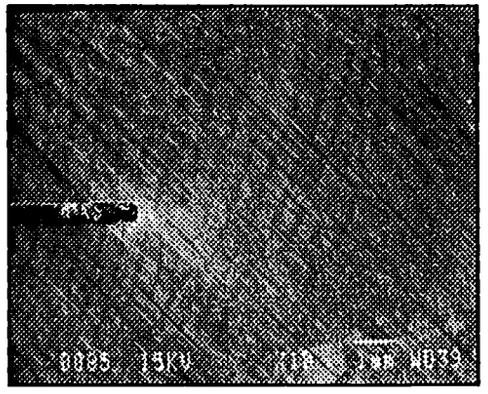

1st 45° ply, 45/0 Interface

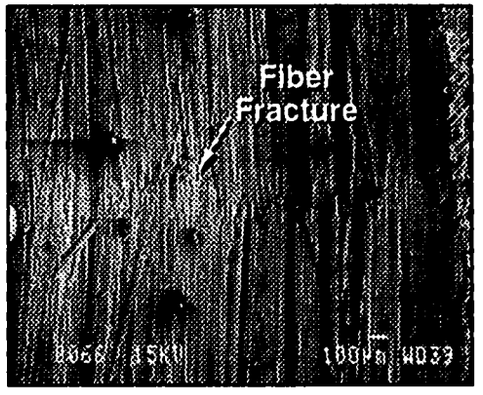

1st 0° ply, 45/0 Interface

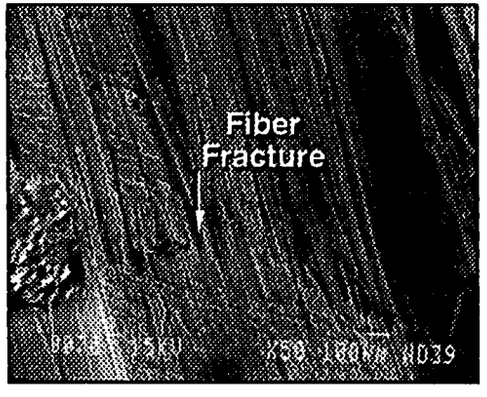

1st -30° ply, 90/-30 Interface

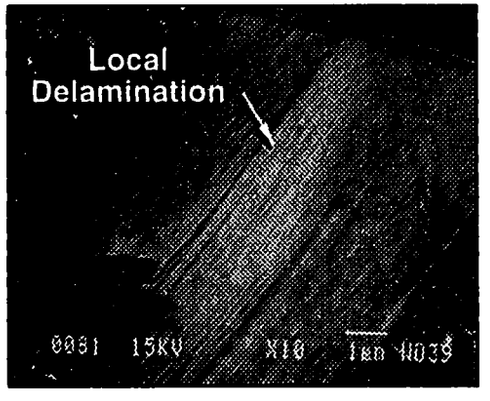

1st 30° ply, -30/30 Interface

Figure12a - Ply Level Fractography of $[-45/45/0/90/-30/30/\bar{0}]_S$ Specimen F5 AK5B Right Notch Tip at 84% of S_{ult}.

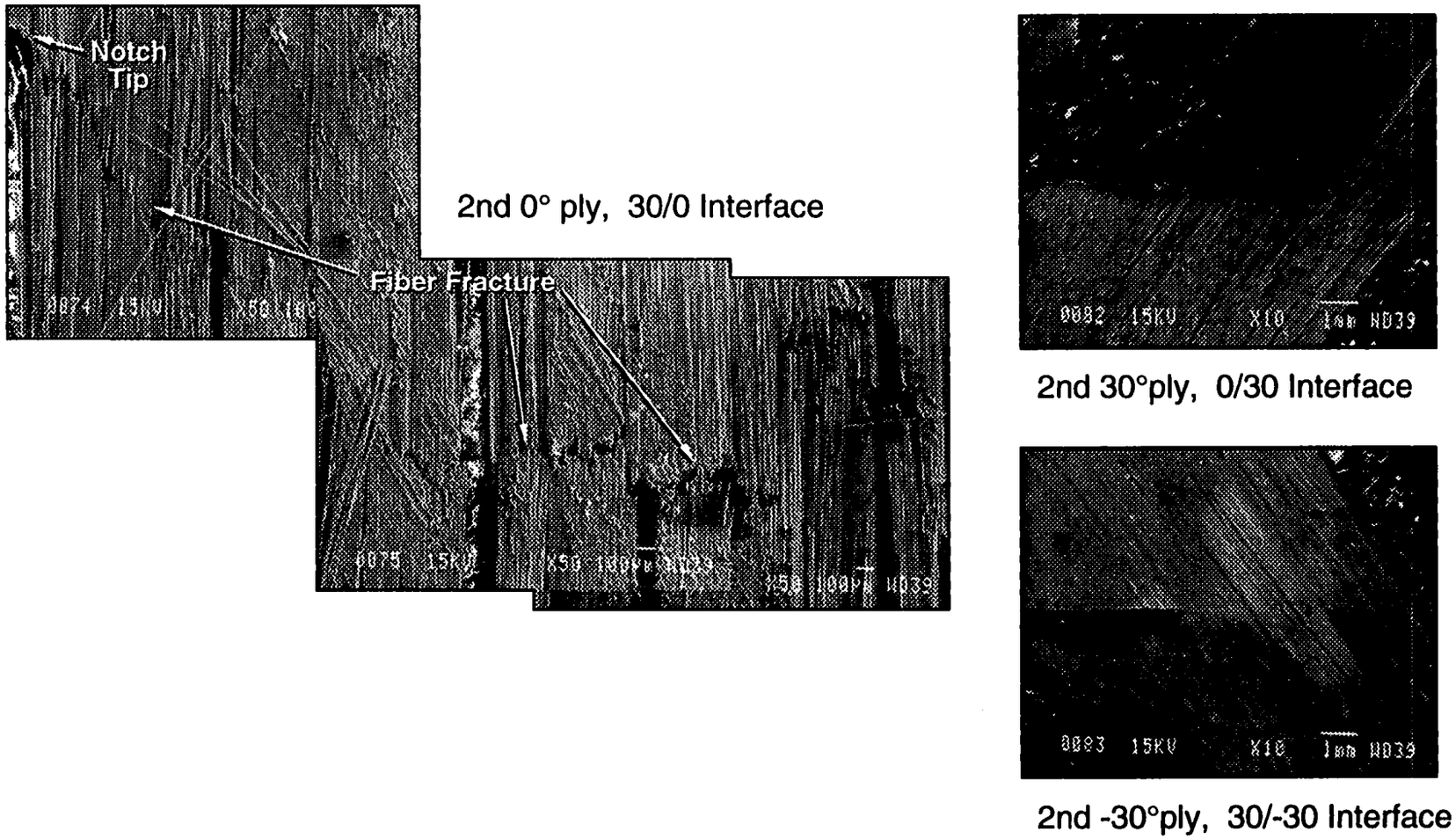

Figure12b - Ply Level Fractography of $[-45/45/0/90/-30/30/\bar{0}]_s$ Specimen F5 AK5B Right Notch Tip at 84% of S_{ult}.

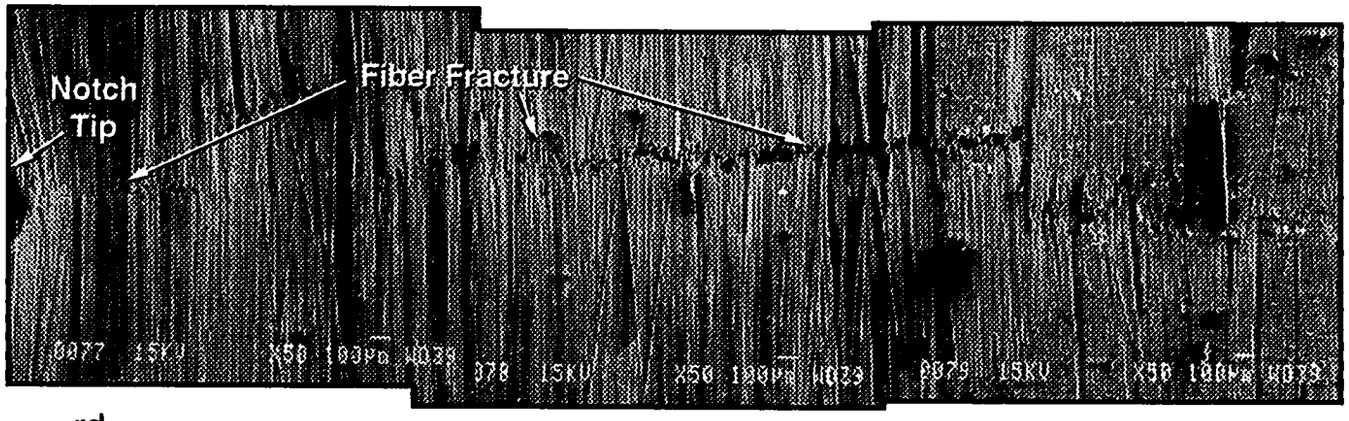

3rd 0° ply, 90/0 Interface

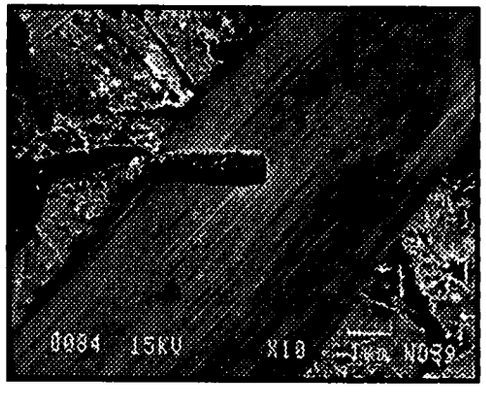

2nd 45° ply, 0/45 Interface

Figure12c - Ply Level Fractography of $[-45/45/0/90/-30/30/\bar{0}]_s$ Specimen F5 AK5B Right Notch Tip at 84% of S_{ult}.

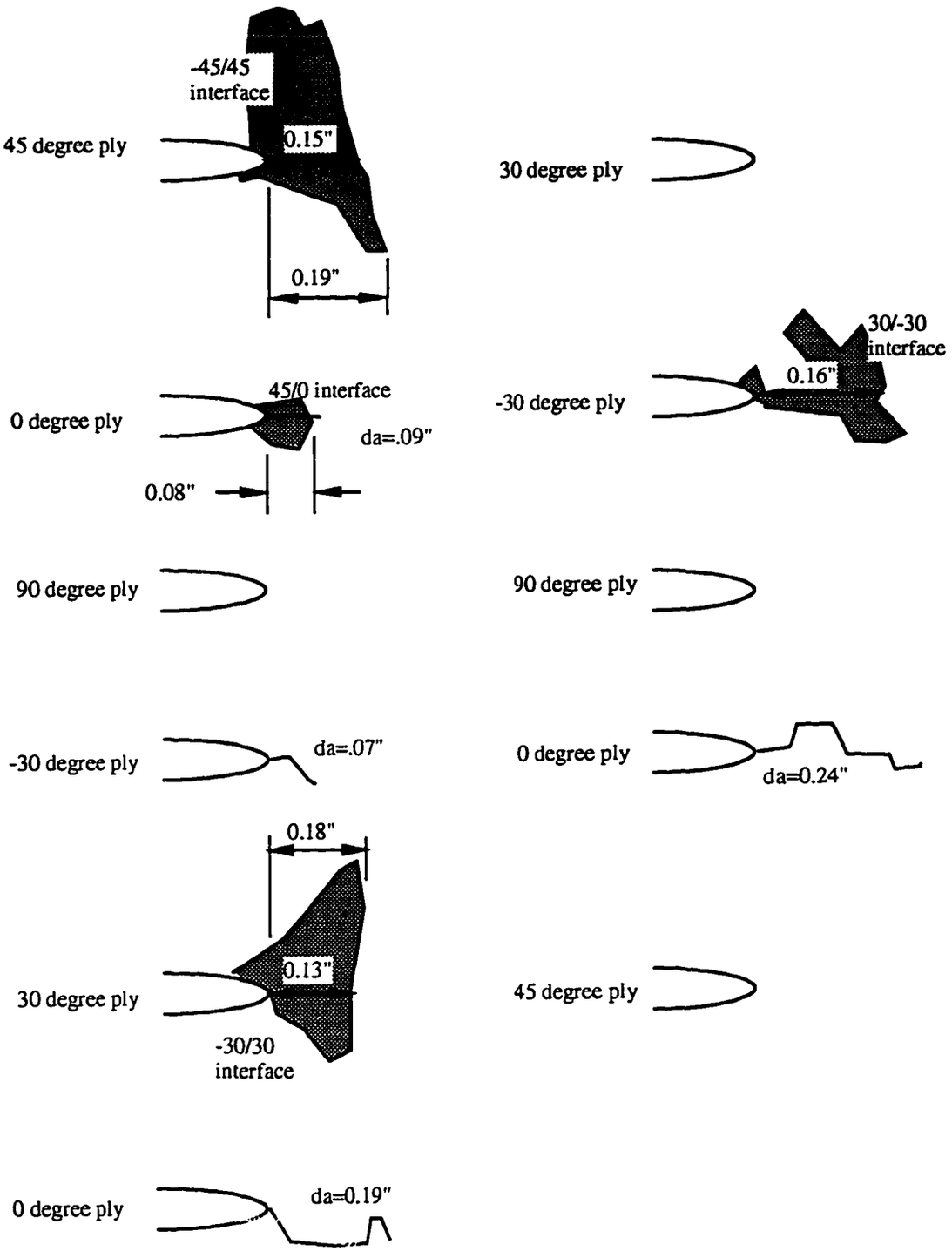

Figure 13 - Fiber Fracture and Delamination Illustration for Specimen F5AK5B, $[-45/45/0/90/-30/30/0]_S$, Right Notch Tip.

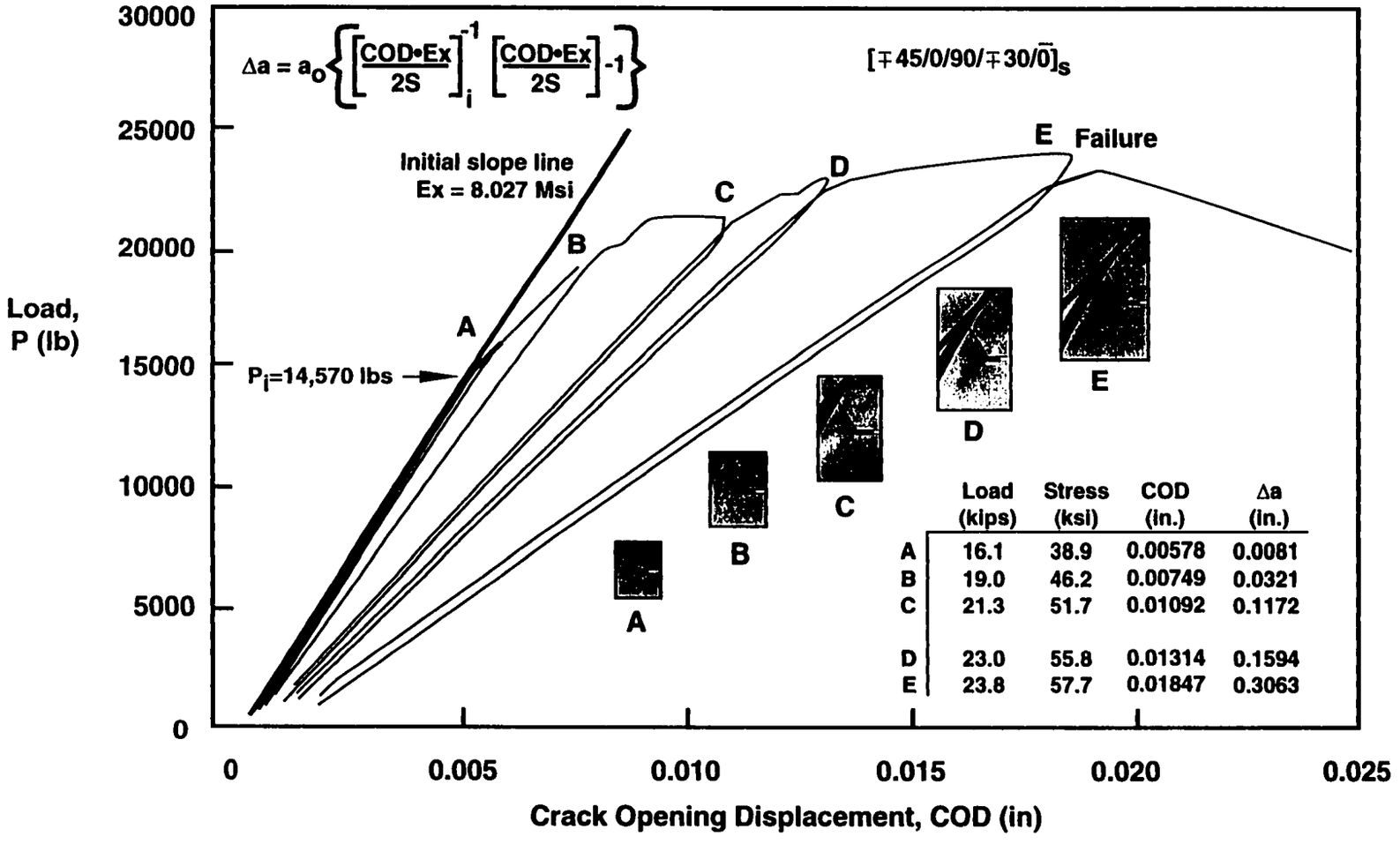

Figure 14 - Crack Opening Displacement for AS4/8553-40, Panel A4AK1.

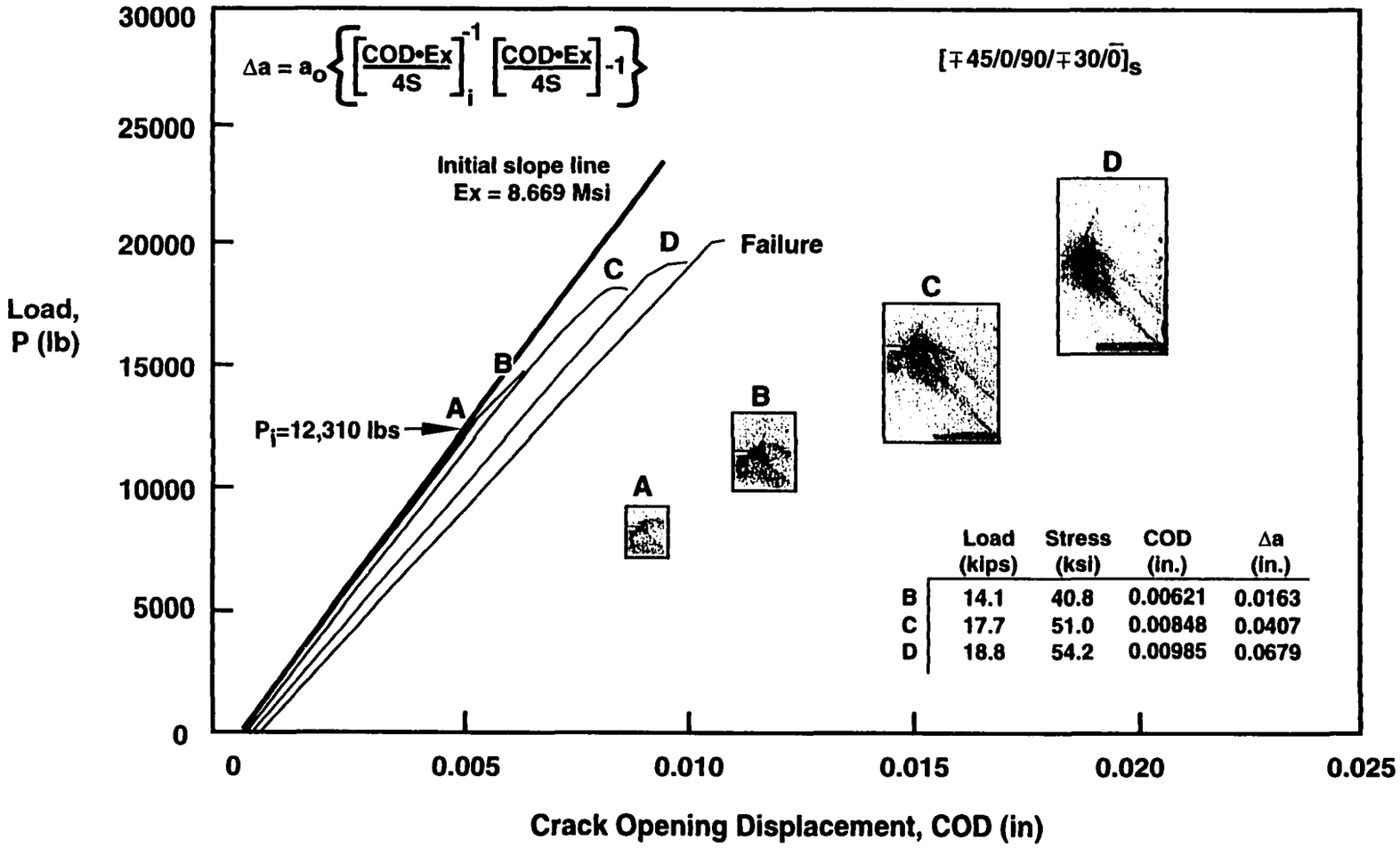

Figure 15 - Crack Opening Displacement for AS4/938, Panel C4AK5A.

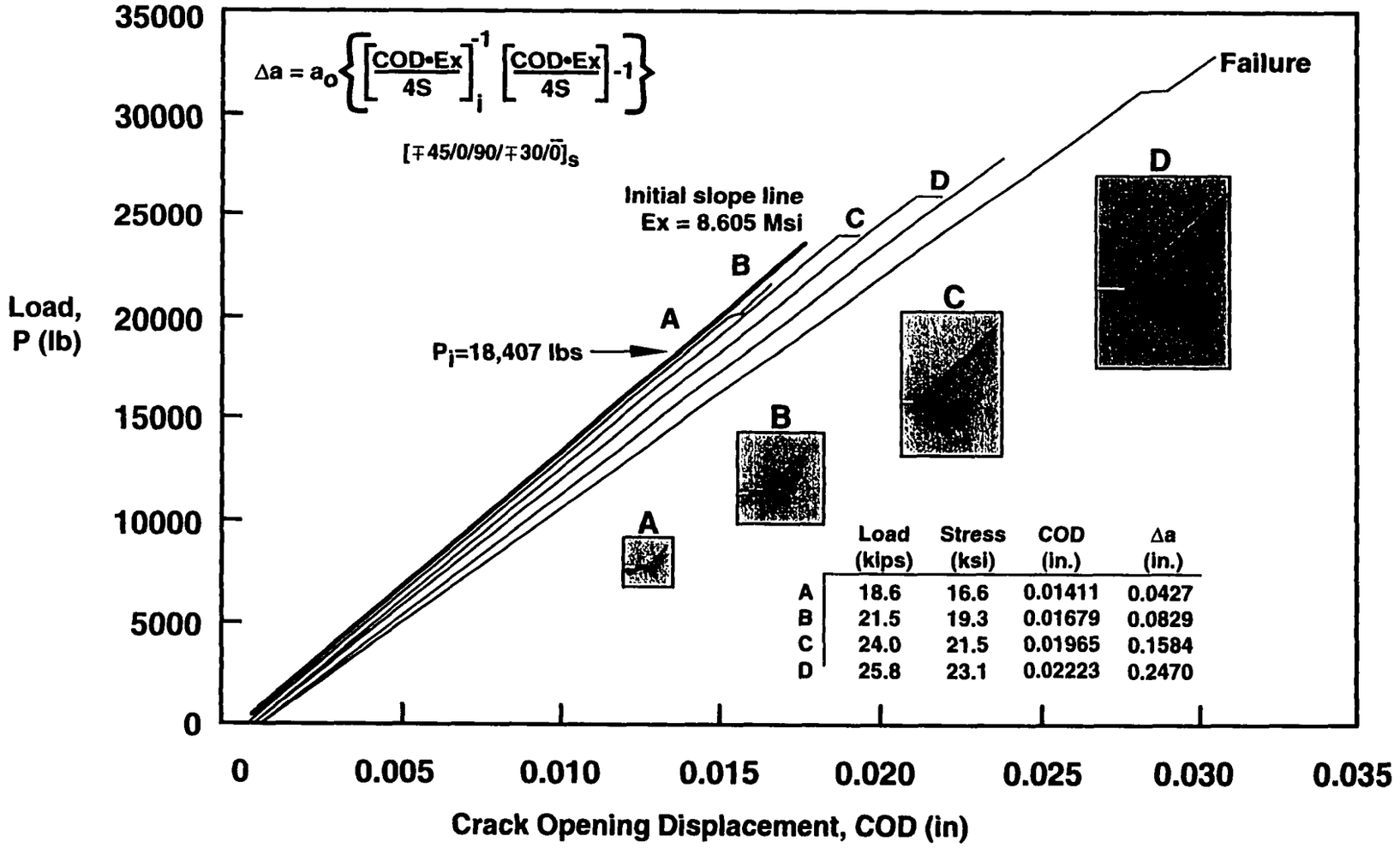

Figure 16 - Crack Opening Displacement for AS4/3501-6, Panel G2 TAPEA.

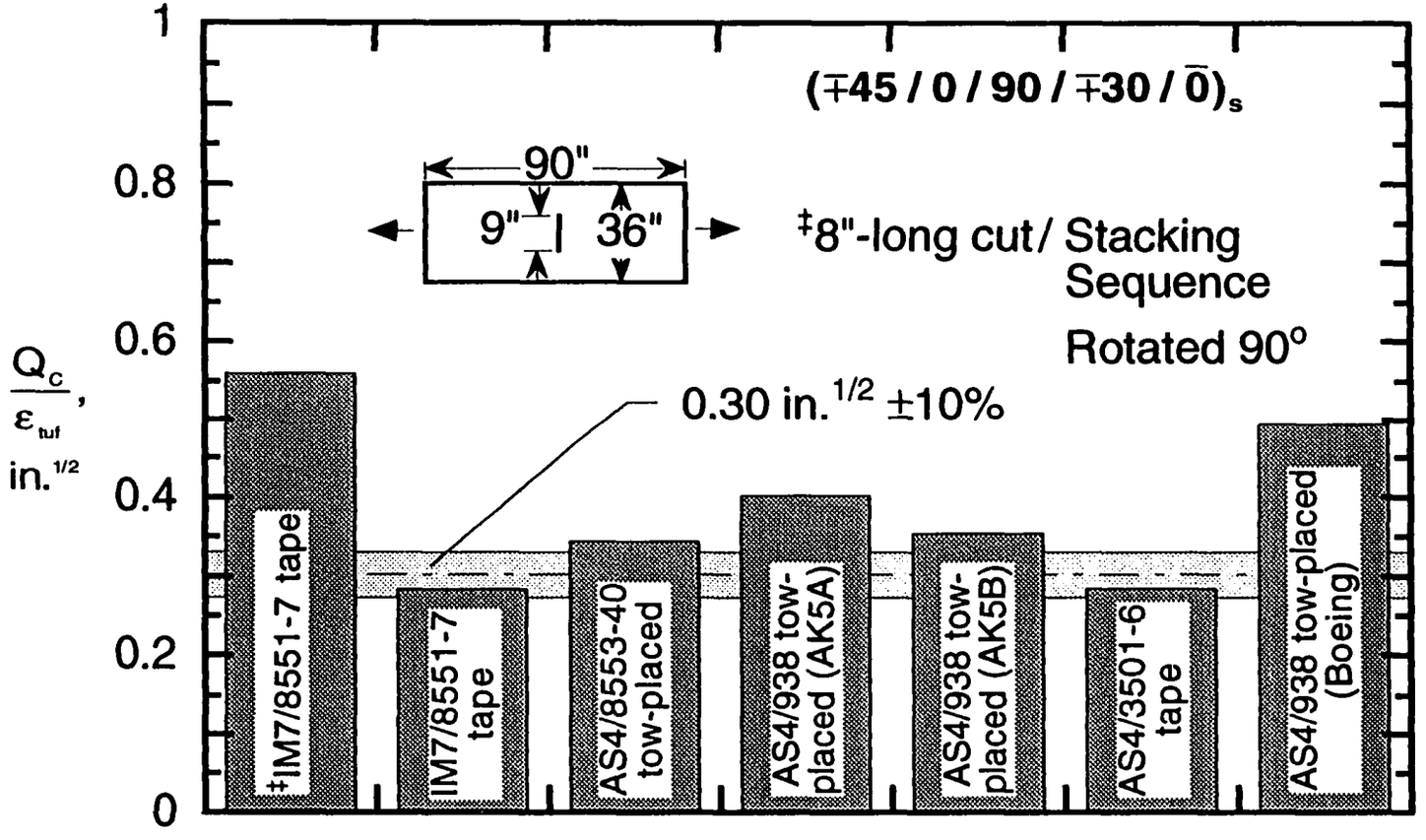

Figure 17 - Fracture Toughness of Large Notched Composite Laminates.

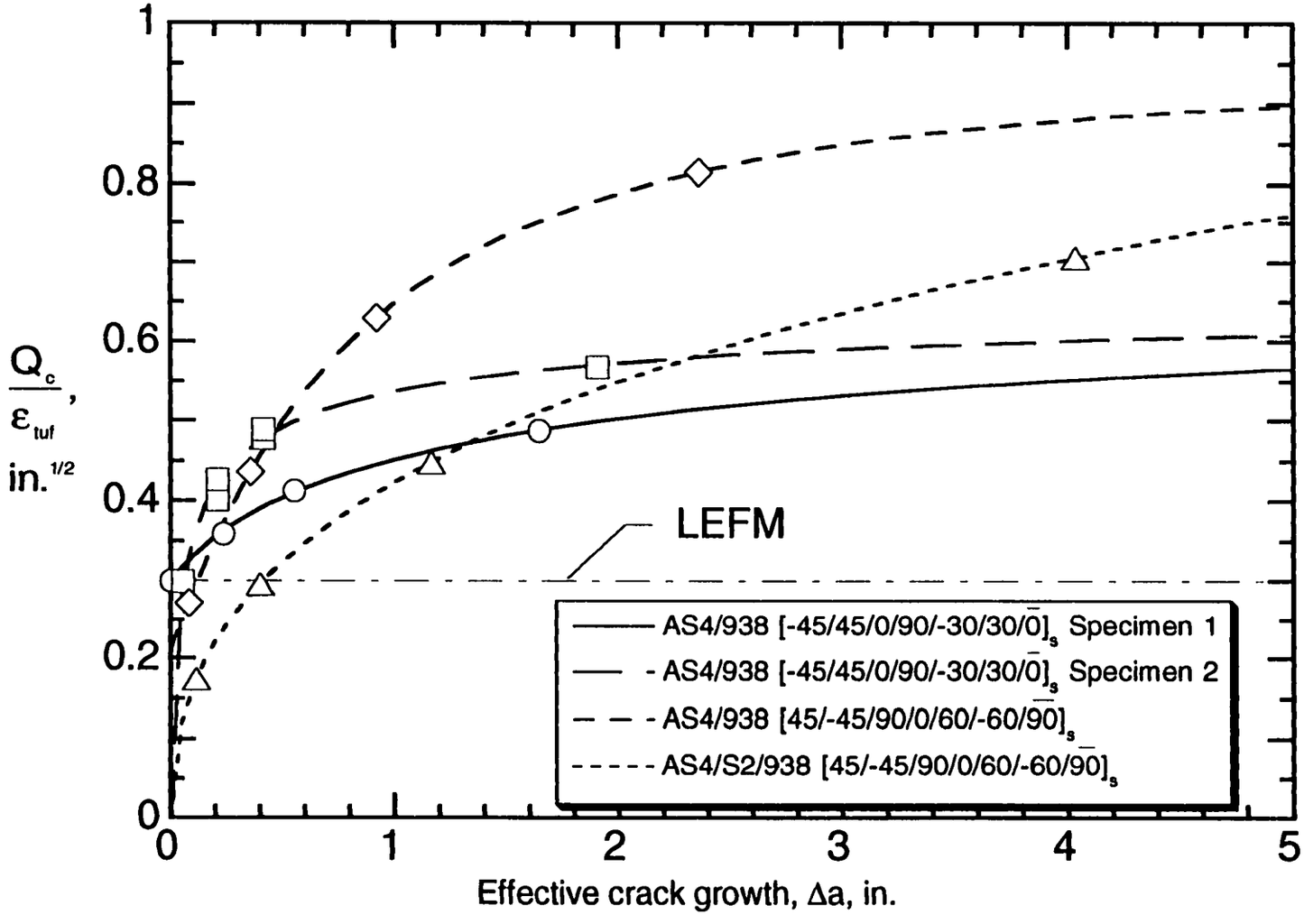

Figure 18 - R-Curves for Large Notched Composite Laminates.

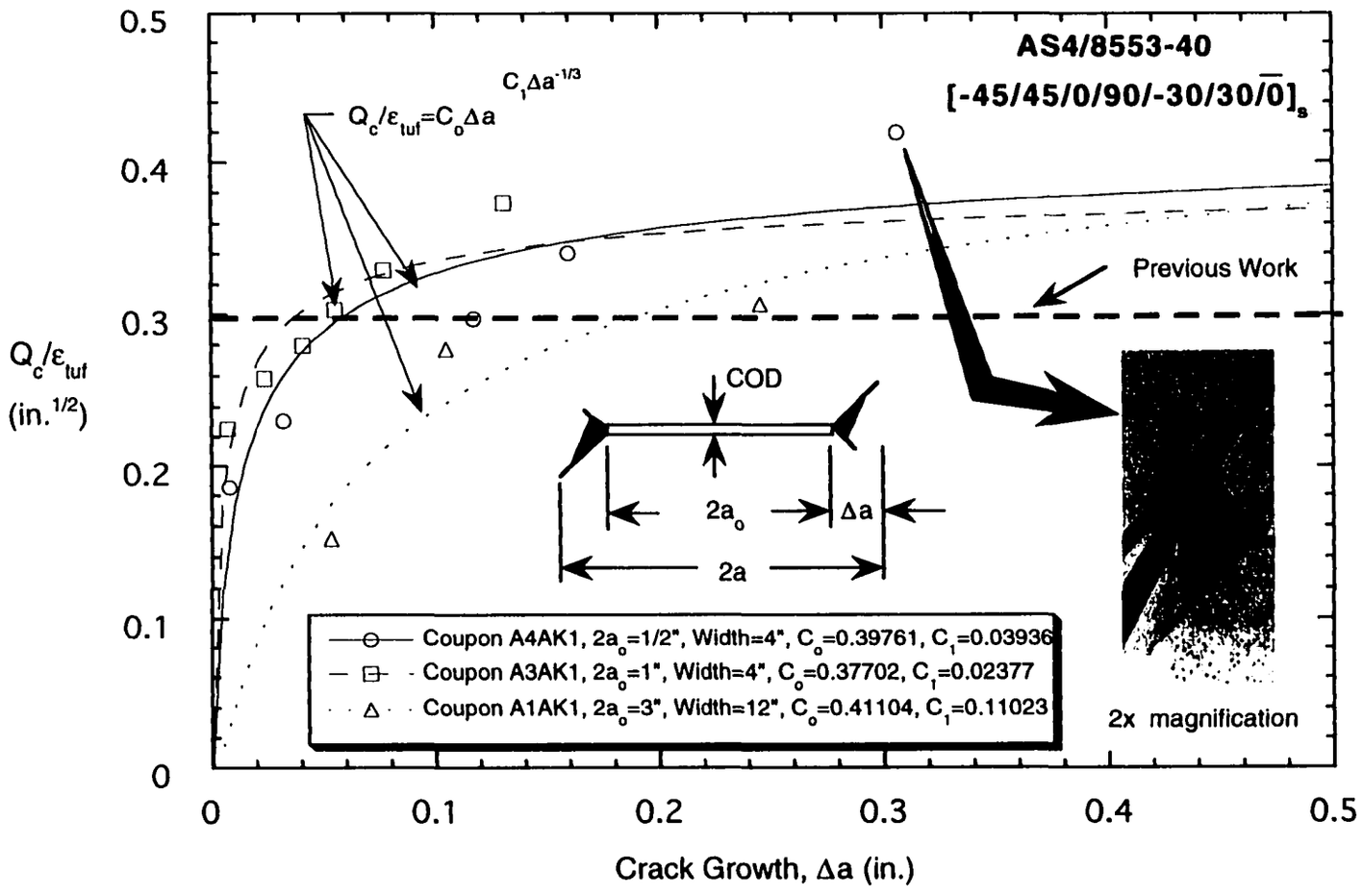

Figure 19 - Crack Growth Resistance in AS4/8553-40 Panels.

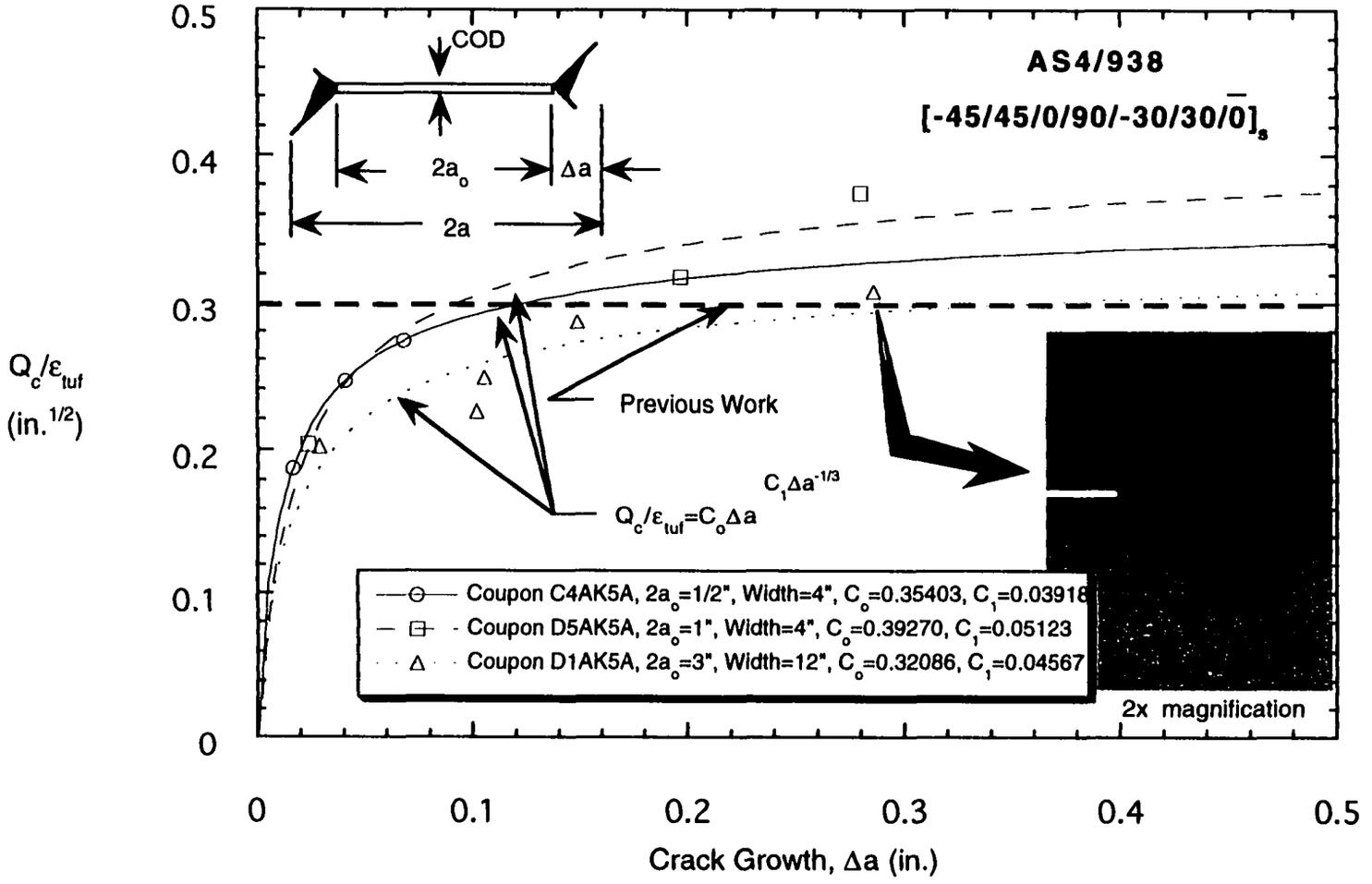

Figure 20 - Crack Growth Resistance in AS4/938 Panels.

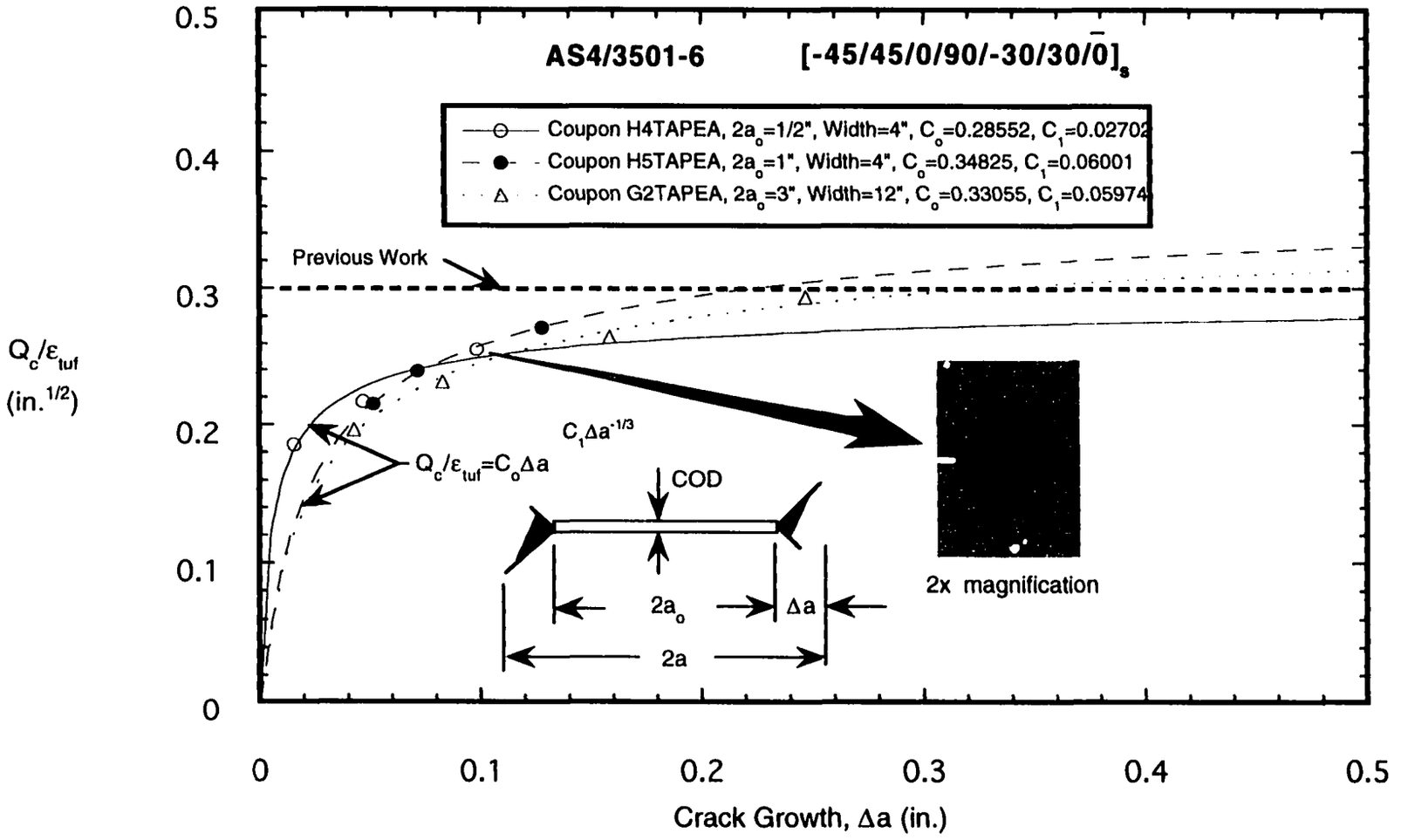

Figure 21 - Crack Growth Resistance in AS4/3501-6 Panels.

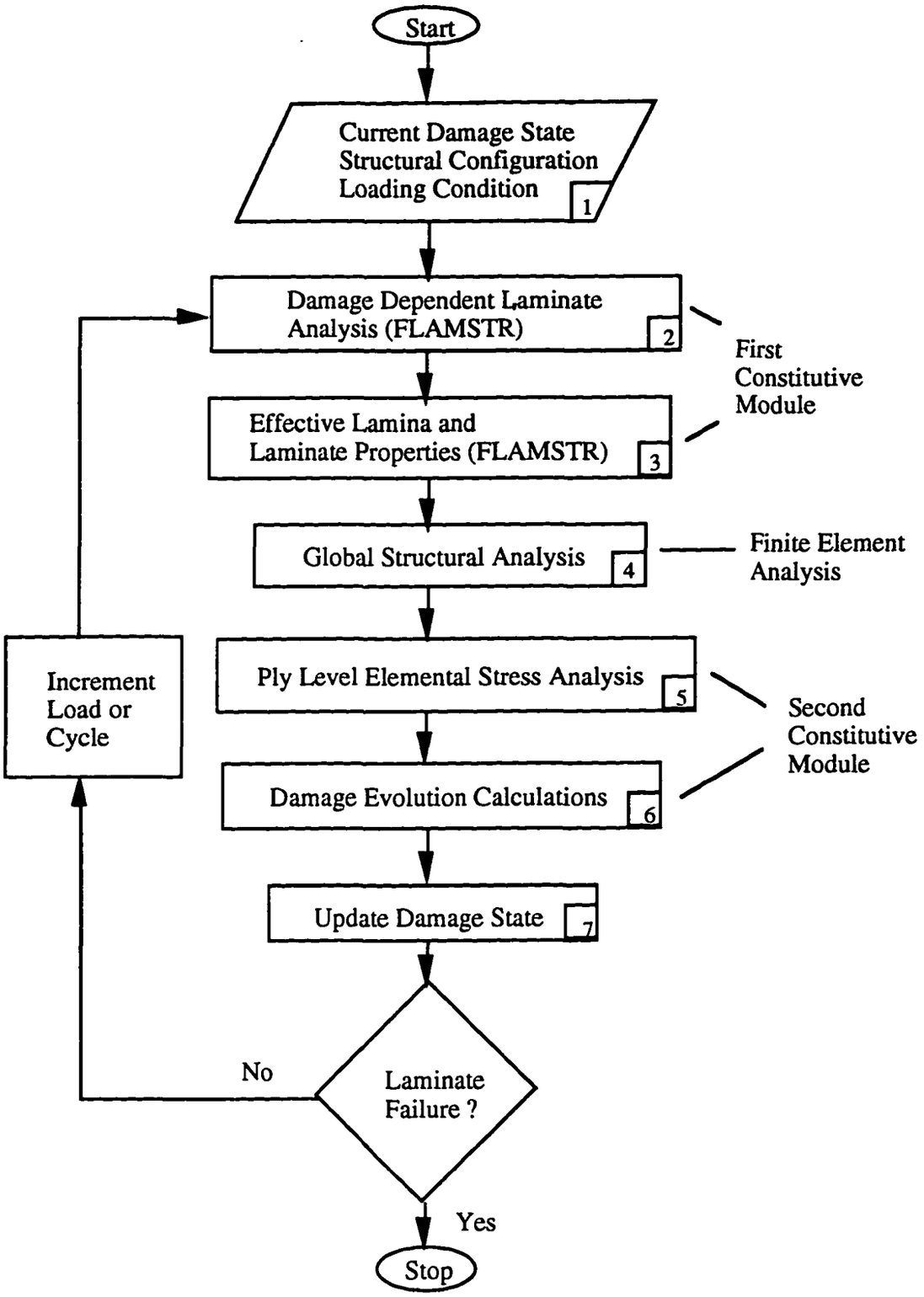

Figure 22 - Progressive Failure Analysis Scheme.

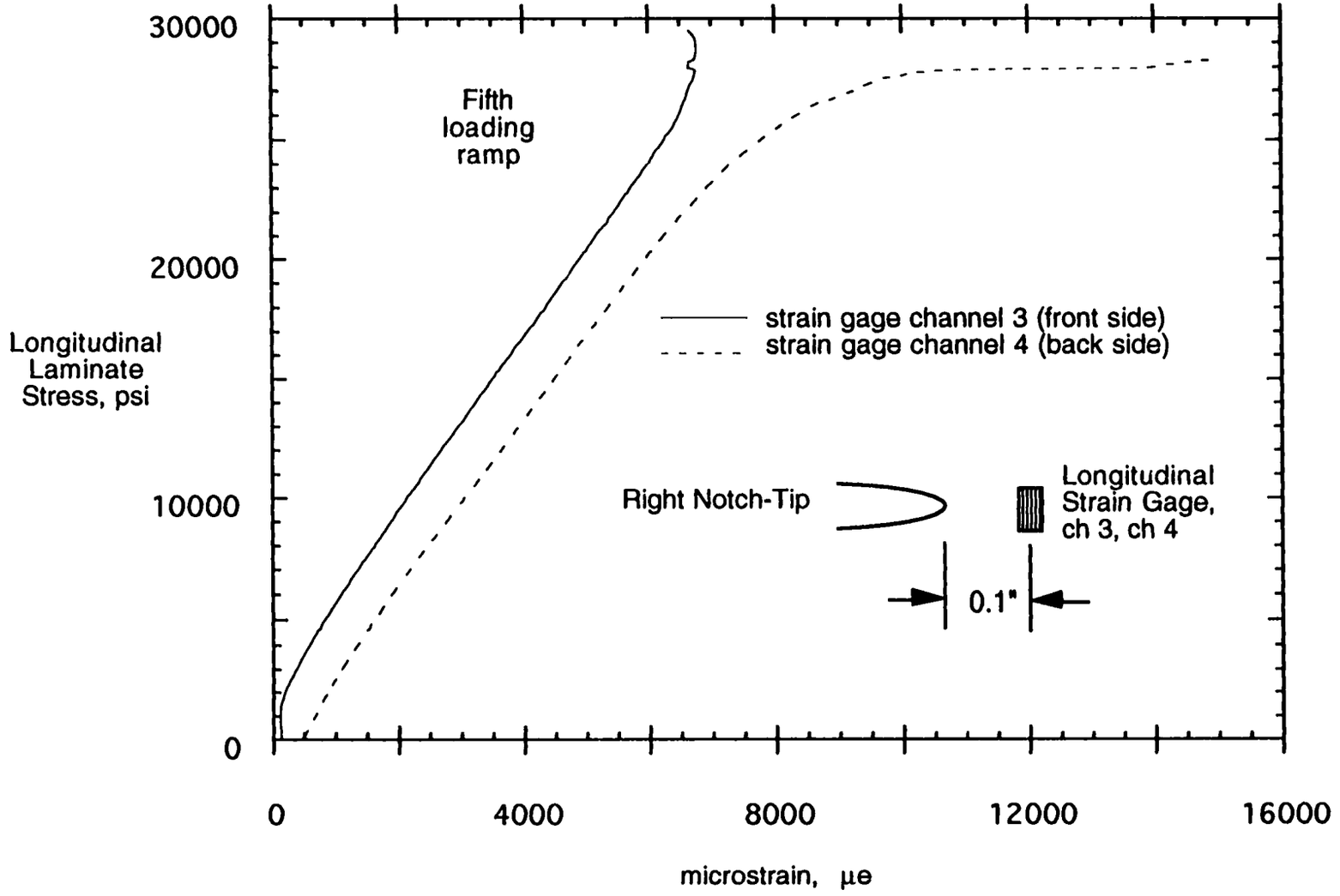

Figure 23 - Notch-Tip Longitudinal Stress/Strain Plots for Panel G2TAPEA, w=12", 3" Notch.

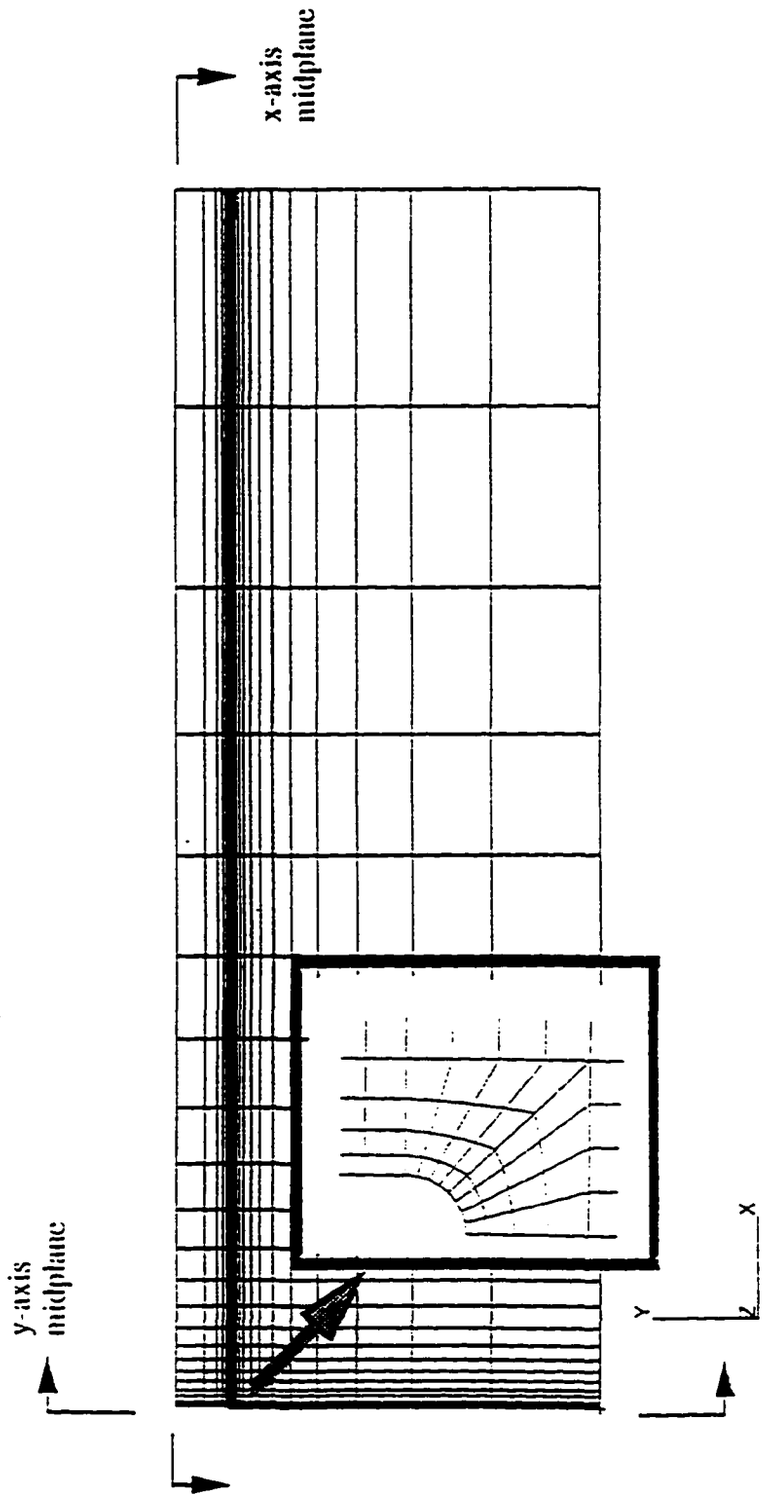

Figure 24 - Quarter Panel Mesh of the Center-Crack Tension Panel. 0.02" Notch, W=4", $2a_o$=1/2", L=12", 570 Nodes, 520 Elements.

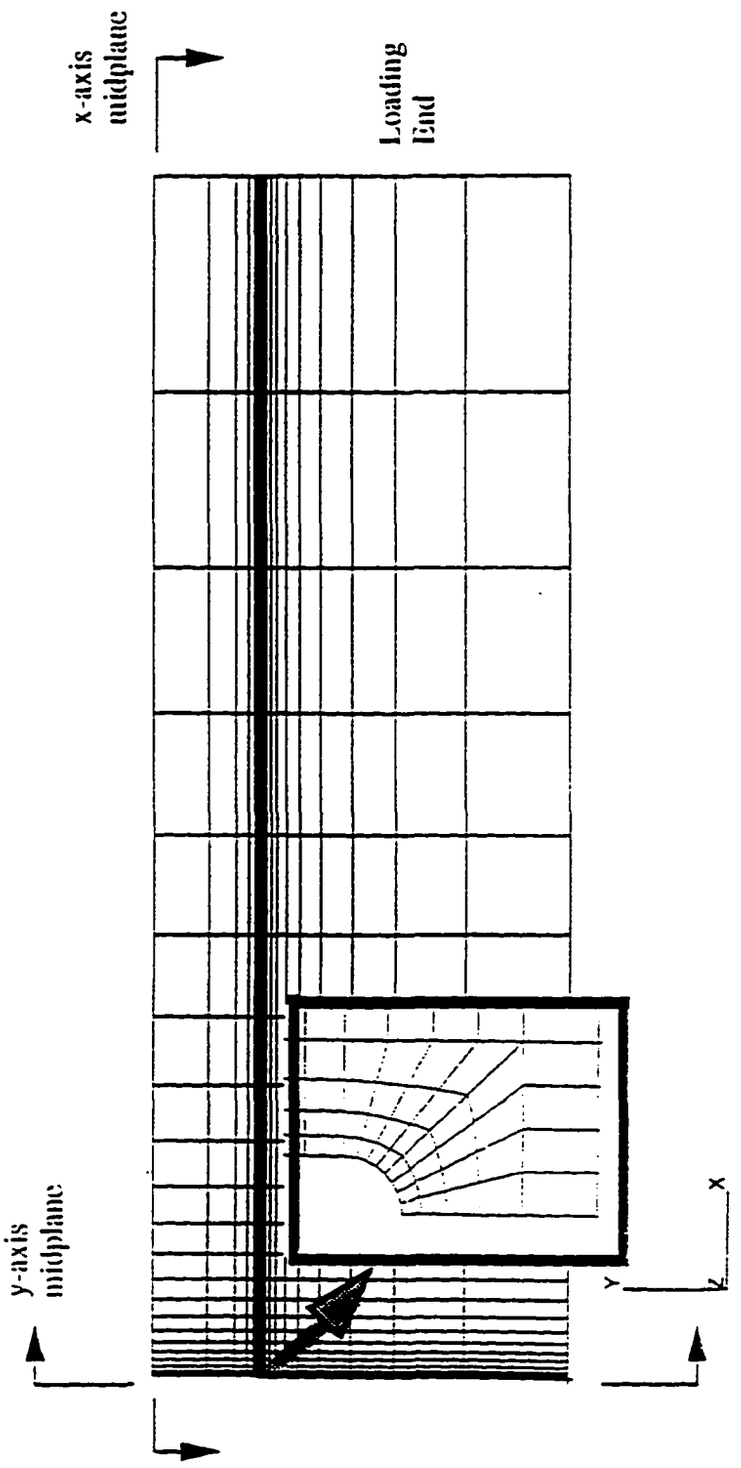

Figure 25 - Quarter Panel Mesh of the Center-Crack Tension Panel. 0.02" Notch, W=4", $2a_0$=1", L=12", 545 Nodes, 496 Elements.

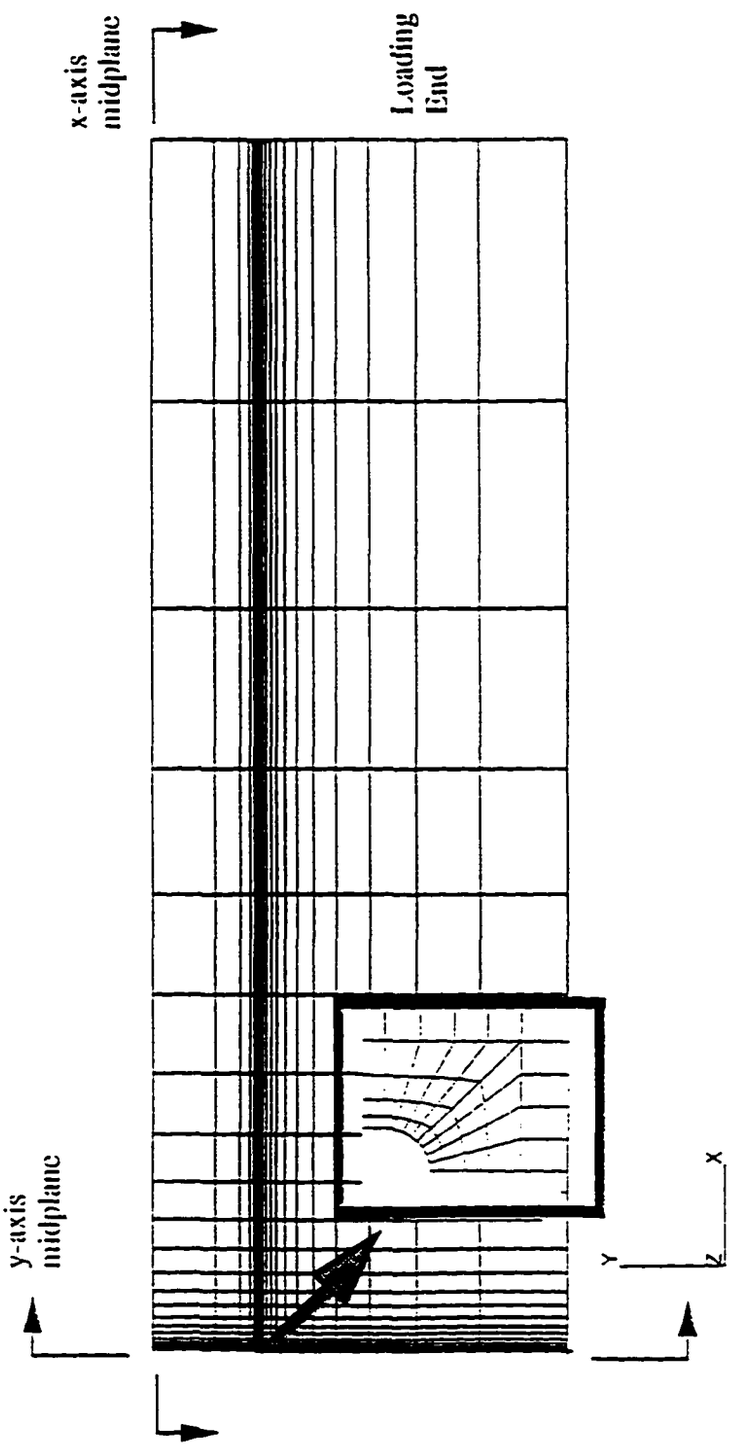

Figure 26 - Quarter Panel Mesh of the Center-Crack Tension Panel. 0.02" Notch, W=12", $2a_o$=3", L=36", 670 Nodes, 616 Elements.

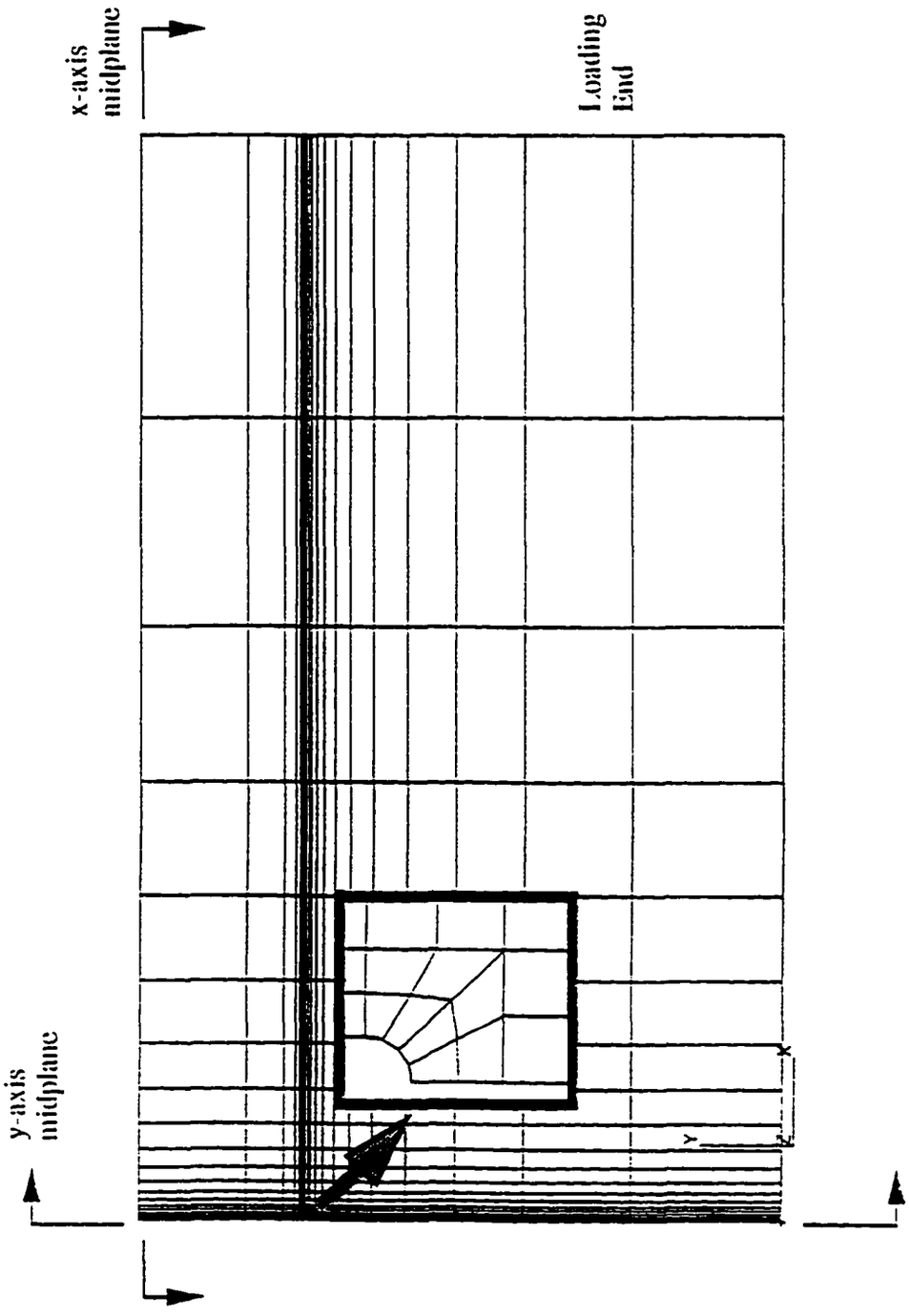

Figure 27 - Quarter Panel Mesh of the Center-Crack Tension Panel. 0.02" Notch, W=36", $2a_0$=9", L=64", 558 Nodes, 510 Elements.

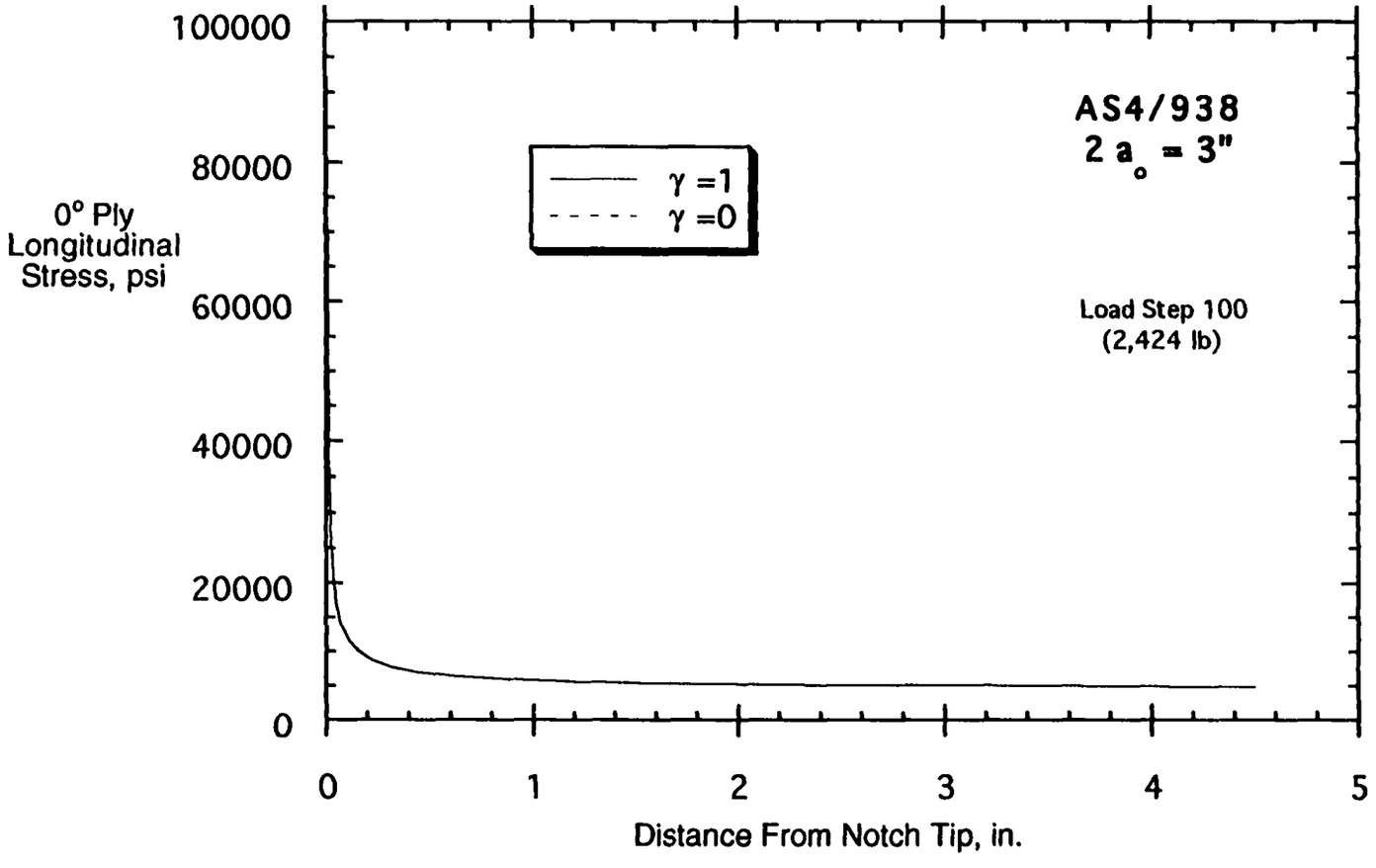

Figure 28 - 0 Degree Ply Longitudinal Stress vs. Distance from the Notch-Tip.

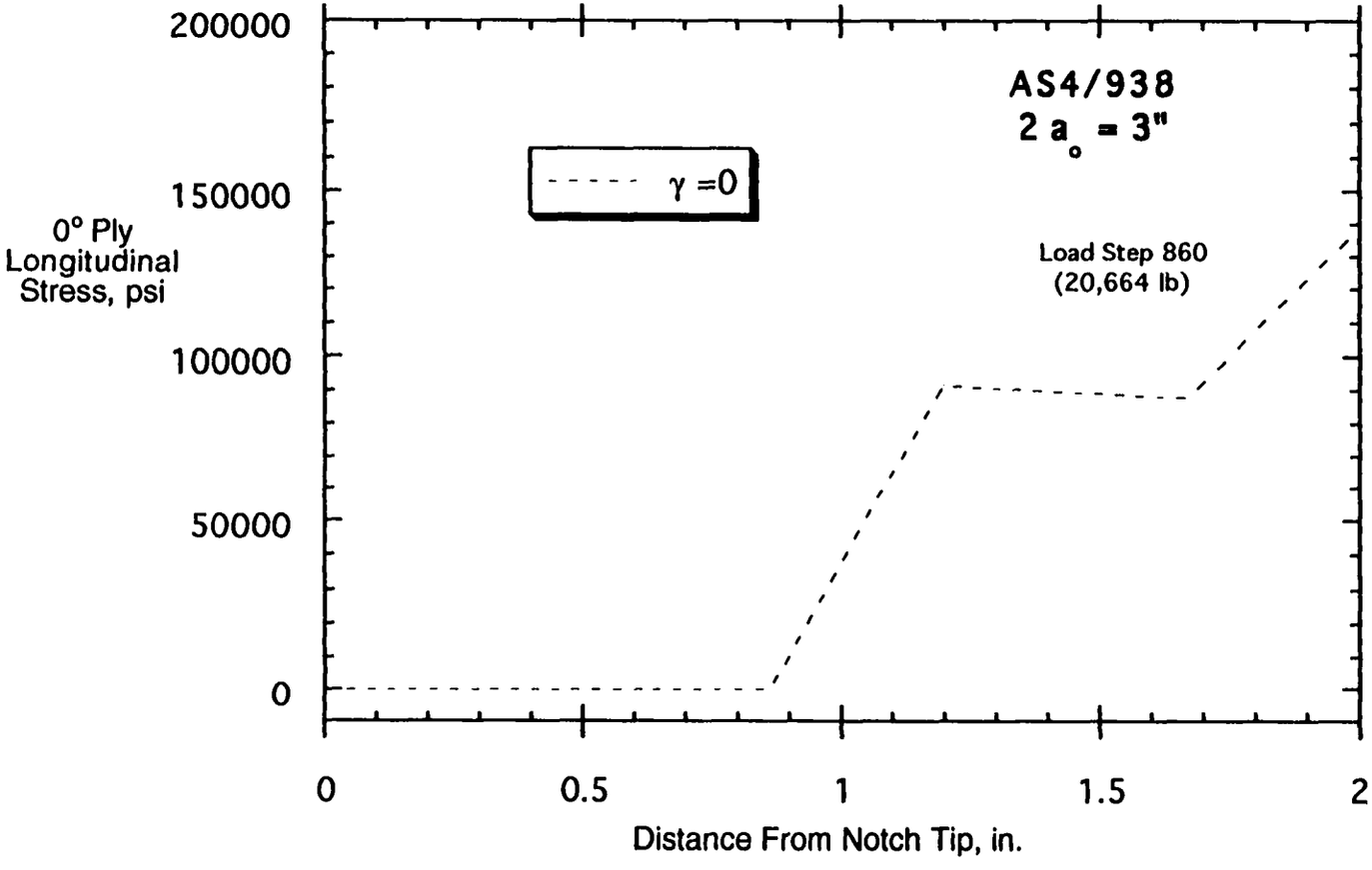

Figure 29 - 0 Degree Ply Longitudinal Stress vs. Distance from the Notch-Tip.

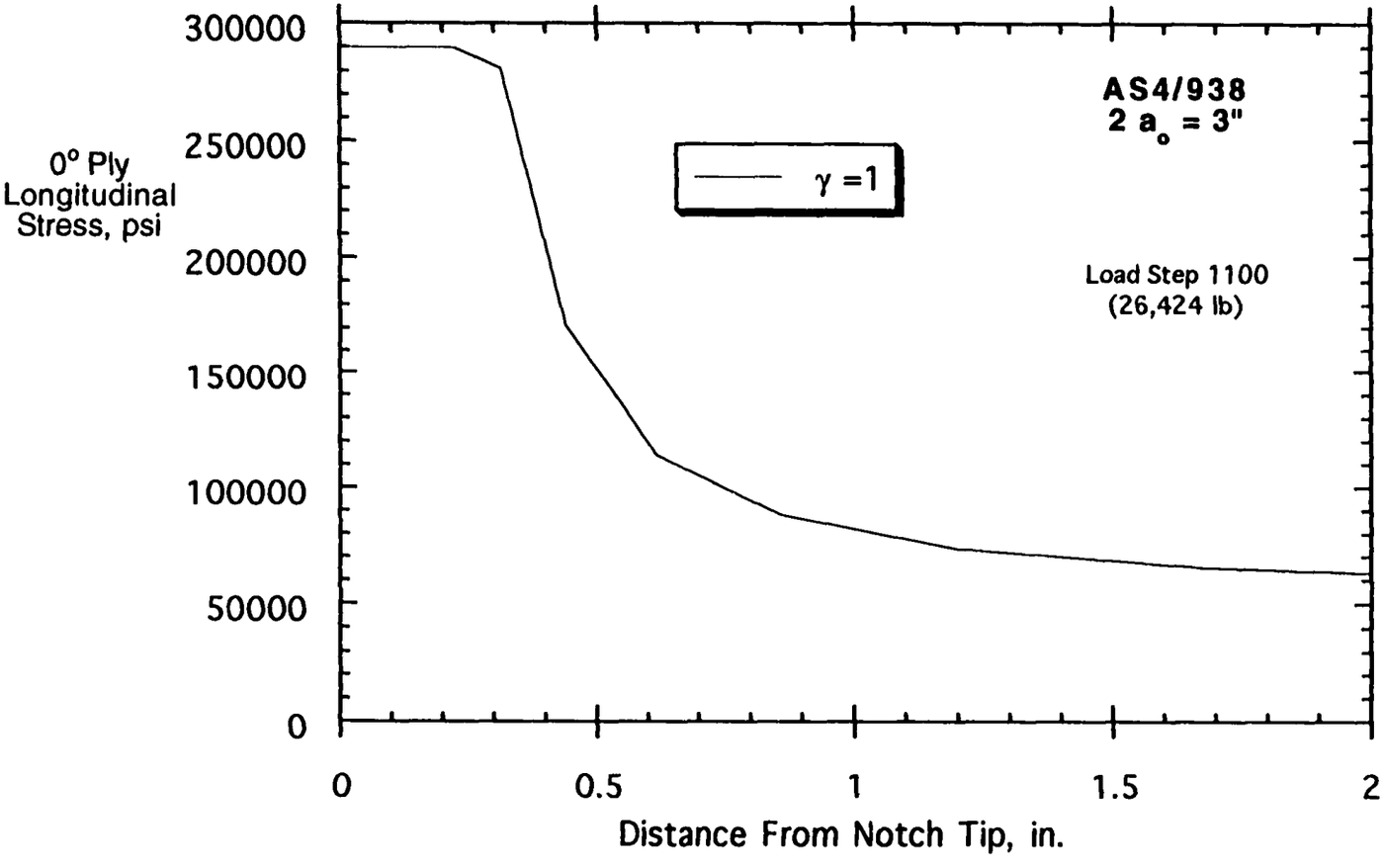

Figure 30 - 0 Degree Ply Longitudinal Stress vs. Distance from the Notch-Tip.

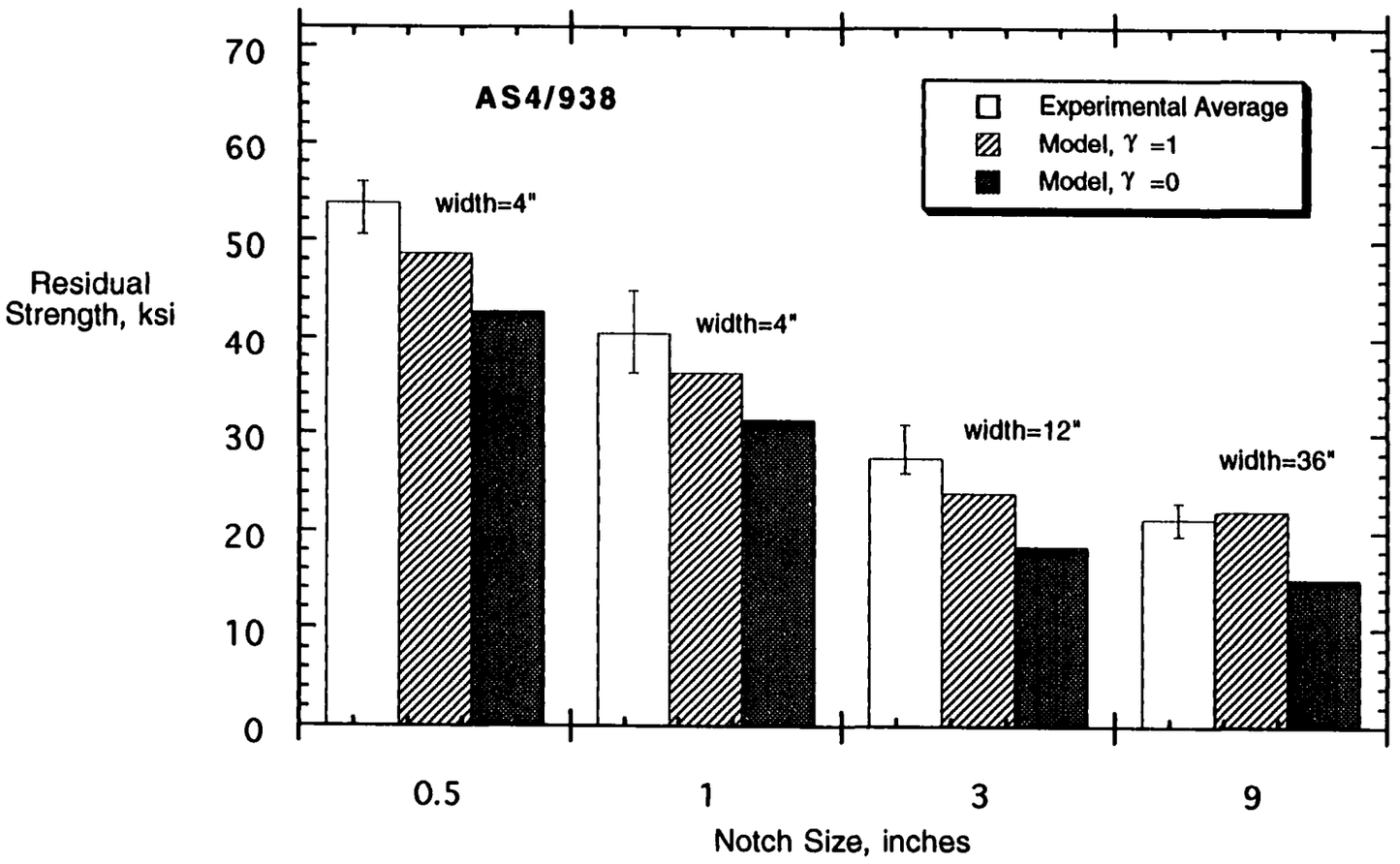

Figure 31 - Residual Strengths of AS4/938 Center-Crack Tension Panels.

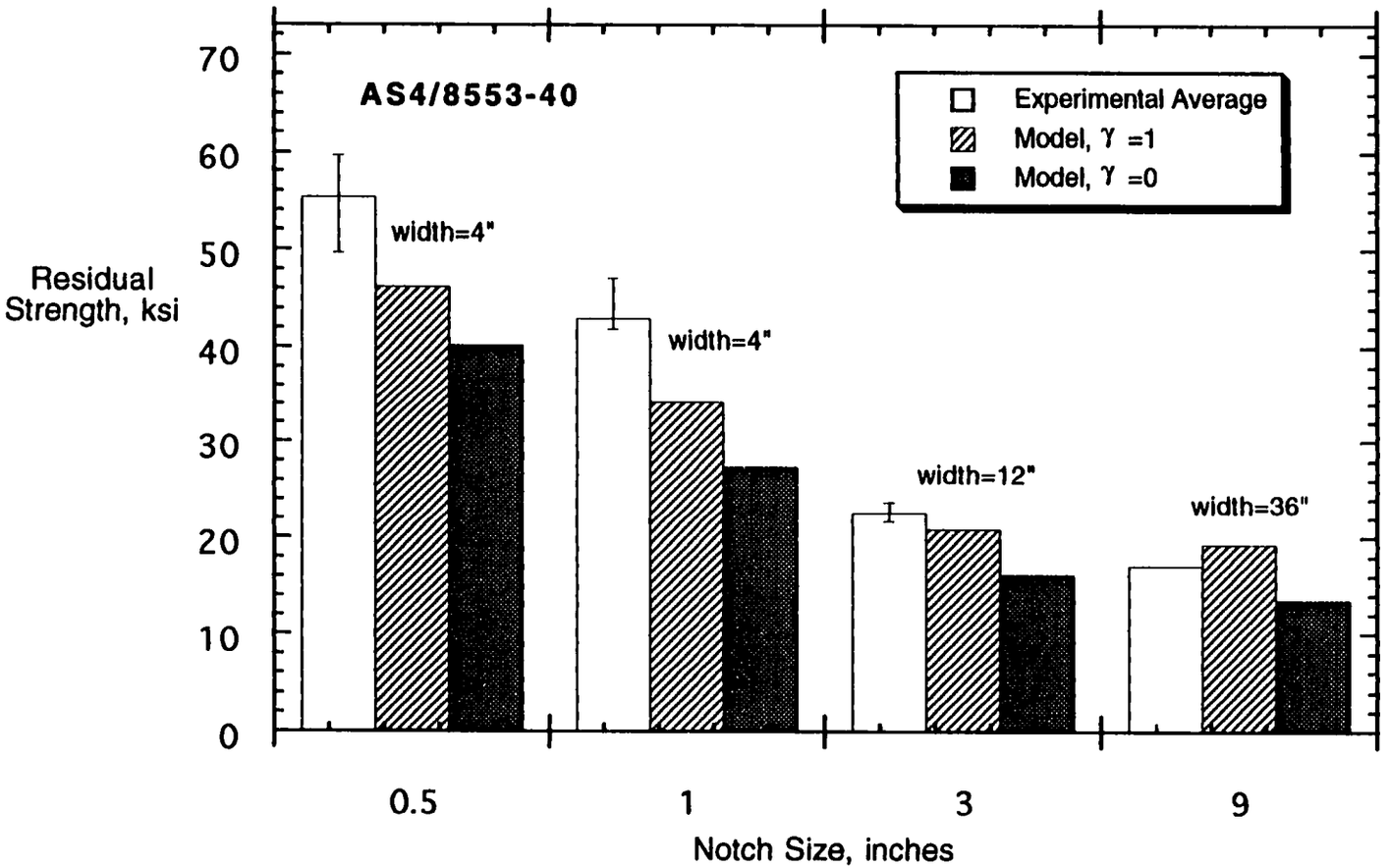

Figure 32 - Residual Strengths of AS4/8553-40 Center-Crack Tension Panels.

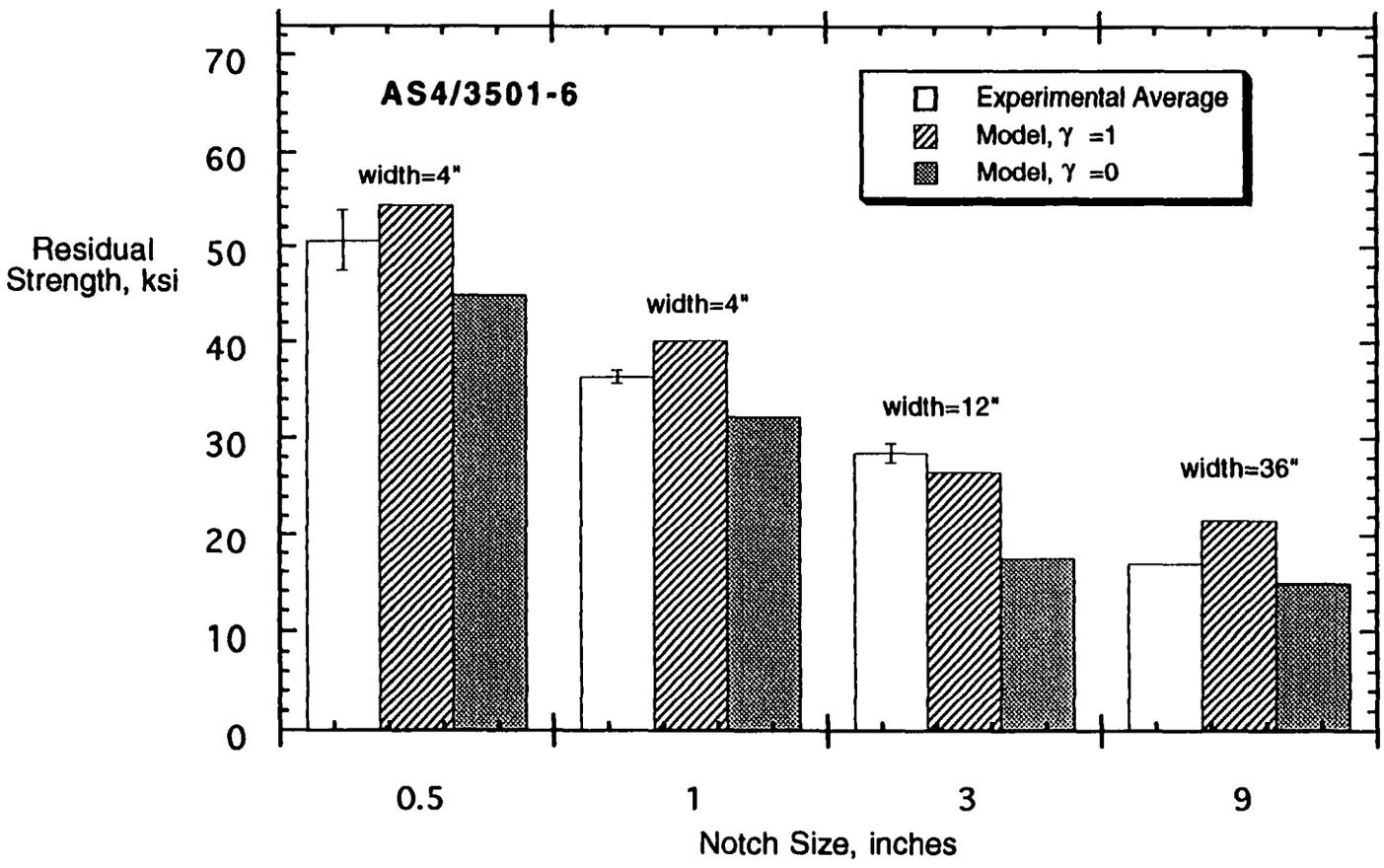

Figure 33 - Residual Strength Predictions of AS4/3501-6 Center-Crack Tension Panels.

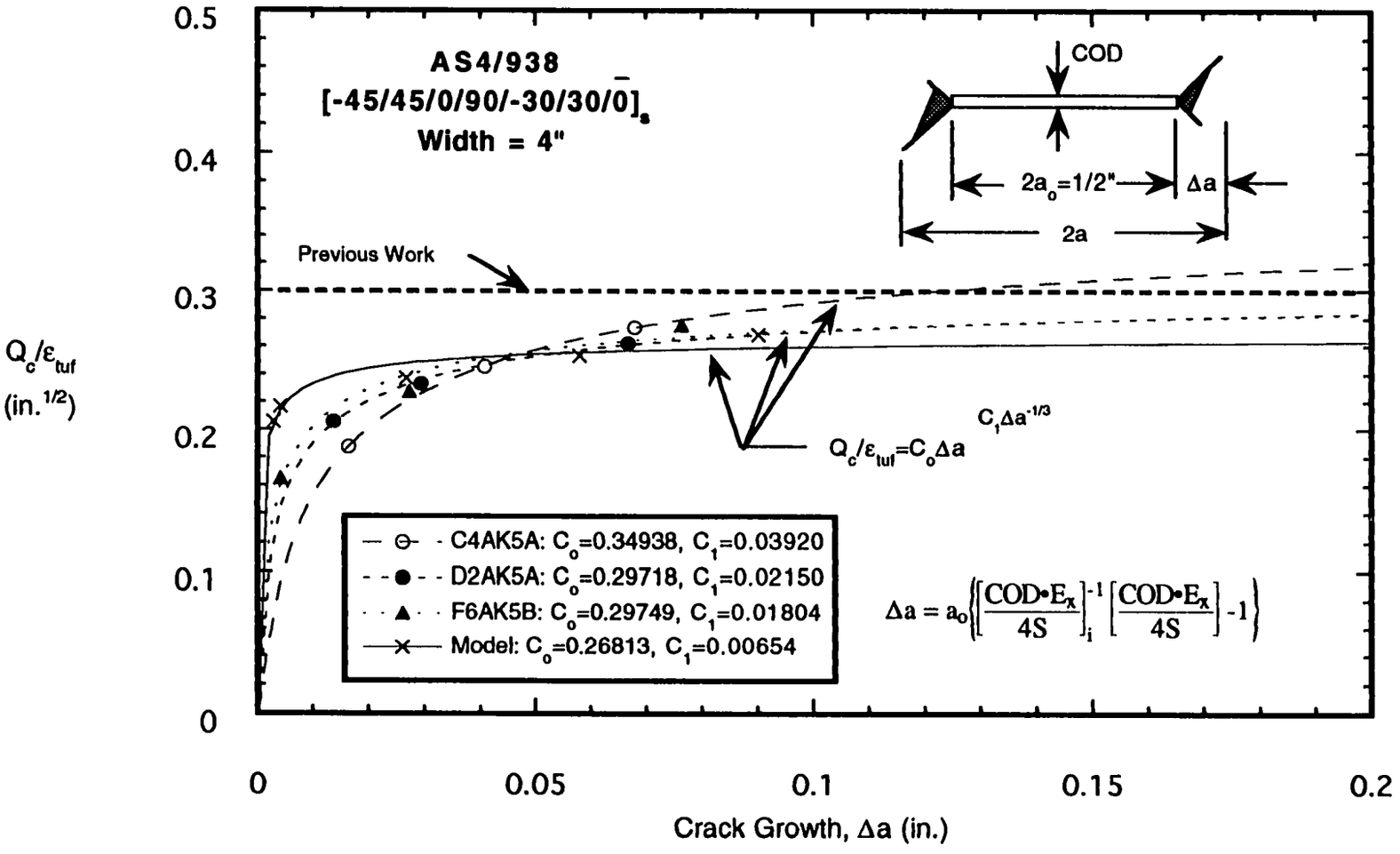

Figure 34 - Experimental and Model Generated R-Curves for AS4/938 Center-Crack Tension Panels, $2a_o$=1/2".

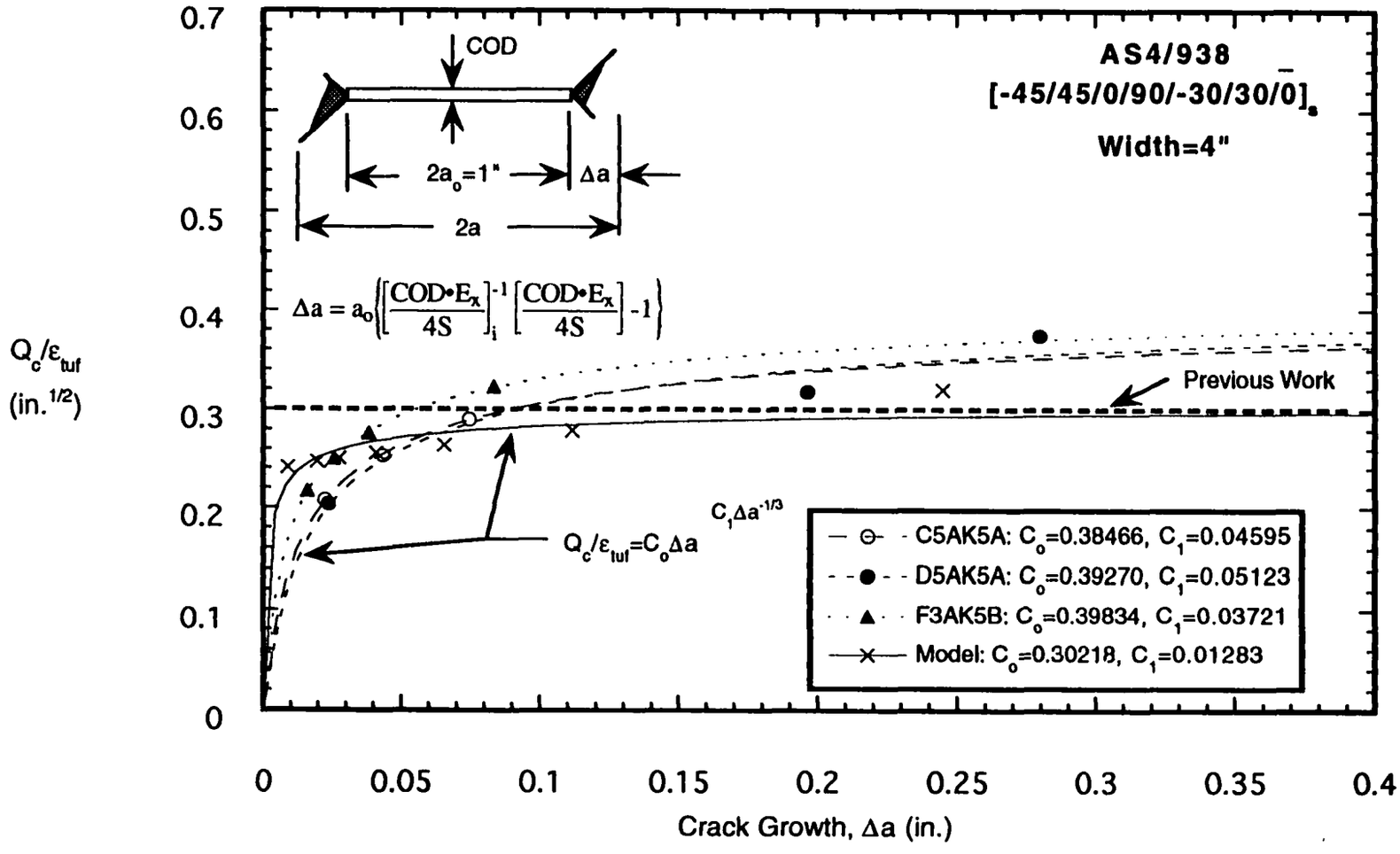

Figure 35 - Experimental and Model Generated R-Curves for AS4/938 Center-Crack Tension Panels, $2a_o$=1".

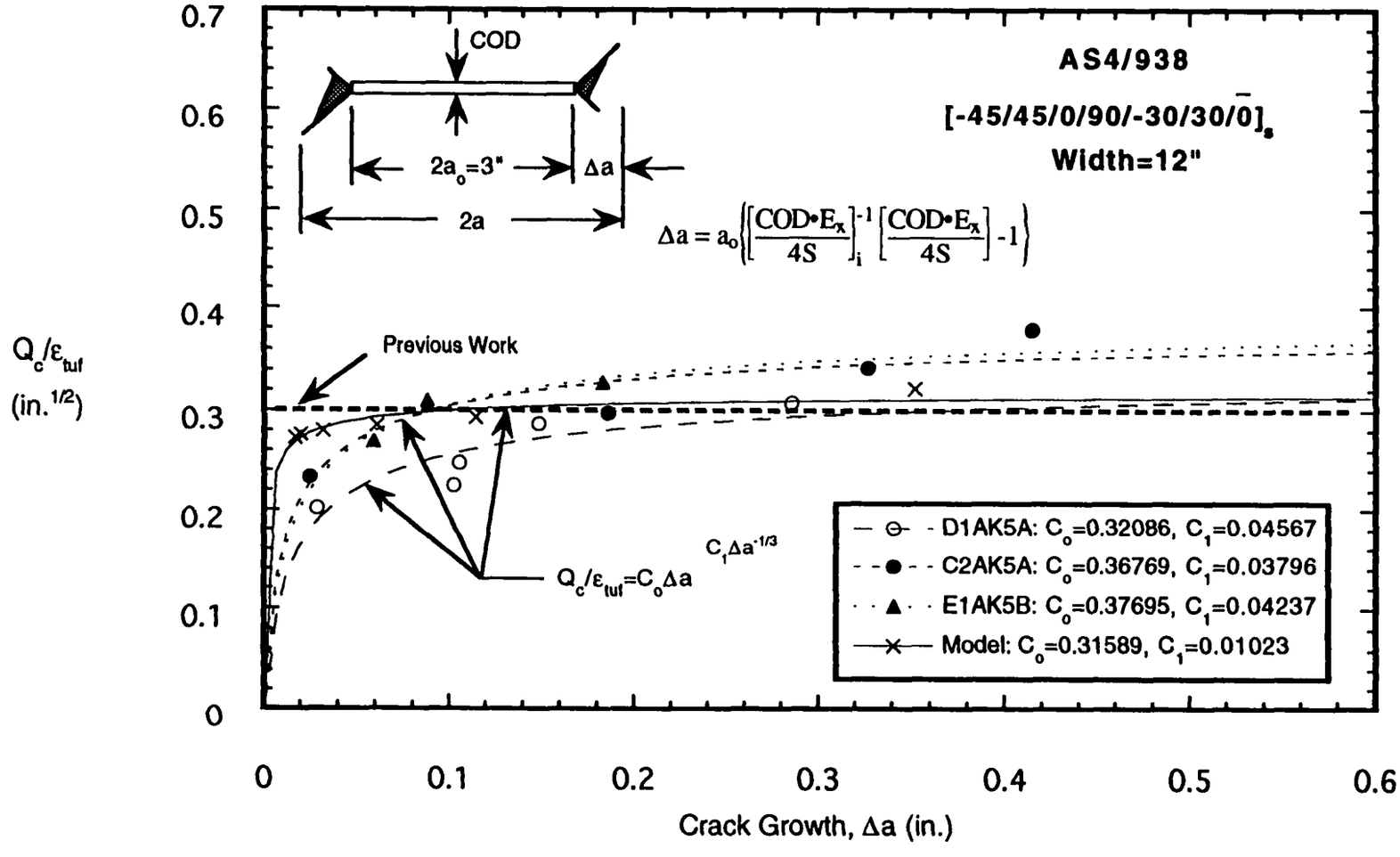

Figure 36 - Experimental and Model Generated R-Curves for AS4/938 Center-Crack Tension Panels, $2a_o$=3".

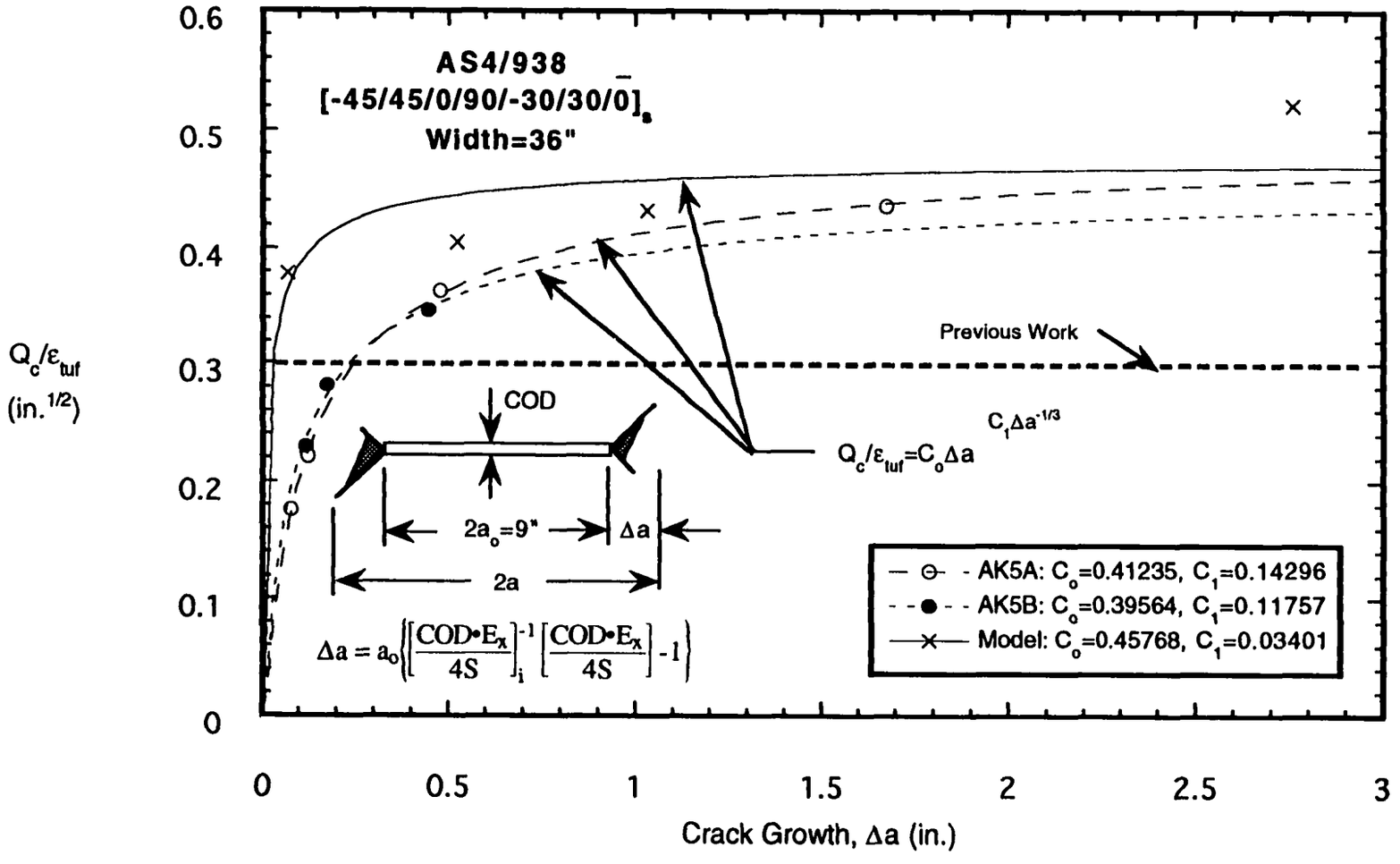

Figure 37 - Experimental and Model Generated R-Curves for AS4/938 Center-Crack Tension Panels, $2a_o$=9".

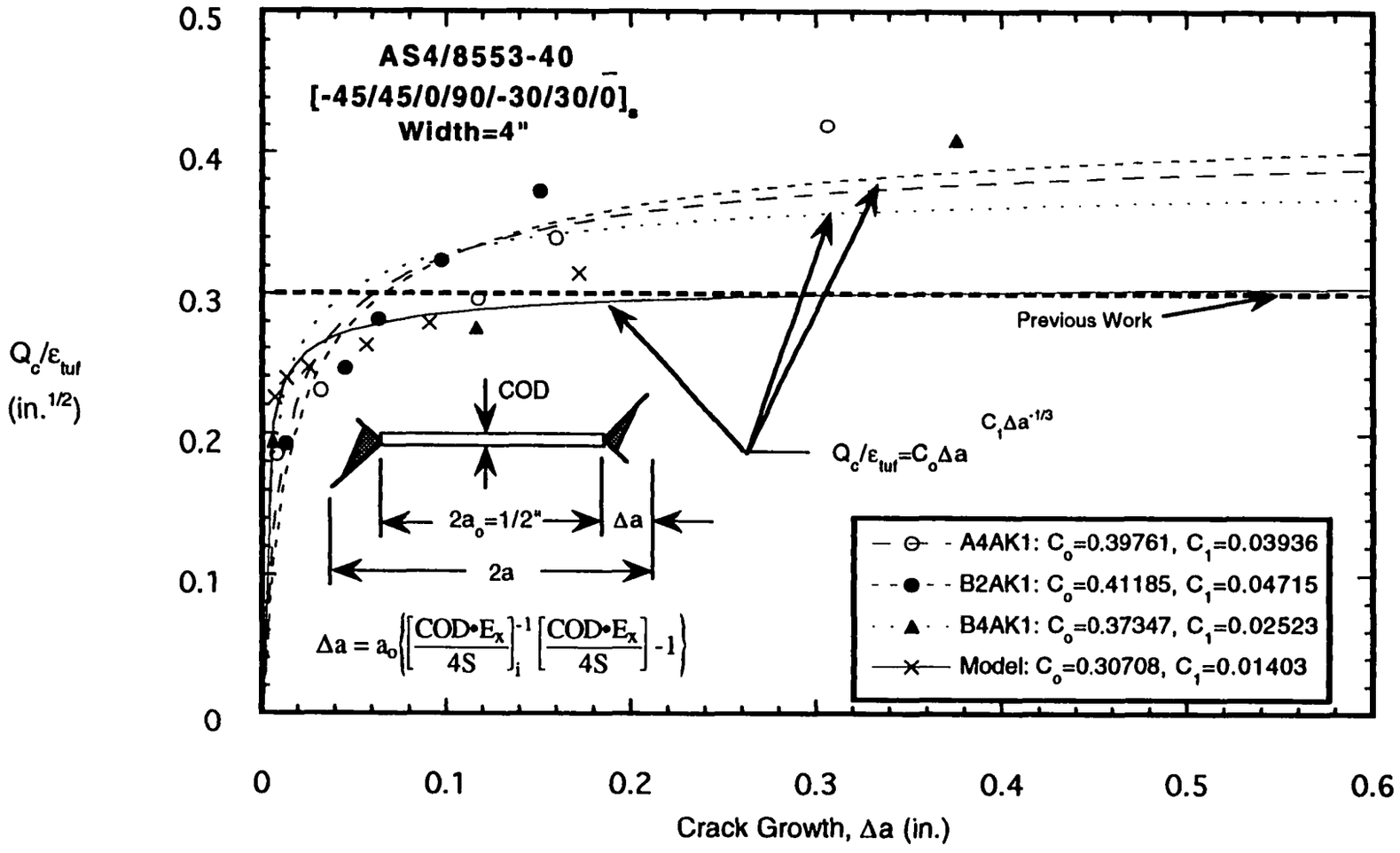

Figure 38 - Experimental and Model Generated R-Curves for AS4/8553-40 Center-Crack Tension Panels, $2a_o$=1/2".

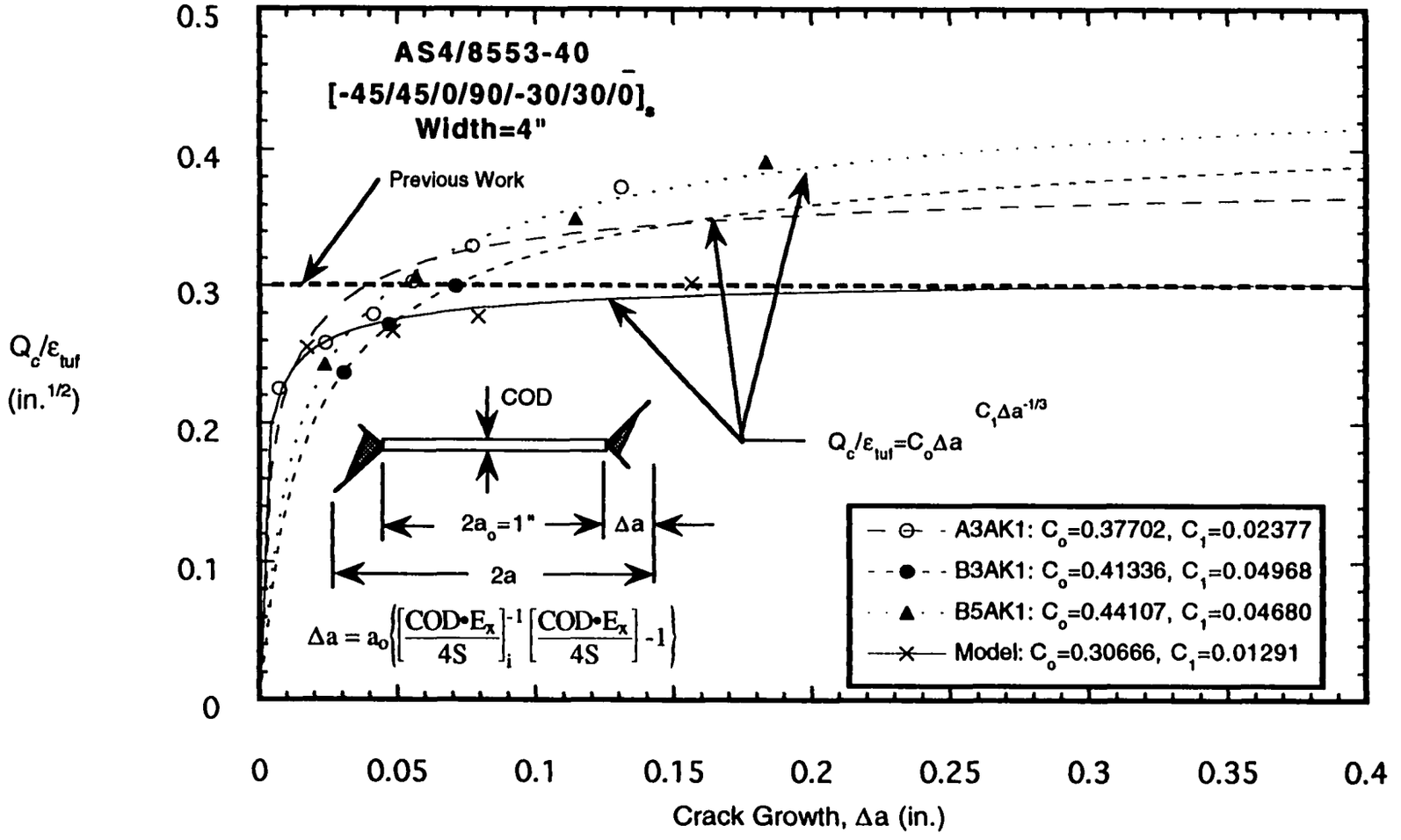

Figure 39 - Experimental and Model Generated R-Curves for AS4/8553-40 Center-Crack Tension Panels, $2a_o$=1".

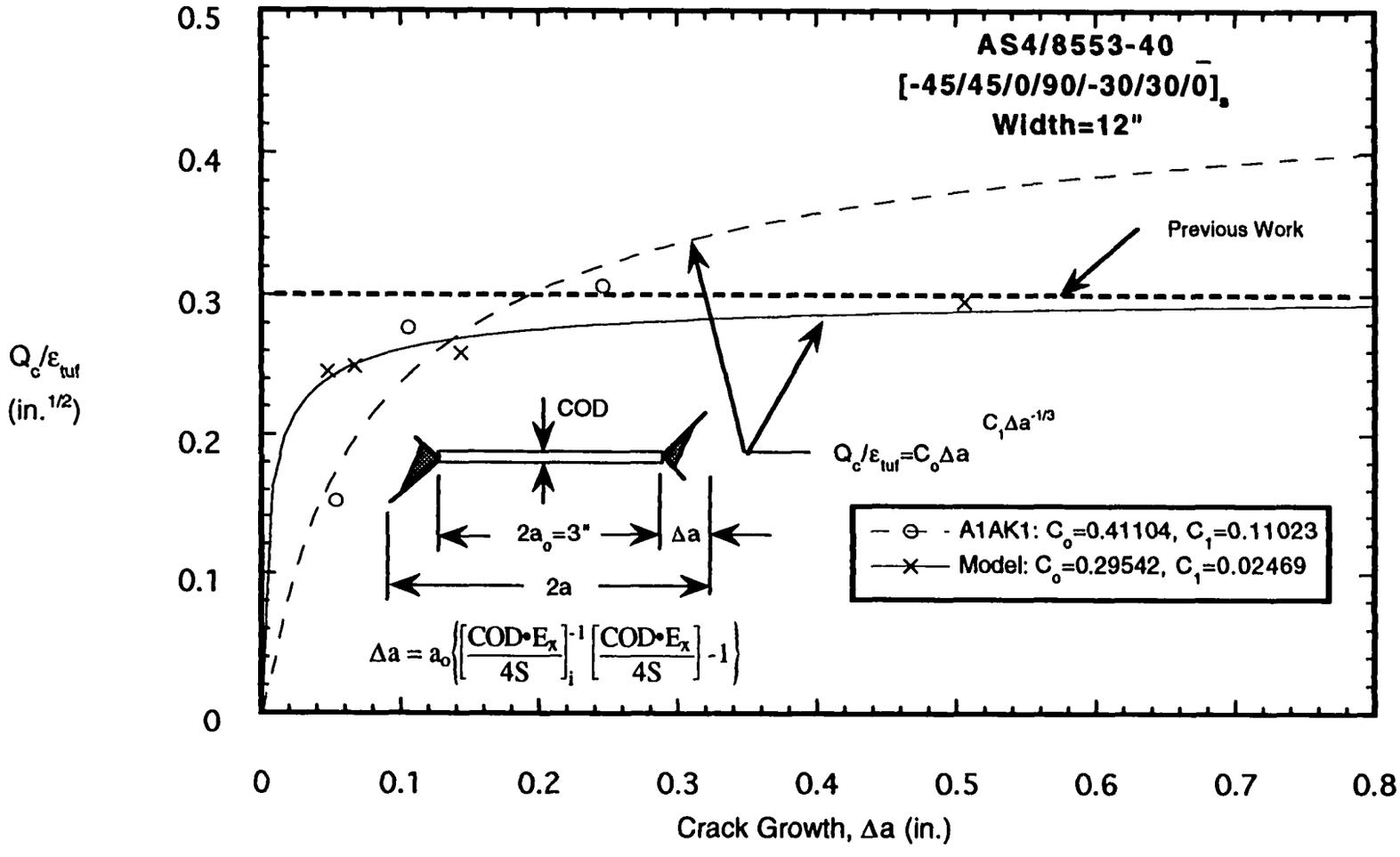

Figure 40 - Experimental and Model Generated R-Curves for AS4/8553-40 Center-Crack Tension Panels, $2a_o$=3".

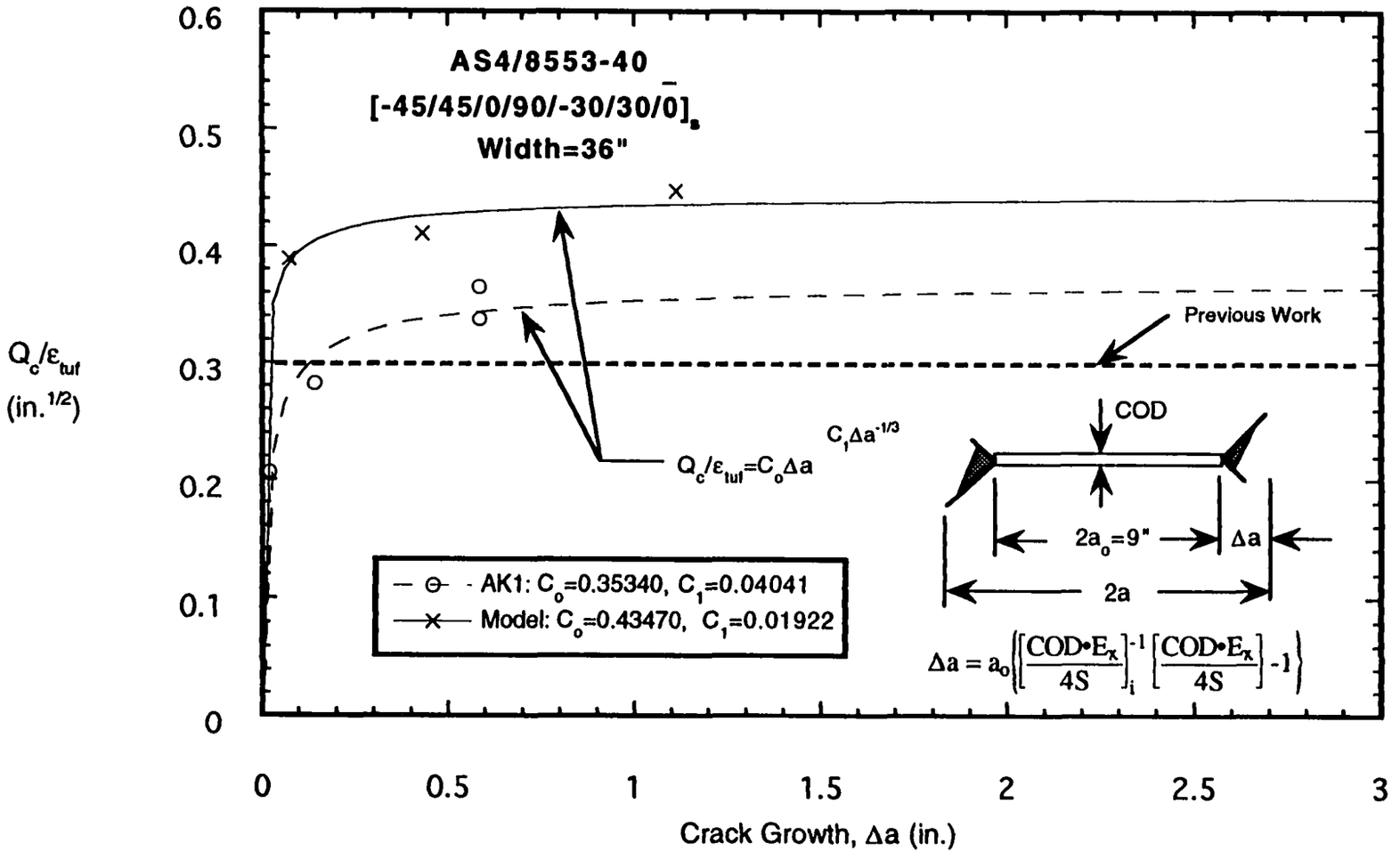

Figure 41 - Experimental and Model Generated R-Curves for AS4/8553-40 Center-Crack Tension Panels, $2a_o$=9".

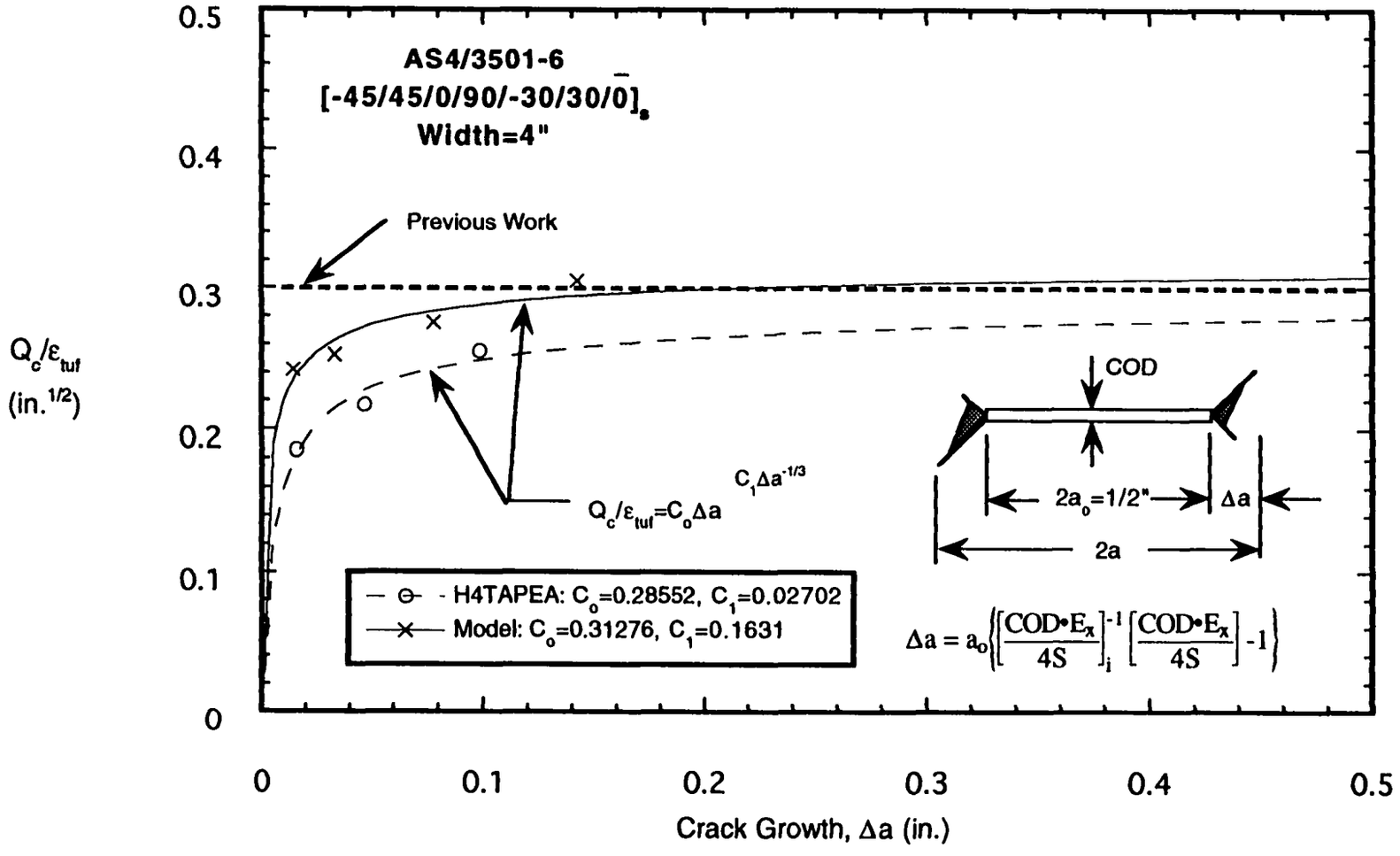

Figure 42 - Experimental and Model Generated R-Curves for AS4/3501-6 Center-Crack Tension Panels, $2a_o$=1/2".

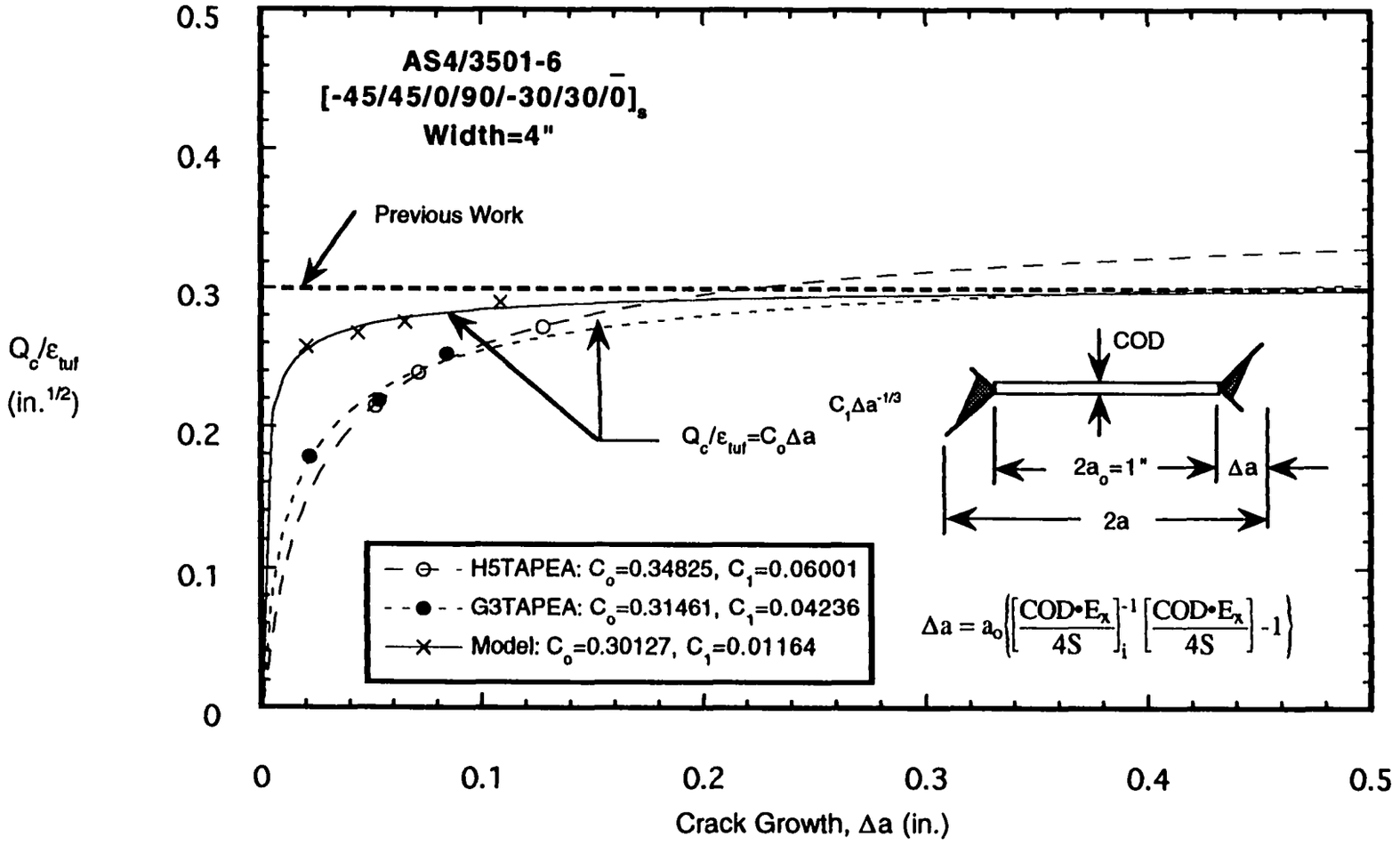

Figure 43 - Experimental and Model Generated R-Curves for AS4/3501-6 Center-Crack Tension Panels, $2a_o$=1".

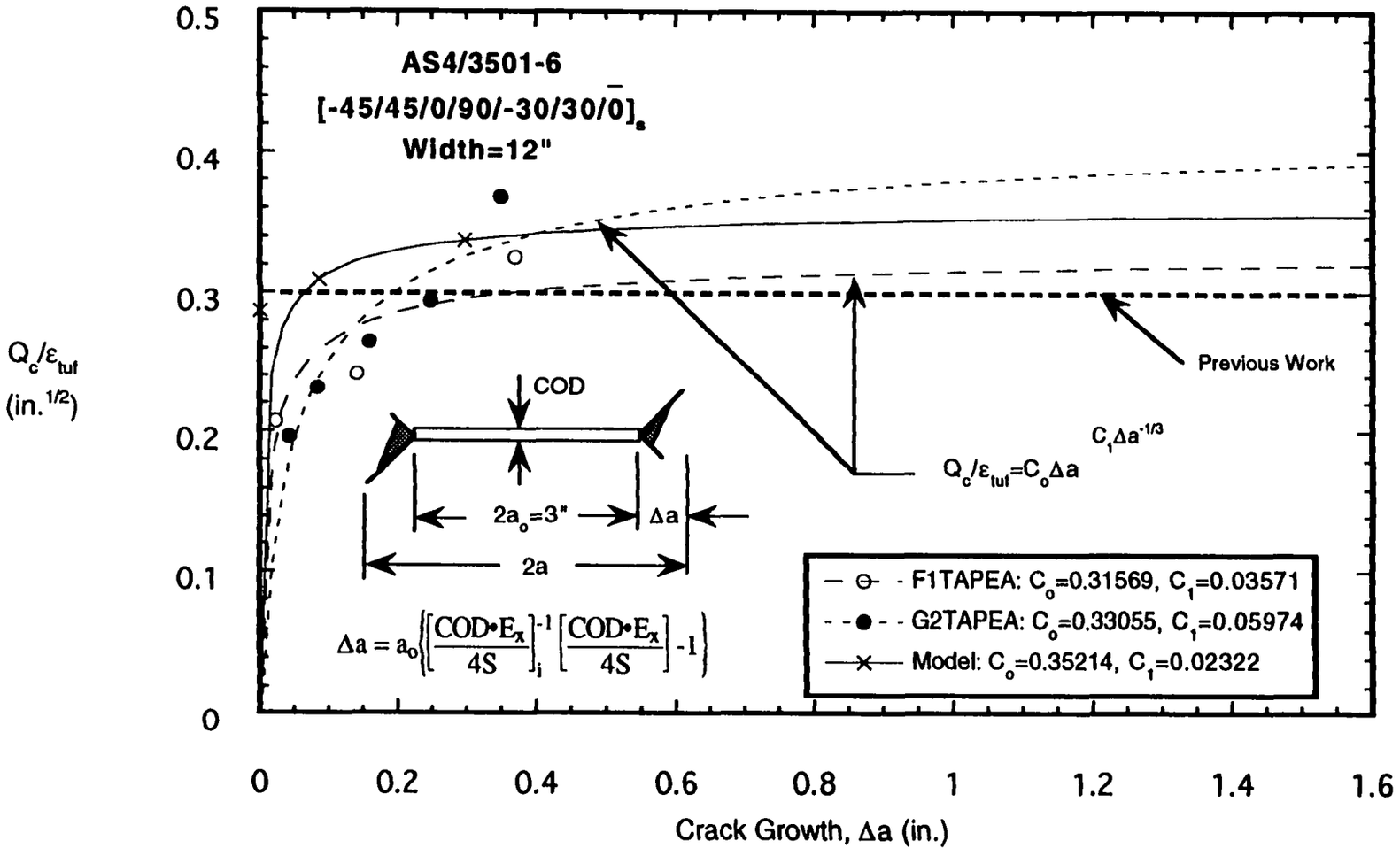

Figure 44 - Experimental and Model Generated R-Curves for AS4/3501-6 Center-Crack Tension Panels, $2a_o$=3".

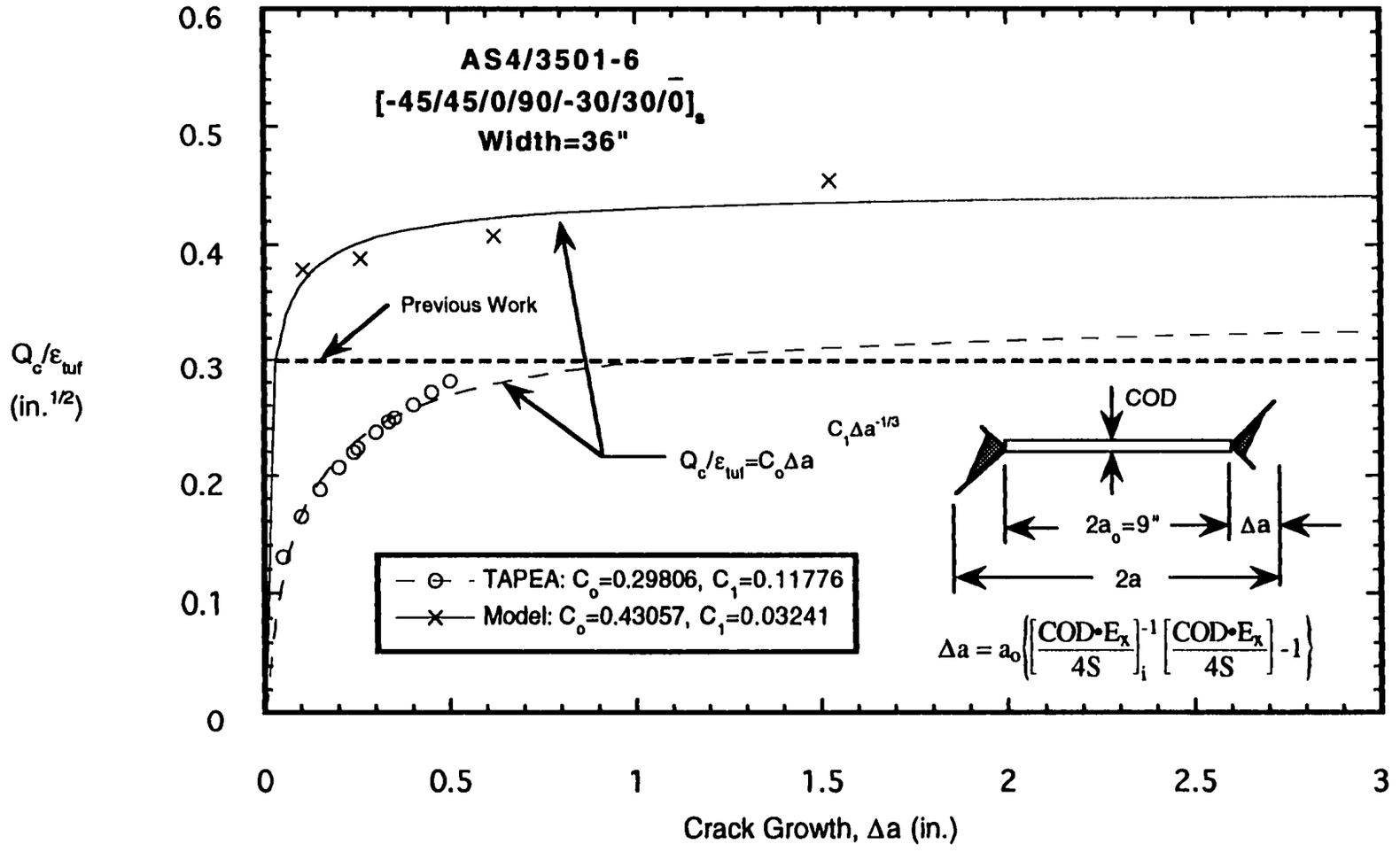

Figure 45 - Experimental and Model Generated R-Curves for AS4/3501-6 Center-Crack Tension Panels, $2a_o$=9".

APPENDIX A
PLY FRACTOGRAPHY SCHEMATICS

Ply fractography for specimen F5AK5B was presented in Figures 12 and 13. The schematics for the rest of the ply fractography specimens will be presented in this appendix. The actual fractographs will not be shown here since the schematics are easier to read. The schematics in Figures A-1 to A-3 show representations of local delamination as dark patches and fiber fracture as "free-hand" drawn lines. Most of the delaminations are dimensioned and the fiber fractures are measured and labeled as *da*. For example, in Figure A-1 the first schematic shows the local delamination at the -45/45 ply interface at the right notch-tip. The ply used for this was the 45 degree ply. The delamination measured 0.31" away from the notch-tip at it's farthest point away. The next ply, a 0 degree ply had delamination and fiber fracture. The fiber fracture is about 0.20" long measured from the notch-tip. All of the dimensions were measured using a machinists scale with 1/100 of an inch divisions. All of the figures in this appendix illustrate the variation in damage occurring from one ply to another. They demonstrate that as translaminate fracture occurrs, the extent of fiber fracture in one ply is not necessarily the same as an adjacent ply. This allows for various avenues of load redistribution and in effect, existence of toughening mechanisms.

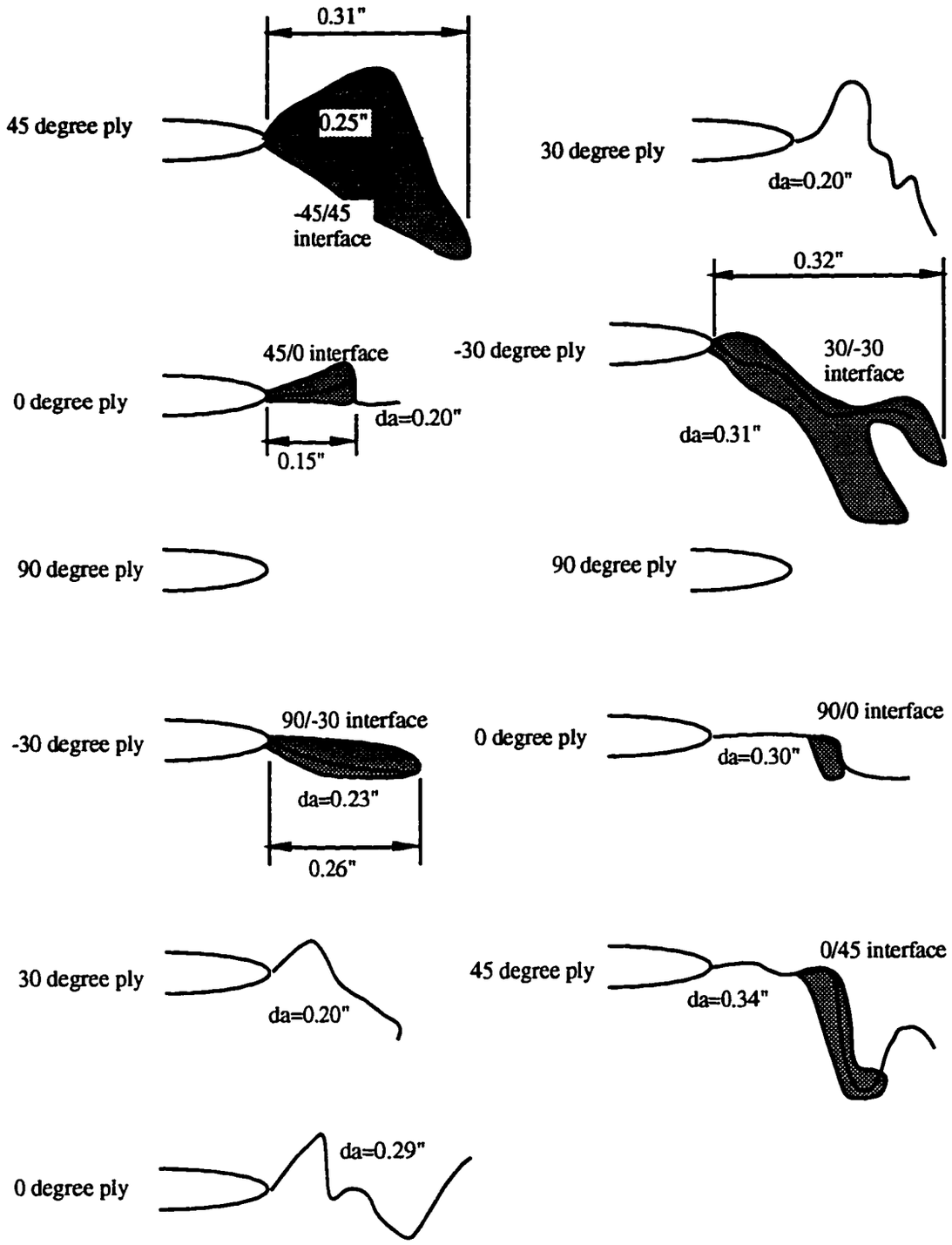

Figure A-1 - AS4/3501-6 Fiber Fracture and Delamination Illustration, Specimen G5TAPEA, $[-45/45/0/90/-30/30/\bar{0}]_S$, Right Notch-Tip, at 61% S_{ult}.

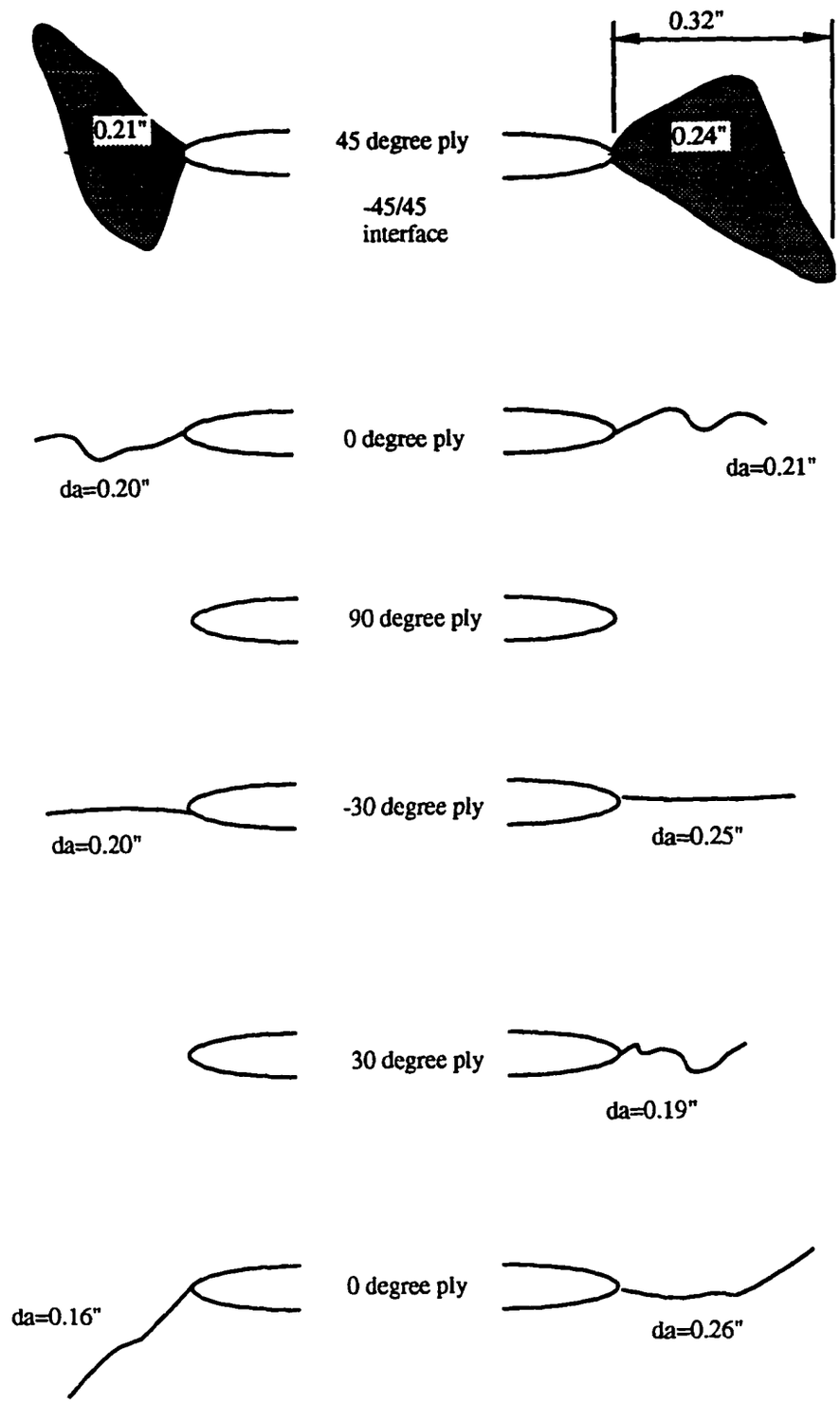

Figure A-2a - AS4\3501-6 Fiber Fracture and Delamination Illustration, Specimen G4TAPEA, $[-45/45/0/90/-30/30/\bar{0}]_S$, Both Notch-Tips, at 88% S_{ult}.

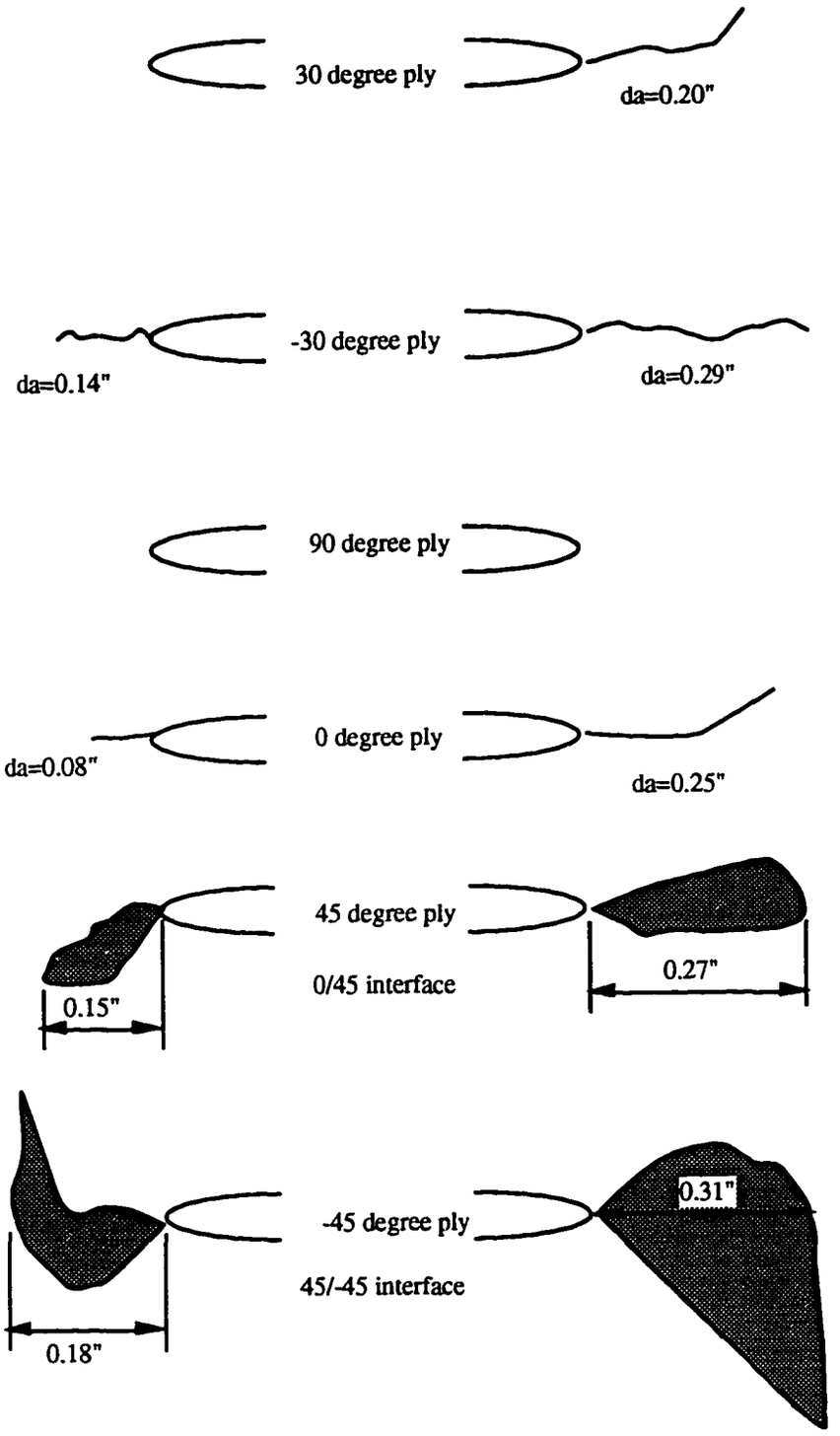

Figure A-2b - AS4/3501-6 Fiber Fracture and Delamination Illustration, Specimen G4TAPEA, $[-45/45/0/90/-30/30/\bar{0}]_S$, Both Notch-Tips, at 88% S_{ult}.

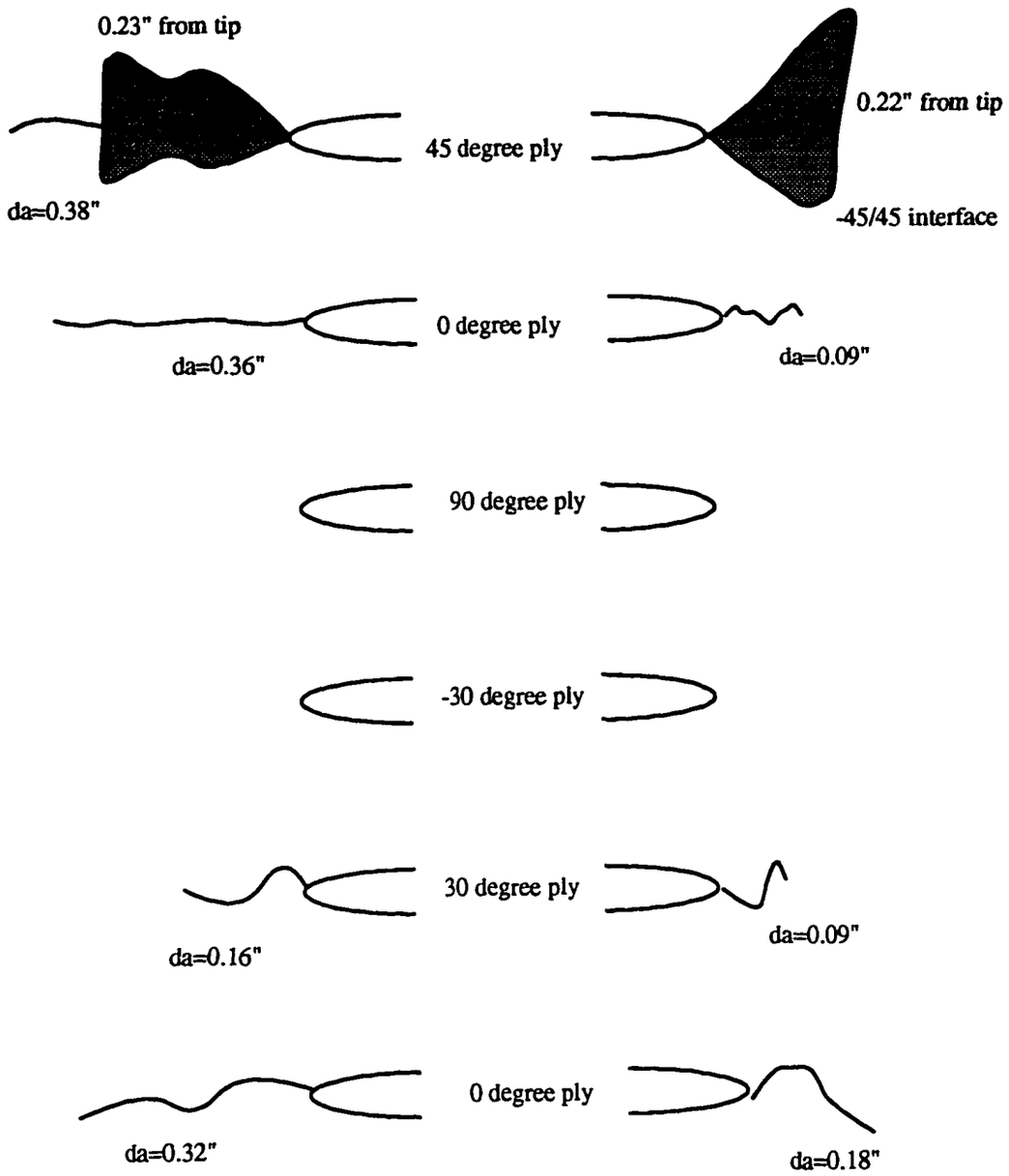

Figure A-3a - AS4/938 Fiber Fracture and Delamination Illustration, Specimen D3AK5A, $[-45/45/0/90/-30/30/\bar{0}]_s$, Both Notch-Tips, at 90% S_{ult}.

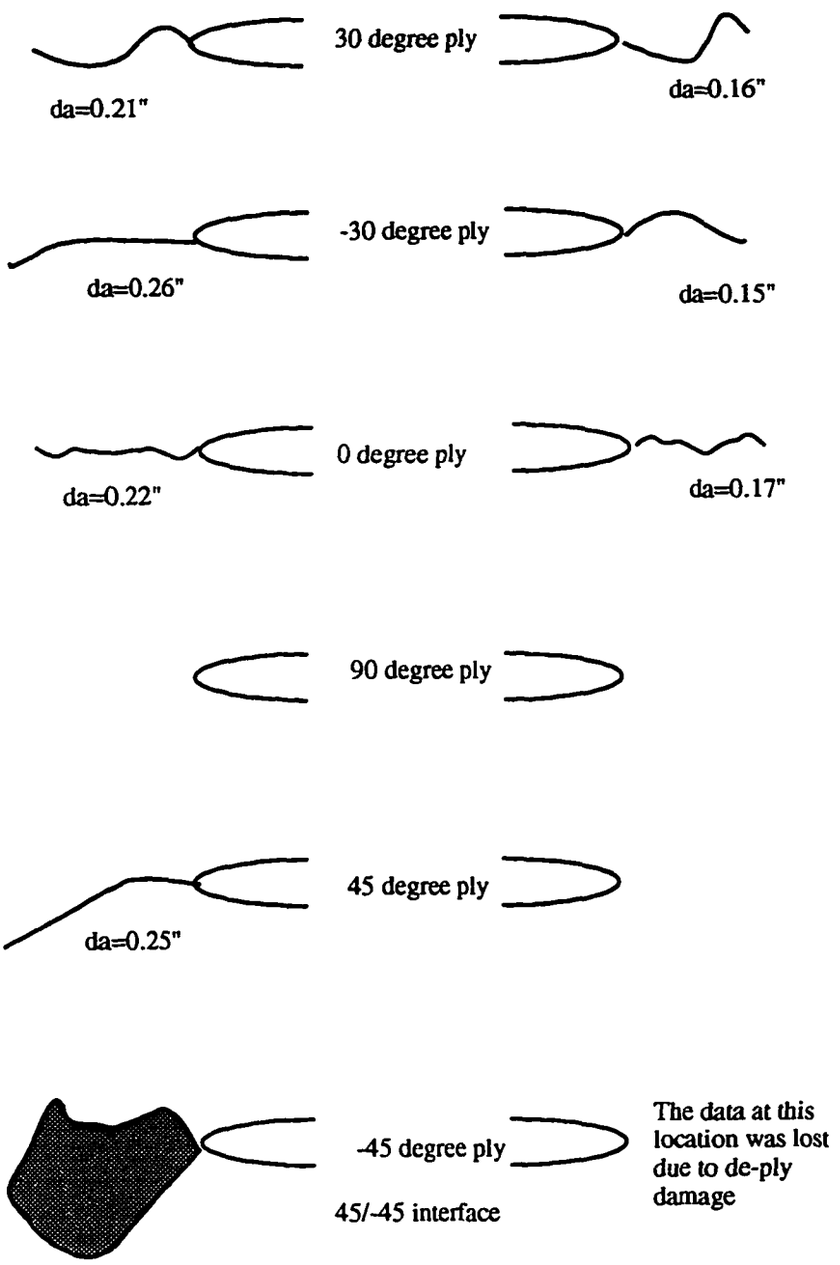

Figure A-3b - AS4/938 Fiber Fracture and Delamination Illustration, Specimen D3AK5A, $[-45/45/0/90/-30/30/\bar{0}]_S$, Both Notch-Tips, at 90% S_{ult}.

APPENDIX B
FIBER BRIDGING

Fiber Bridging Literature Survey

Fiber bridging has been scrutinized and studied as a crack growth inhibitor since the 1980's. Since then much research has been done to model and predict fiber bridging behavior. Initially, there were typically two types of fiber bridging models - the steady-state fiber bridging (SSFB) models and the generalized fiber bridging (GFB) models. Aveston et al. [B.1] and Budiansky et al. [B.2] used an energy balance approach in SSFB models to derive an expression for K_m, the stress intensity factor (S.I.F.) for the matrix, in terms of composite microstructural parameters under conditions of steady-state cracking during monotonic loading. The steady-state S.I.F. is independent of crack length. A continuum fracture mechanics analysis is combined with a micromechanics analysis in a GFB model to derive S.I.F. solutions for matrix cracks of arbitrary size. The constraint due to the intact fibers in the wake of the matrix crack is idealized as an unknown closure pressure. The models developed by Marshall et. al., McCartney, and McMeeking and Evans [B.3-B.5] are all GFB models and are commonly referred to as the MCE, MC, and ME fiber bridging models, respectively.

The works of Aveston, Budiansky, Marshall, etc., initiated and inspired further studies of fiber bridging. Sensmeier and Wright [B.6] studied the effects of fiber bridging on fatigue crack growth in titanium matrix composites. The framework for this analysis was the MCE [B.3] fiber bridging model. Further utilization of the GFB models by Bukuckas and Johnson [B.7] was in a study of matrix fatigue crack growth behavior in

center-notched titanium matrix composites. They assumed the intact fibers in the wake of the crack are idealized as a crack closure pressure in their use of the MCE, MC, and ME [B.3-B.5] fiber bridging models. Finally, Chan [B.8] presents a theoretical analysis that examines the effects of cyclic degradation of interface on fiber bridging of fatigue cracks in metal matrix or intermetallic matrix composites. He calculated frictional stresses on individual fiber/matrix interfaces using crack tip micromechanics and the fiber bridging models based on the works of Marshall et. al. [B.3] as well as Hutchinson Jensen [B.9].

Fiber bridging models that are somewhat independent of the MCE, MC, and ME models have been under development. Bao and Song [B.10] derived crack bridging traction laws that are based on a fiber pull-out analysis coupled with three proposed fiber/matrix interface assumptions. Yin [B.11] introduced a fiber bridging model based on crack closure tractions and applies a superposition to the stress intensity factor solution of a center-cracked tension specimen to provide a modified stress intensity factor which includes the effects of fiber bridging.

In light of the idea that fiber bridging increases fracture toughness and can be construed as a crack growth resistance mechanism, much research has occurred to correlate the effects of fiber bridging with crack growth resistance curves (R-curves). Suo et. al. [B.12] developed crack closure tractions in the form of spring laws (linear and non-linear are compared) which are inferred from experimental delamination R-curves. Miyajima and Sakai [B.13] used the experimental R-curve to study fiber bridging where the fiber bridging tractions are estimated by the Dugdale approach. Similarly, Sakai et.al. [B.14] used the Dugdale approach to estimate fiber bridging tractions. Fiber pull-out and bridging processes in the wake of the propagating crack tip are discussed in relation to experimental R-curves.

An experimental investigation of the role of fiber bridging in the delamination resistance was conducted by Spearing and Evans [B.15]. The results were compared with fiber bridging models utilizing a softening traction law. This led to schemes for

predicting trends in delamination resistance with specimen geometry and crack length. Hu and Mai [B.16] uses a crack bridging theory which considers the difference in experimental and theoretical compliances to determine the fiber bridging stresses in the form of a crack closure or softening law. They showed that the delamination R-curve is consistent with the observation of fiber bridging in the delaminated region. Finally, influence of the bridging zone length on the resistance curve behavior was examined by Zok and Hom [B.17]. Experiments are correlated with fiber bridging models and compared with R-curves. They demonstrated, with a model utilizing a crack closure pressure, that resistance curves for composites depend on both the absolute length of the bridging zone and the length of the bridging zone relative to the total crack length and specimen width.

Fiber Bridging and Translaminate Fracture

There are currently three types of fiber bridging; elastic fiber bridging, frictional fiber bridging, and pull-out fiber bridging, Figure B-1. Elastic fiber bridging is the case where the crack circumvents the fiber such that the fiber and matrix interface remain intact. The interfacial shear strength, in frictional fiber bridging, is exceeded causing interfacial debonding and frictional stretching without fiber fracture. Finally, in pull-out fiber bridging, the fiber is shorter than the debond length and/or fractures within the debond length. For all three types of fiber bridging, previous works have stated and shown that fiber bridging is a crack growth resistance mechanism (toughening mechanism). However, all three types of fiber bridging are matrix cracks being bridged by intact fibers.

Consider the shear lag model [B.18, B.19]. In the concept of shear lag, there is a region where interfacial shear stresses exceed the strength of the interface. It is in this region where there is relative sliding between the fiber and matrix. This often results in fiber bridging - fibers within the wake of the crack remain intact, Figure B-2. It can be

said then that fiber bridging is a toughening mechanism and is therefore a contributing factor in the R-curve behavior. The controlling mechanism for the case of shear lag is the high interfacial shear stress.

The work herein focuses on translaminate fracture, not just matrix cracking alone. The bridging effects in translaminate fracture differ from the current fiber bridging configurations as is illustrated in Figure B-3. Typically, for translaminate fracture, there exists a fractured ply bridged by neighboring intact plies; usually a 0 degree ply bridged by off-axis plies. The ply bridging affects the redistribution of load into the neighboring plies. For a better understanding of this, it is a good idea to compare the behavior of metals to fiber reinforced composites, Figure B-4. We know that there are a lot of similarities in the mechanical behavior of metals to fiber-reinforced composites but their toughening mechanisms are different. For instance, the Dugdale plastic zone considers an effective crack longer than the physical crack. Crack edges in front of the physical crack carry the yield stress, tending to close the crack. The size of Δa is chosen such that the stress singularity is eliminated. It is proposed here that a similar phenomenon to the crack closure in the plastic zone is occurring in fiber reinforced composites, Figure B-5. Here, the fracture toughness is equal to the toughness found from the applied loading plus the additional toughness due to the bridging effects. The difference from the Dugdale approach is that the toughening mechanism and the calculations of the bridging effects are entirely different. Recent works by Poe [B.20, B.21] state that the general fracture toughness parameter, Q_c in Figure 33, is solely a material parameter. However, if the structural effects of fiber bridging are present, the general fracture toughness parameter will be affected by its presence.

References

[B.1] Aveston, J., Cooper, G.A., and Kelly, A., "Single and Multiple Fracture," *The Properties of Fibre Composites*, Conference Proceedings, National Physical Laboratory, Guildford. IPC Science and Technology Press, pp. 15-26, 1971.

[B.2] Budiansky, B., Hutchinson, J.W., and Evans, A.G., "Matrix Fracture in Fiber-Reinforced Ceramics," *J. Mech. Phys. Solids*, Vol. 34, No. 2, pp. 167-189, 1986.

[B.3] Marshall, D.B., Cox, B.N., and Evans, A.G., "The Mechanics in Matrix Cracking in Brittle-Matrix Fiber Composites," *Acta. Metall.*, Vol. 33, No. 11, pp. 2013-2021, 1985.

[B.4] McCartney, L.N., "Mechanics of Matrix Cracking in Brittle-Matrix Fiber-Reinforced Composites," *Proc. R. Soc. Lond.*, A 409, pp. 329-350, 1987.

[B.5] McMeeking, R.M.and Evans, A.G., "Matrix Fatigue Cracking in Fiber Composites," *Mech. of Matls.*, Vol. 9, pp. 217-227, 1990.

[B.6] Sensmeier, M.D. and Wright, P.K., "The Effect of Fiber on Fatigue Crack Growth in Titanium Matrix Composites," *Fundamental Relations Between Microstructure and Mechanical Properties of Metal-Matrix Composites*, P.K. Liaw and M.N. Gungor, Eds., The Minerals, Metals, and Materials Society, 1990, pp. 441-457.

[B.7] Bakuckus, Jr., J.G. and Johnson, W.S., "Application of Fiber Bridging Models to Fatigue Crack Growth in Unidirectional Titanium Matrix Composites," *J. of Comp. Tech. and Res.*, JCTRER, Vol. 15, No. 3, Fall 1993, pp. 242-255.

[B.8] Chan, K.S., " Effects of Interface Degradation on Fiber Bridging of Composite Fatigue Cracks," *Acta. Metall. Mater.*,Vol. 41, No. 3, pp. 761-768, 1993.

[B.9] Hutchinson, J.W. and Jensen, H.M., "Models of Fiber Debonding and Pullout in Brittle Composites with Friction," *Mech. Mater.*, Vol. 9, pp.139, 1990.

[B.10] Bao, G. and Song, Y., "Crack Bridging Models for Fiber Composites With Slip-Dependent Interfaces," *J. Mech. Phys. Solids*, Vol. 41, No. 9, pp. 1425-1444, 1993.

[B.11] Yin, S.W., "A Fiber Bridging Model for the Fracture of Brittle Matrix Composites," *Engr. Fract. Mech.*, Vol. 46, No. 5, pp. 887-894, 1993.

[B.12] Suo, Z. Bao, G., and Fan, B., "Delamination R-Curve Phenomena Due to Damage," *J. Mech. Phys. Solids*, Vol. 40, No. 1, pp. 1-16, 1992.

[B.13] Miyajima, T. and Sakai, M., "Fiber Bridging of a Carbon Fiber-Reinforced Carbon Matrix Lamina Composite," *J. Mater. Res.*, Vol. 6, No. 3, March 1991.

[B.14] Sakai, M., Miyajima, T., and Inagaki, M., "Fracture Toughness and Fiber Bridging of Carbon Fiber Reinforced Carbon Composites," *Comp. Sci. and Tech.*, Vol. 40, pp. 231-250, 1991.

[B.15] Spearing, S.M. and Evans, A.G., "The Role of Fiber Bridging in the Delamination Resistance of Fiber-Reinforced Composites," *Acta. Metall. Mater.*, Vol. 40, No. 9, pp. 2191-2199, 1992.

[B.16] Hu, X.Z. and Mai, Y.W., "Mode I Delamination and Fiber Bridging in Carbon-Fiber/Epoxy Composites With and Without PVAL Coating," *Comp. Sci. and Tech.*, Vol. 46, pp. 147-156, 1993.

[B.17] Zok, F. and Hom, Z.L., "Large Scale Bridging in Brittle Matrix Composites," *Acta. Metall. Mater.*, Vol. 38, No. 10, pp. 1895-1904, 1990.

[B.18] Zweben, C., "Fracture Mechanics and Composite Materials: A Critical Analysis," Amer. Society for Testing and Materials, pp.65-97, 1973.

[B.19] Goree, J.G. and Autar, K.K., "Shear Lag Analysis of Notched Laminates with Interlaminar Debonding," NASA Contractor Report 3798, May 1984.

[B.20] Poe, C.C., Jr., Harris, C.E., Coats, T.W., and Walker, T.H., "Tension Strength with Discrete Source Damage," *Proceedings of the Fifth NASA/DOD Advanced Composites Technology Conference*, NASA CP 3294, May 1995.

[B.21] Poe, C.C., Jr., "A Unifying Strain Criterion for Fracture of Fibrous Composite Laminates," *Engineering Fracture Mechanics*, Vol. 17, No. 2, pp. 153-171, 1983.

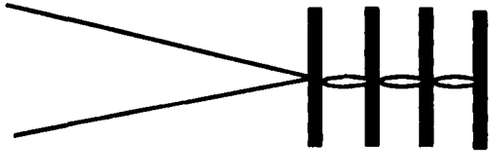

Elastic Fiber Bridging
Crack Circumvents the fiber such that the fiber and matrix interface remain intact

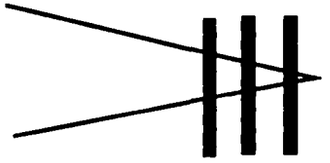

Frictional Fiber Bridging
The interfacial shear strength is exceeded causing interfacial debonding and frictional stretching without fiber fracture

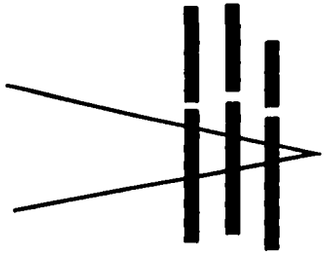

Pull-Out Fiber Bridging
Fiber is shorter than the debond length and/or fractures within the debond length

Figure B-1 - Three (Current) Types of Fiber Bridging.

Shear Lag

- Interface Shear Stresses Exceed Strength of the Interface
- Relative Sliding Between the Fiber and Matrix
- Fiber Bridging

Toughening Mechanism: Fiber Bridging

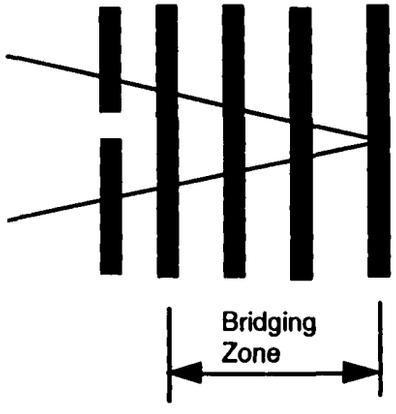

Controlling Mechanism: High Interfacial Shear Stresses

Figure B-2 - The Fiber Bridging and Shear Lag Relationship.

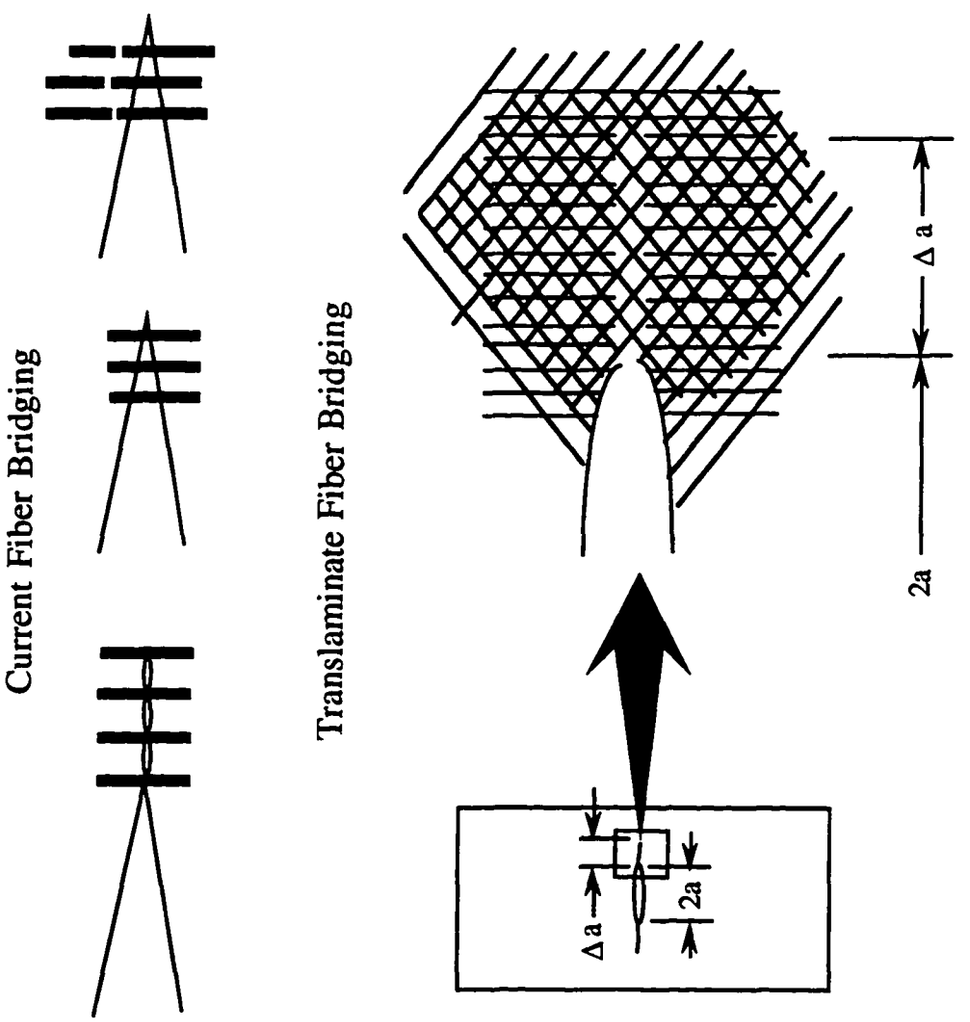

Figure B-3 - Current Fiber Bridging Configurations and Translaminate Fiber Bridging.

Classical LEFM

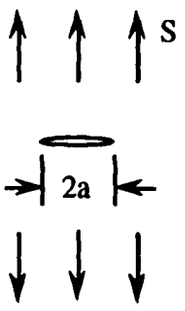

$$K = S\sqrt{\pi a}\sqrt{\sec\frac{\pi a}{W}}$$

Irwin Plastic Zone

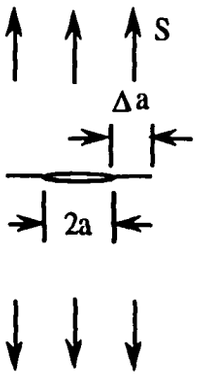

$$K = S\sqrt{\pi(a+\delta a)}\sqrt{\sec\frac{\pi(a+\delta a)}{W}}$$

where $\delta a = \Delta a + r_p$

r_p is the plastic zone diameter

Dugdale Plastic Zone

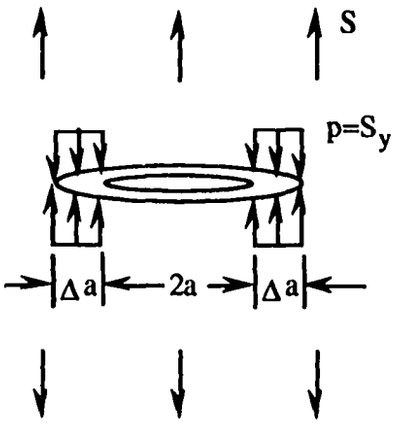

Choose Δa such that $K = 0$

$$K = K_{app} + K_p$$

$$K_{app} = S\sqrt{\pi(a+\Delta a)}$$

$$K_p = \frac{p}{\sqrt{\pi a}}\int_a^{\Delta a}\left\{\sqrt{\frac{a+x}{a-x}} + \sqrt{\frac{a-x}{a+x}}\right\}dx$$

$$S\sqrt{\pi(a+\Delta a)} = 2S_y\sqrt{\frac{a+\Delta a}{\pi}}\arccos\frac{a}{a+\Delta a}$$

Figure B-4 - Fracture Toughness Solutions for Metals.

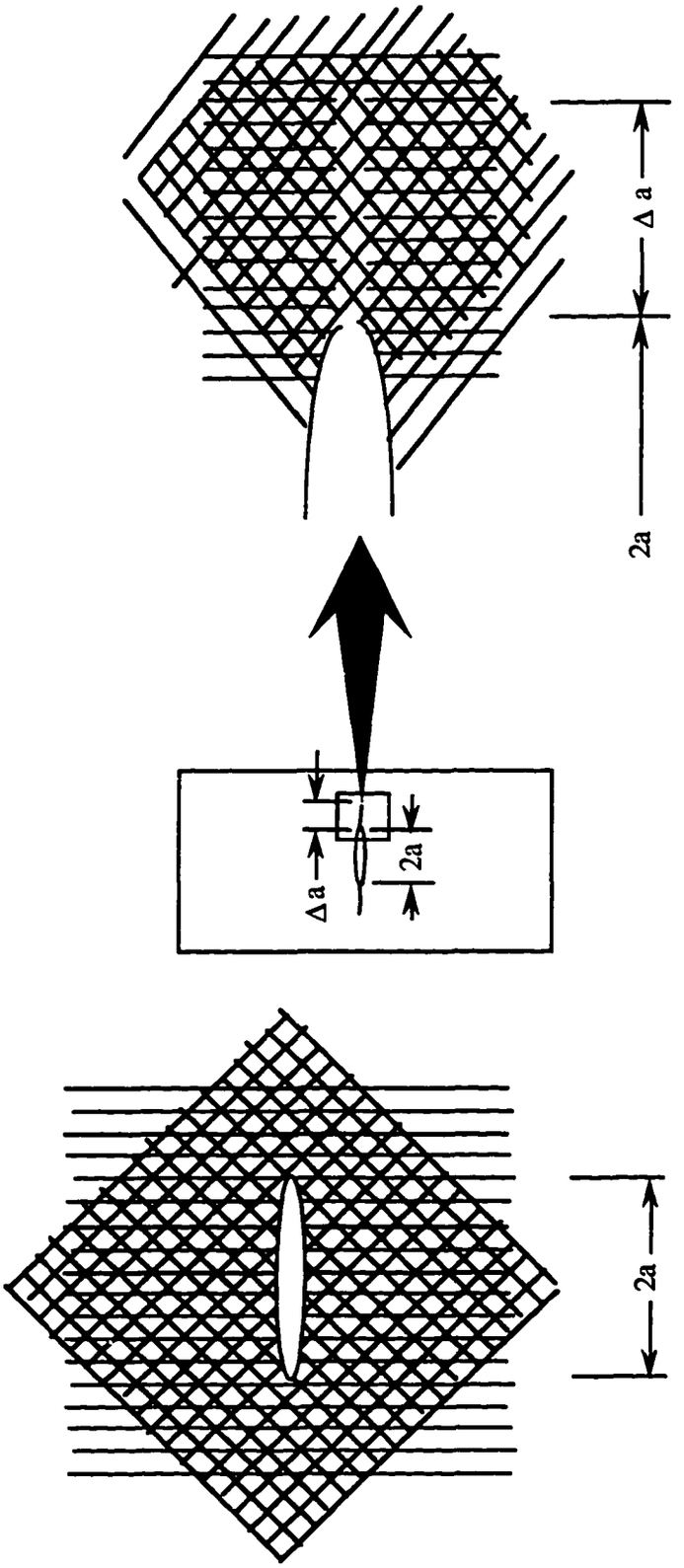

$$Qc = \varepsilon_c \sqrt{\pi a \sec \frac{\pi a}{w}(\xi)}$$

$$Qc = \varepsilon_c \left[\pi(a+\Delta a) \sec \frac{\pi(a+\Delta a)}{W} \right]^{1/2} (\xi) + Qc(p(x))$$

Figure B-5 - General Fracture Toughness and Translaminate Bridging.

APPENDIX C
OPEN-HOLE TENSION MESH REFINEMENT STUDY

Previous work [34] demonstrated the ability of the progressive damage model to accurately predict stiffness loss of open-hole IM7/5260 composite laminates loaded in tension-tension fatigue, Figure C-1. As part of the development of the residual strength methodology, a mesh refinement study of the open-holestrength cases was conducted.

Four quarter-panel meshes were generated for the one inch wide and eight inch long open-hole specimens. Only about a third of the length is shown for illustrative purposes in Figure C-2. The result of this study is given in Figure C-3 which leads to the conclusion that the solution converges very well for the open-hole tension tests. Residual strength predictions for the open-hole laminates is given in Figure C-4 for completeness.

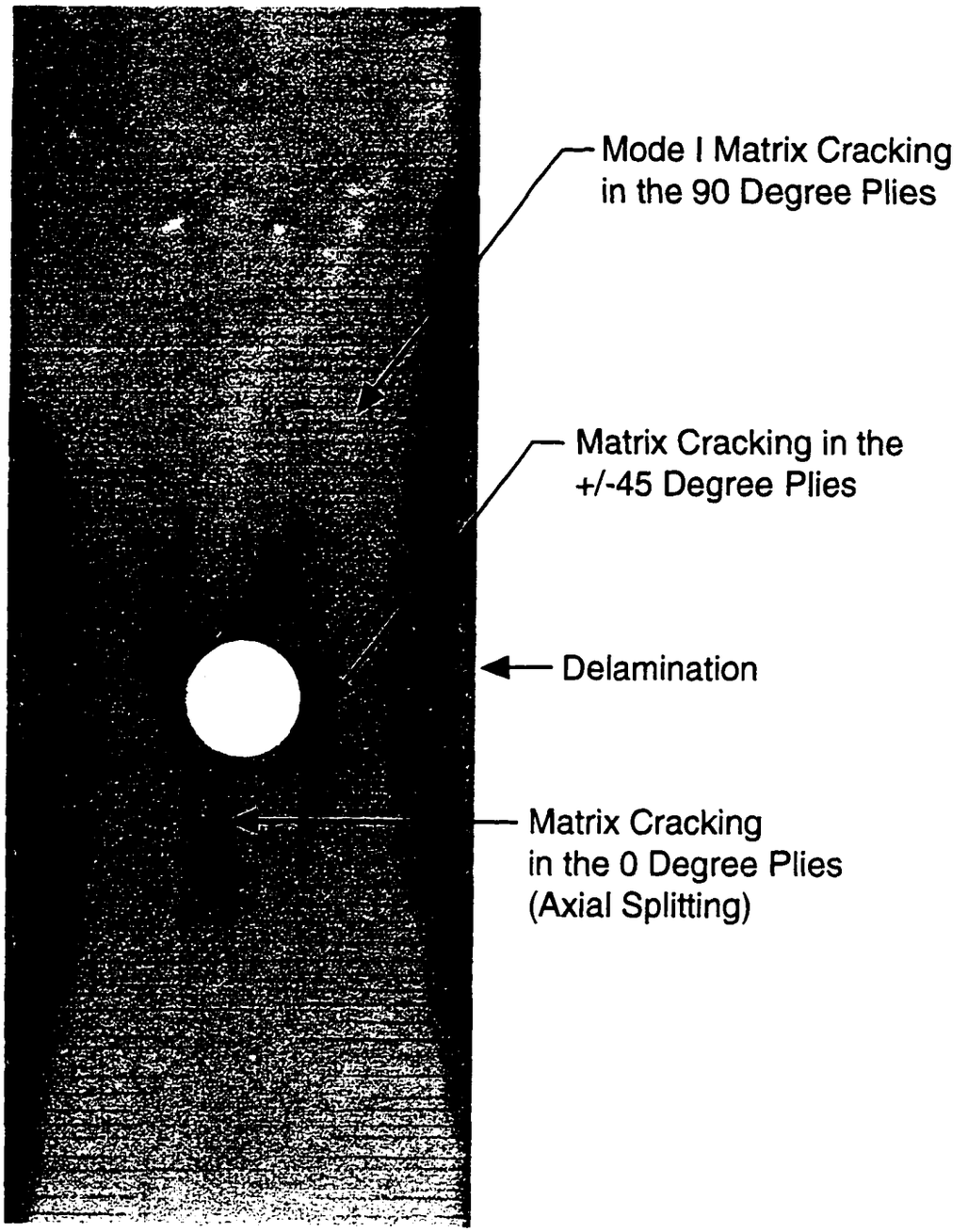

Figure C-1 - Tension-Tension Fatigue Damage in a Notched $[0/45/-45/90]_S$ IM7/5260 Laminate.

Mesh 1. 387 nodes 336 elements

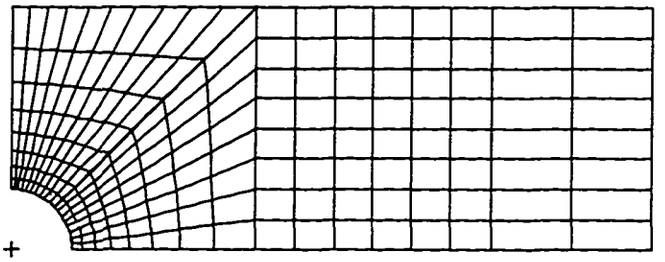

Mesh 2. 1071 nodes 992 elements

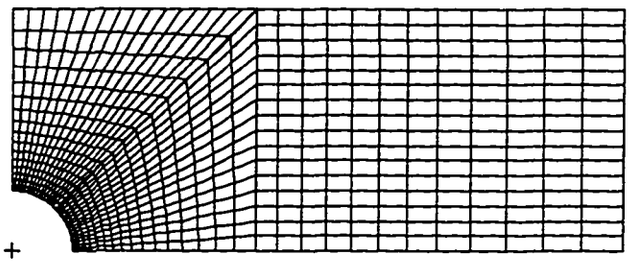

Mesh 3. 2225 nodes 2112 elements

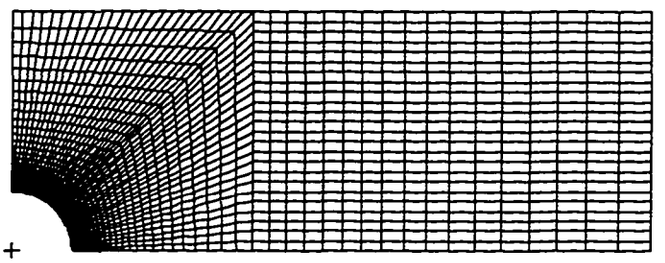

Mesh 4. 2813 nodes 2688 elements

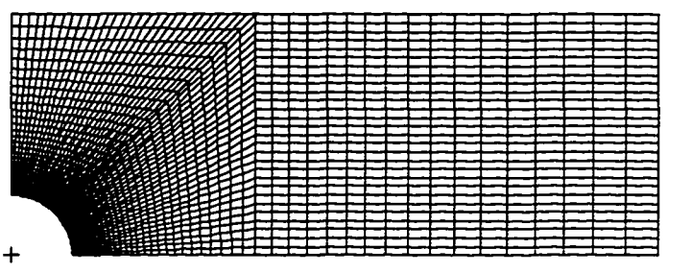

Figure C-2 - Finite Element Meshes Used in the Convergence Study.

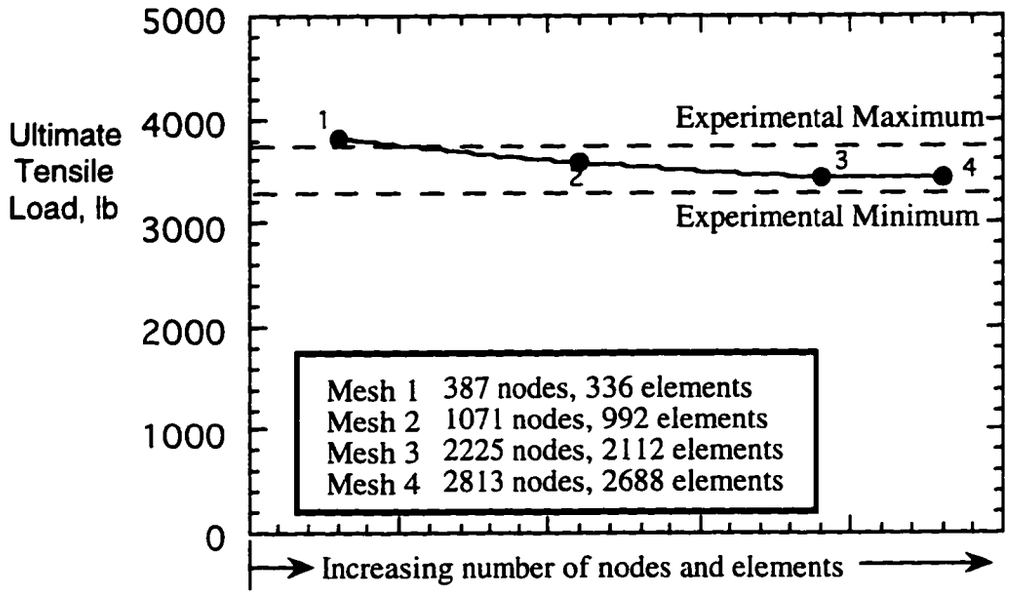

Figure C-3 - Mesh Refinement Study for the Residual Strength Predictions of the $[0/45/-45/90]_s$ Laminate Open-Hole Geometry.

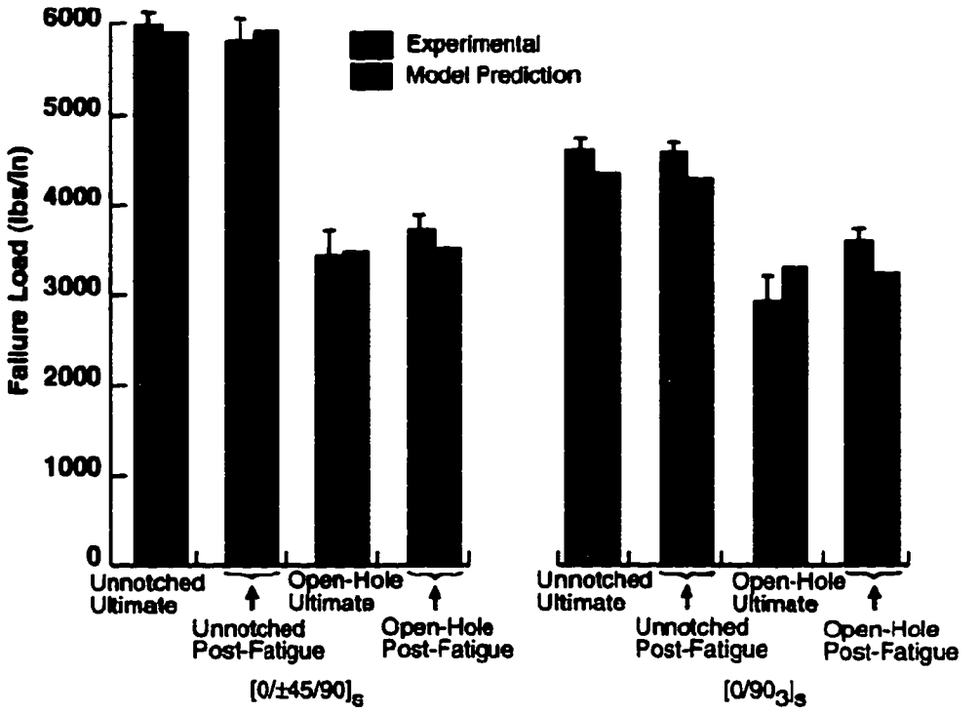

Figure C-4 - Predictions of Residual Strength.

APPENDIX D
R-CURVES / CHARACTERISTIC CRACK LENGTHS

The R-curves in Figures 34-45 were developed from the calculated effective crack growth, Δa. Another way to determine the effective crack growth is to simply measure it from the x-ray radiograph. This method is subjective because one needs to determine from the x-ray radiograph exactly what represents Δa. This may vary from person to person and from one x-ray radiograph to the next. An example is given to illustrate the procedure used to generate the R-curves, both for the measured Δa as well as for the closed form solution Δa. This example uses data from one of the experiments and is representative of all of the calculations involved in generating the R-curves in this study, including the predicted R-curves.

Discontinuities along the load/cod plot in Figure D-1 are labled *A*, *B*, *C*, and *D*. It is at these discontinuities that the specimen was unloaded and x-ray radiographs were taken just like the ones in Figures 14-16. The damage at the notch-tip was measured transversely from the tip of the notch toward the outer edge of the specimen with a machinists scale with divisions of 1/100 of an inch. The x-ray radiographs were enlarged to make this task easier. Table D-1 illustrates the steps taken to arrive at the Δa measurements given in Figure D-1.

To determine Δa from the closed form solution shown in Figure D-2, a straight line is drawn up the initial slope to aid in obtaining the initial point of nonlinearity. The load at this initial point is labeled P_i and is about 12.3 kips for this specimen. Given that E_x=8.669 Msi, and the plot shows S_i=34,442 psi and cod_i=0.00492 in., then $[cod \cdot E_x/4S]_i$ has a value of 0.3096. Table D-2 demonstrates the final steps to calculating Δa and

fracture toughness. The failure values in Table D-2 were calculated for the point of catastrophic failure. These values are not represented by data points in the plots, they were only calculated for the fracture toughness values in Tables 5-8. The R-curves using the measured crack growth, Figures D-3 to D-11, include experimental and predicted plots.

Table D-1 Measured Characteristic Crack Growth Results

Discontinuity	X-ray Radiograph Magnification	Magnified Δa (in.)	Characteristic Crack Growth, Δa (in.)	Stress, σ (psi)	Q_c/ε_{tuf} ($\sqrt{in.}$)
A	3.72 x	0.40	0.1075	34,442	0.1852
B	3.72x	0.57	0.1532	40,808	0.2343
C	3.72x	0.97	0.2608	51,048	0.3357
D	3.72x	1.19	0.3199	54,229	0.3810

Table D-2 Calculated Characteristic Crack Growth Results

Discontinuity	COD (in.)	Load, P (lb)	Stress, σ (psi)	Characteristic Crack Growth, Δa (in)	Q_c/ε_{tuf} ($\sqrt{in.}$)
B	0.0062	14,114	40,808	0.0163	0.1875
C	0.0085	17,656	51,048	0.0407	0.2456
D	0.0099	18,756	54,229	0.0679	0.2736
Failure	0.0108	20,261	58,579	0.0726	0.2975

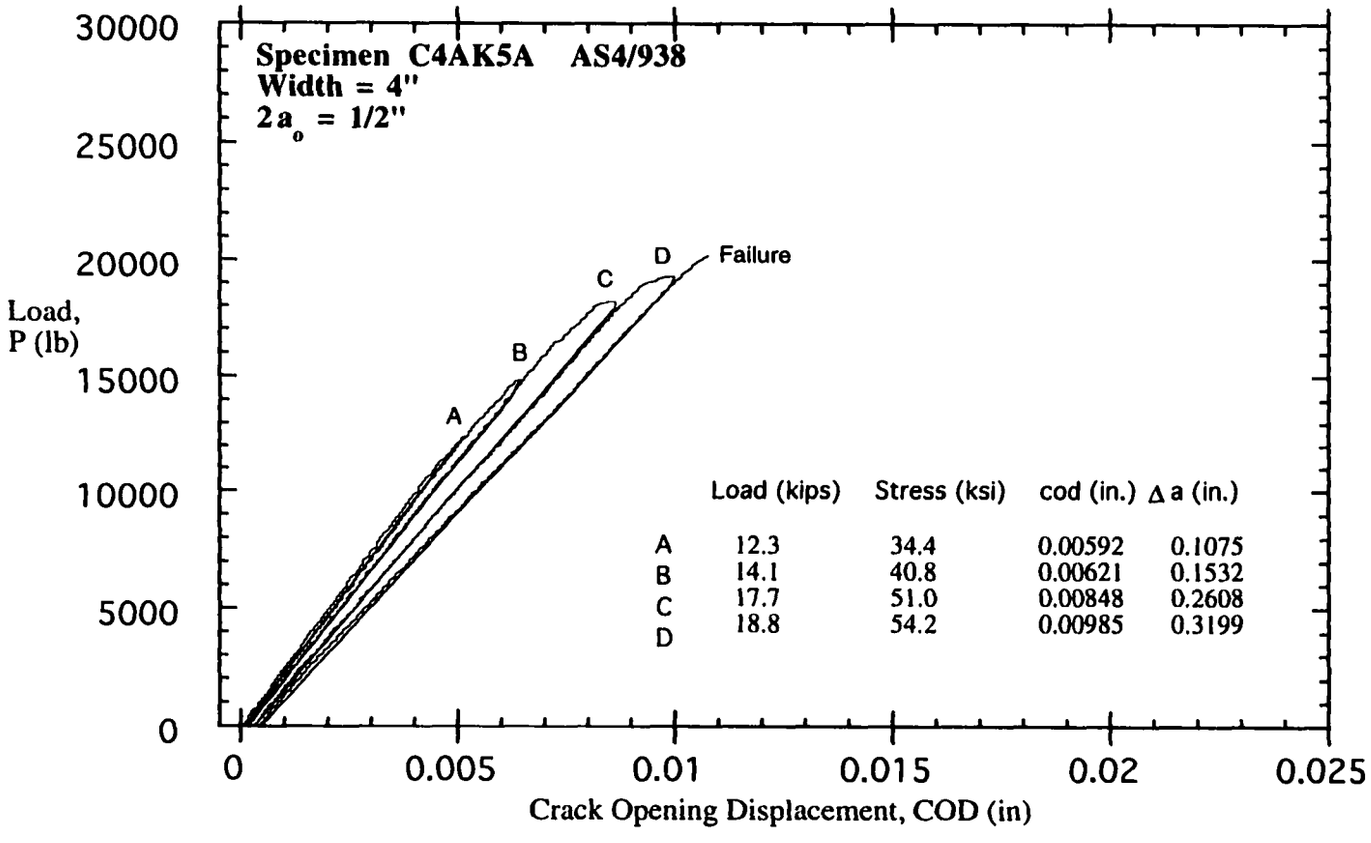

Figure D-1 - Load/COD Plot for the Illustration of Crack Growth Measurements.

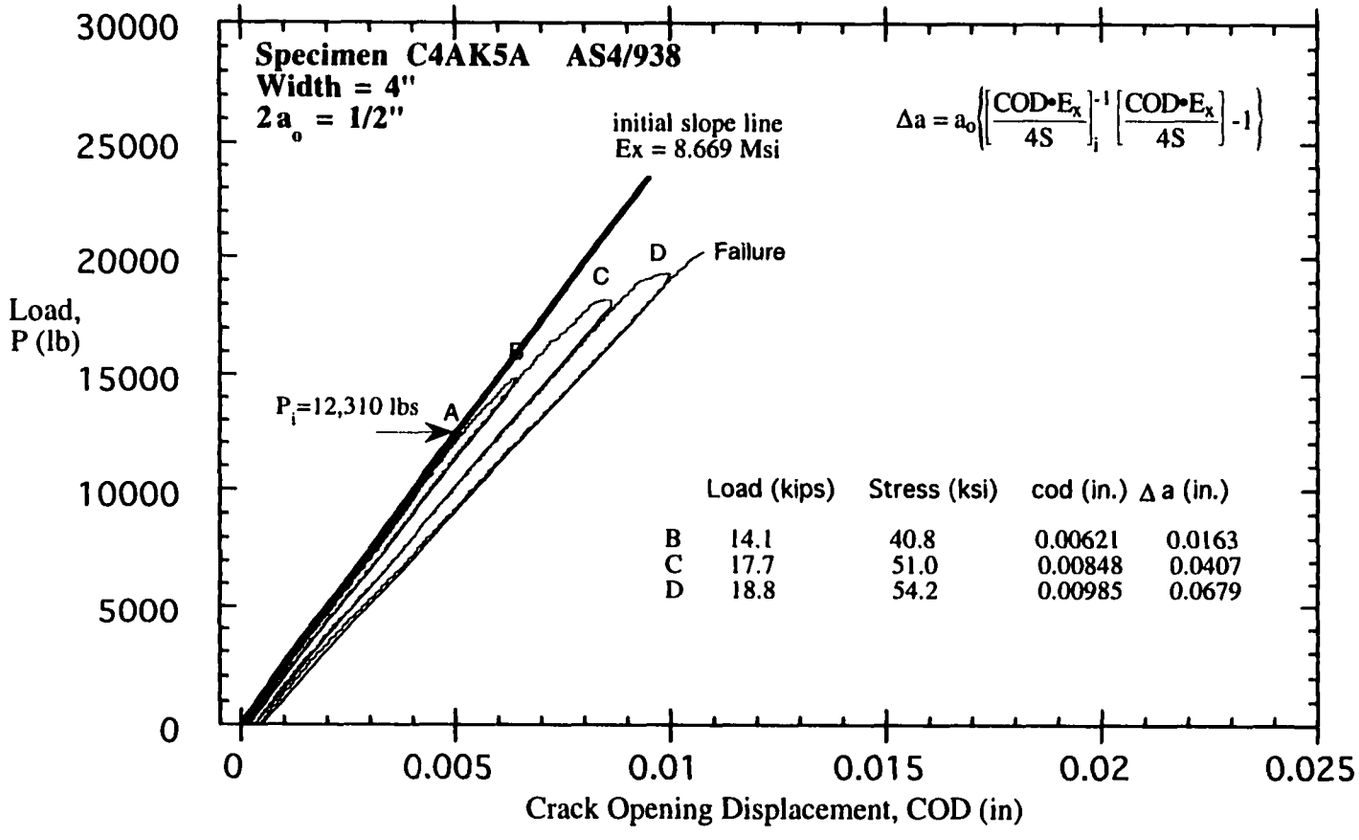

Figure D-2 - Load/COD Plot for the Illustration of Crack Growth Calculations.

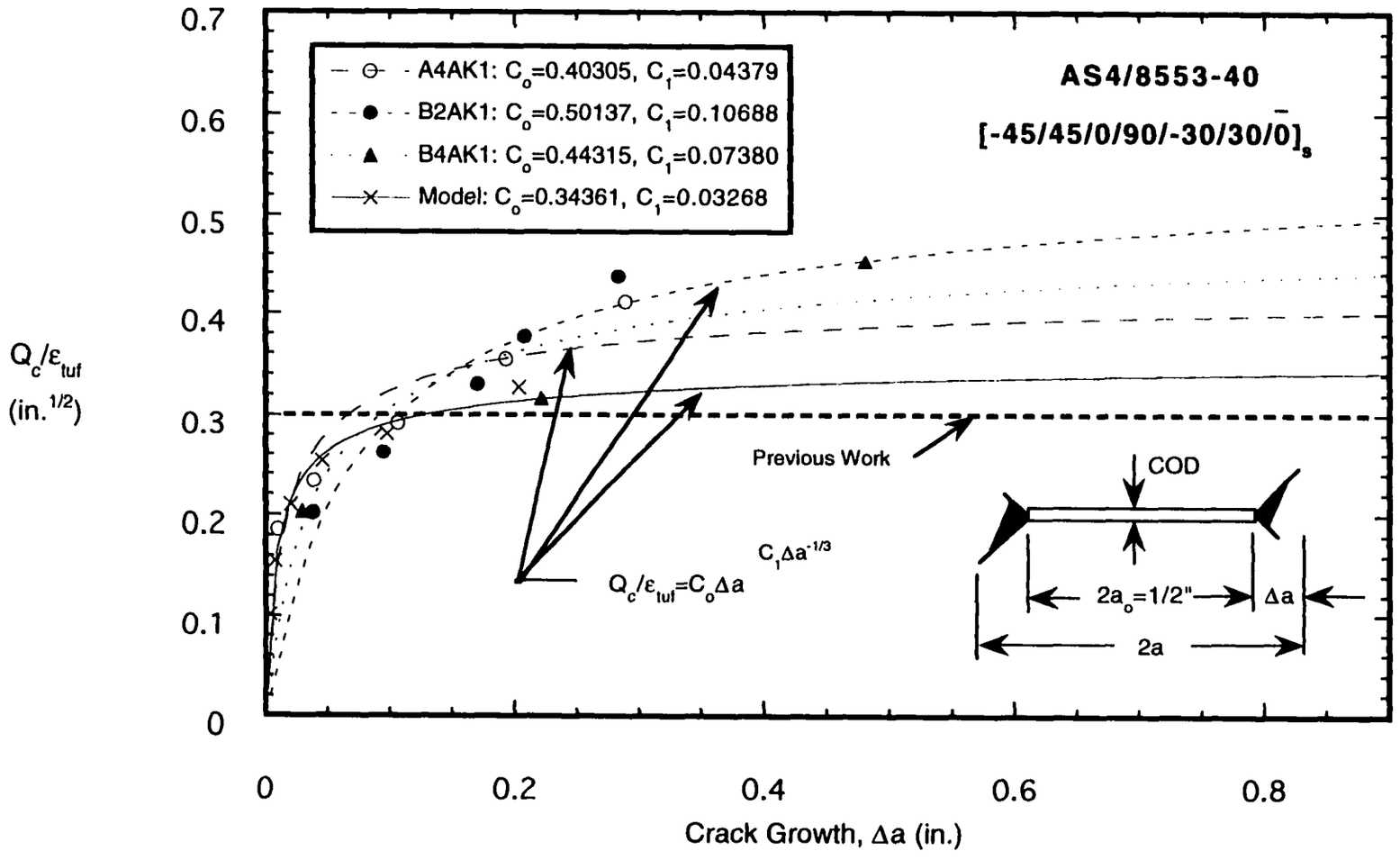

Figure D-3 - Experimental and Model Generated R-Curves Using Δa Measured from X-Ray Radiographs.

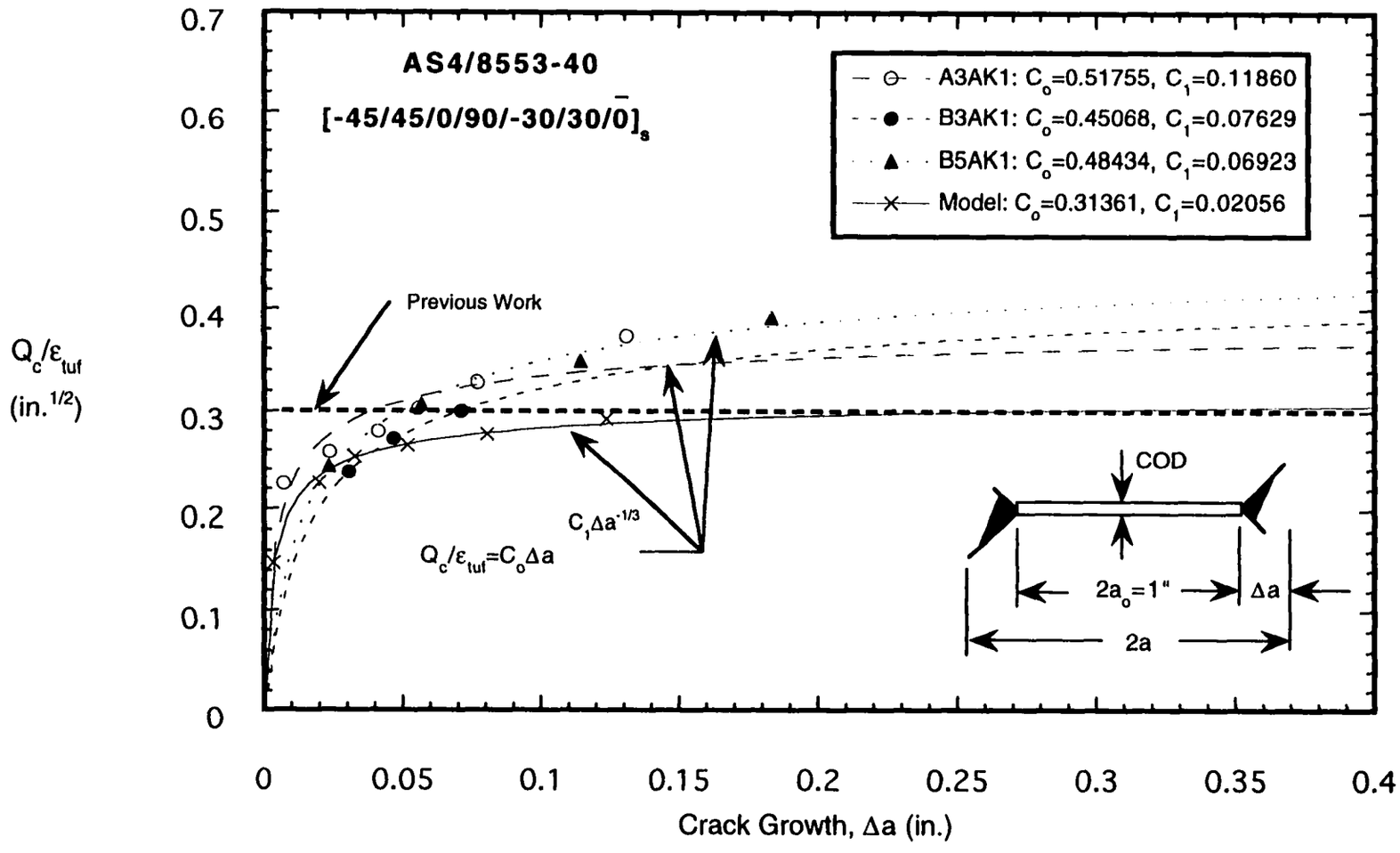

Figure D-4 - Experimental and Model Generated R-Curves Using Δa Measured from X-Ray Radiographs.

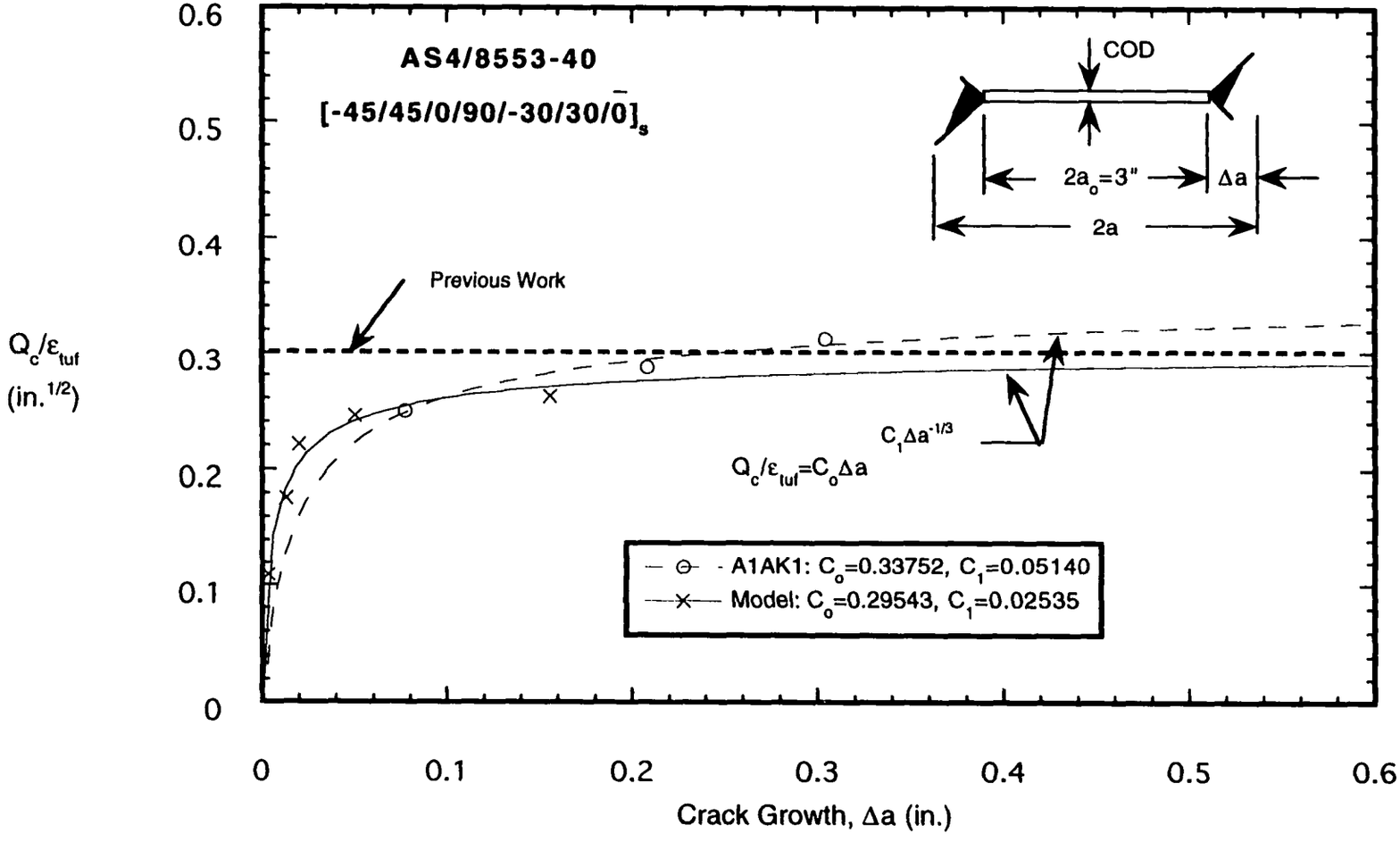

Figure D-5 - Experimental and Model Generated R-Curves Using Δa Measured from X-Ray Radiographs.

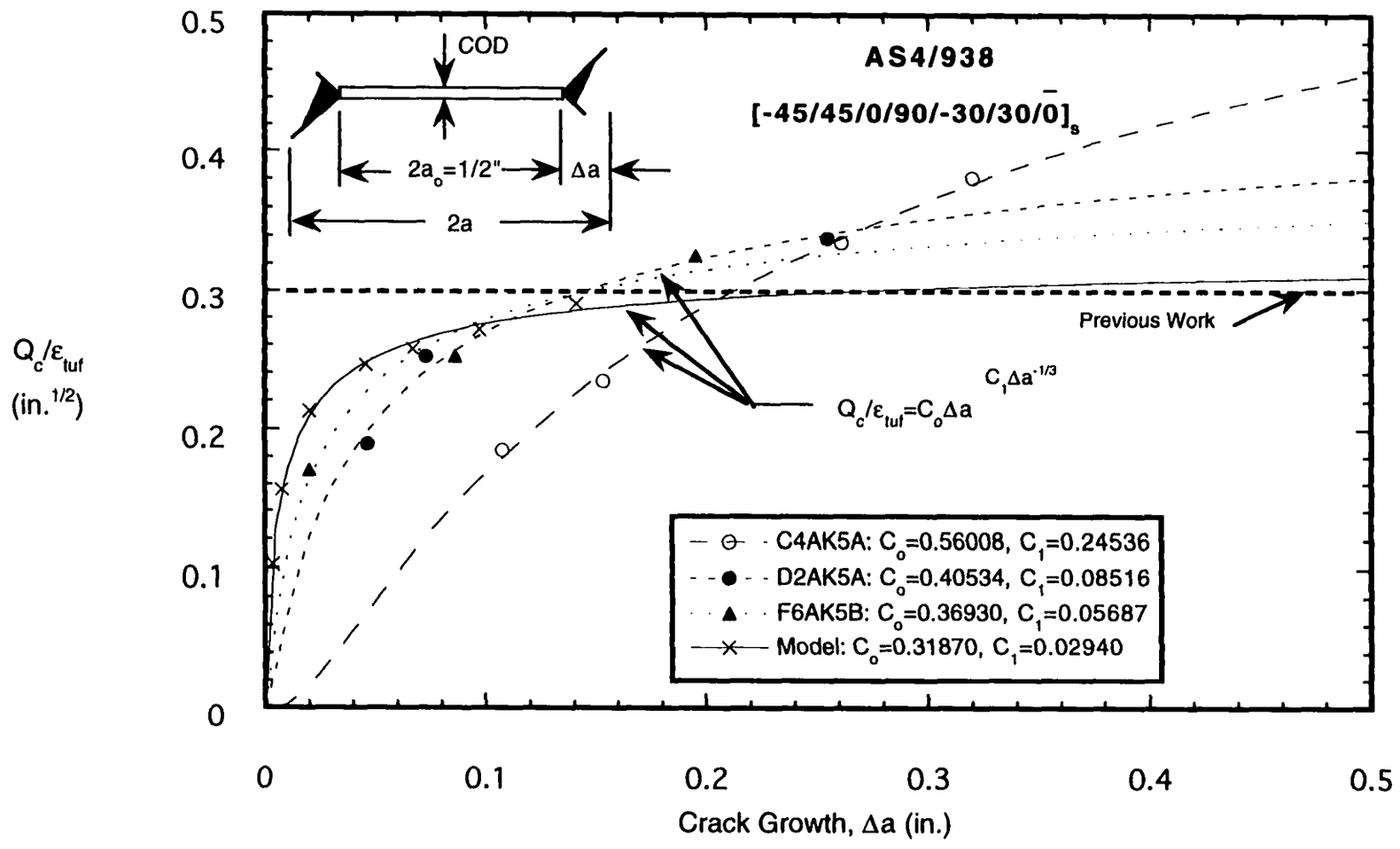

Figure D-6 - Experimental and Model Generated R-Curves Using Δa Measured from X-Ray Radiographs.

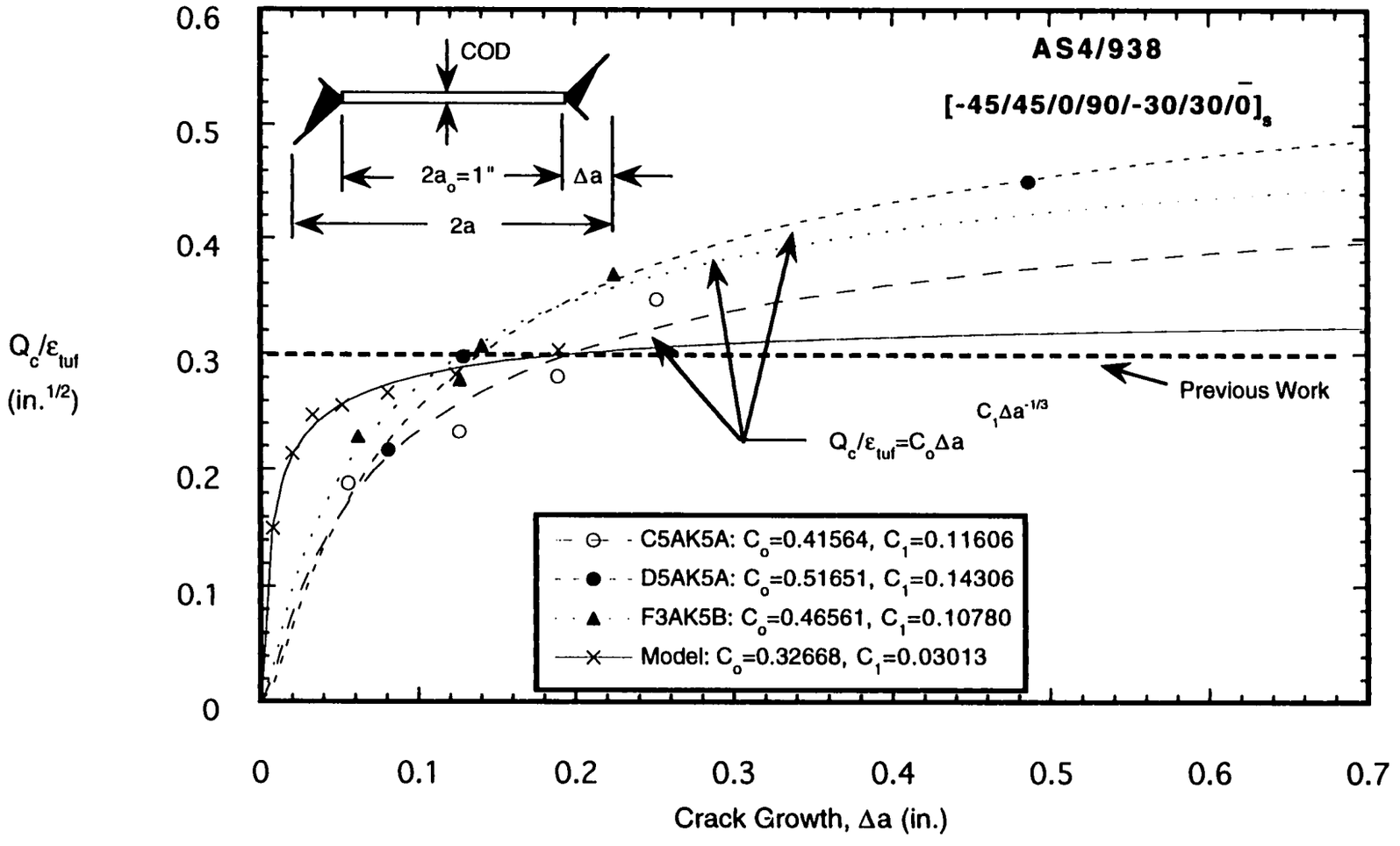

Figure D-7 - Experimental and Model Generated R-Curves Using Δa Measured from X-Ray Radiographs.

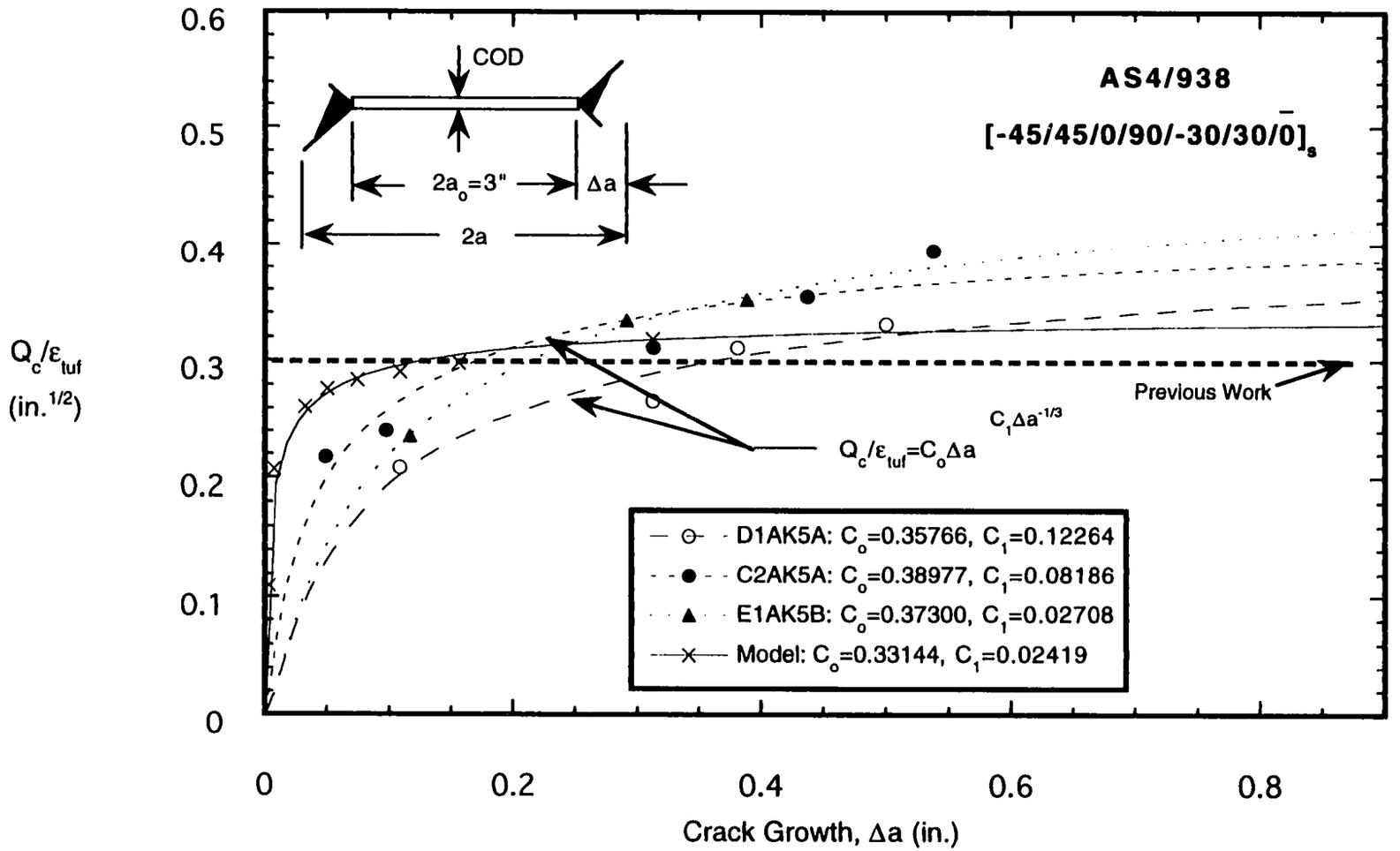

Figure D-8 - Experimental and Model Generated R-Curves Using Δa Measured from X-Ray Radiographs.

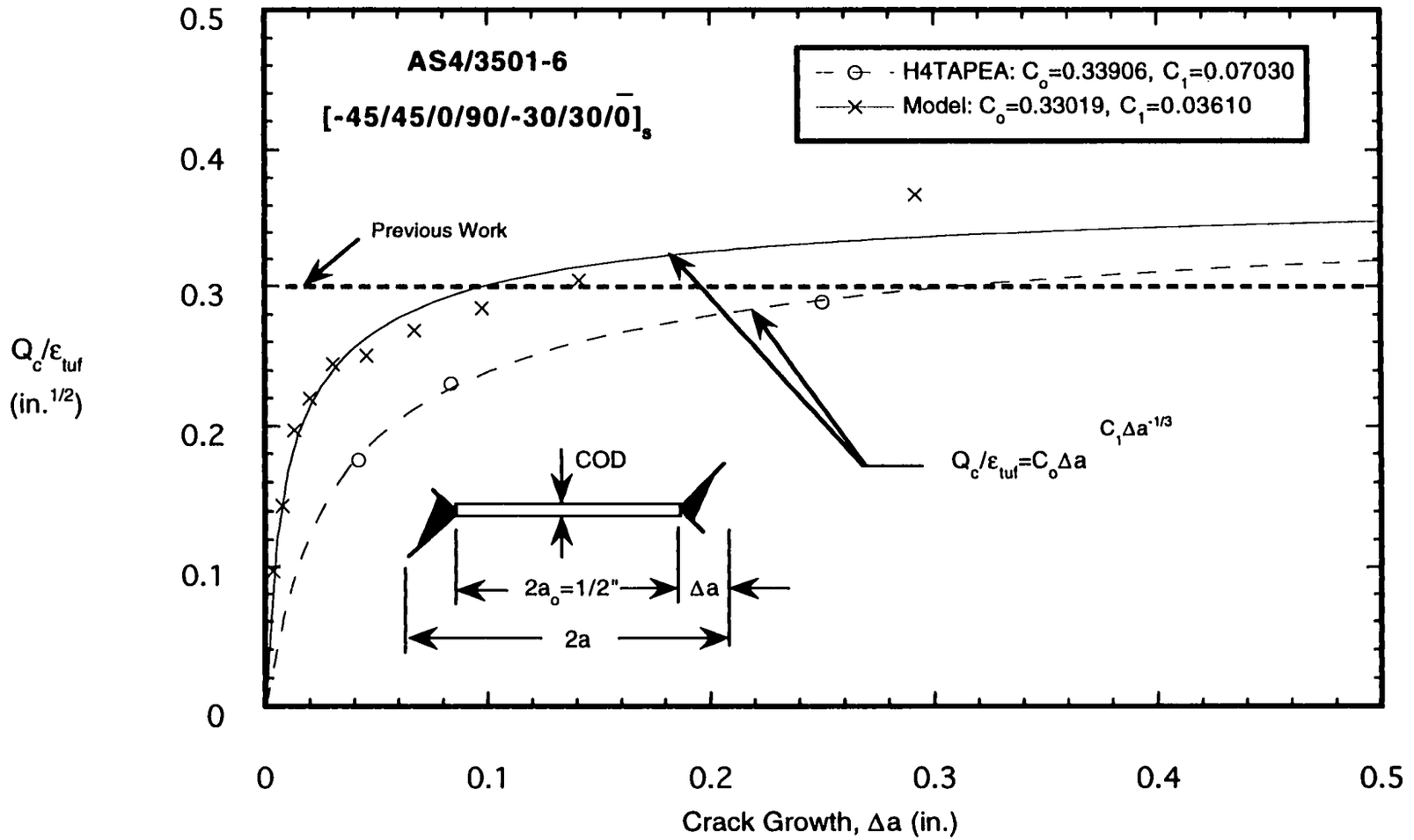

Figure D-9 - Experimental and Model Generated R-Curves Using Δa Measured from X-Ray Radiographs.

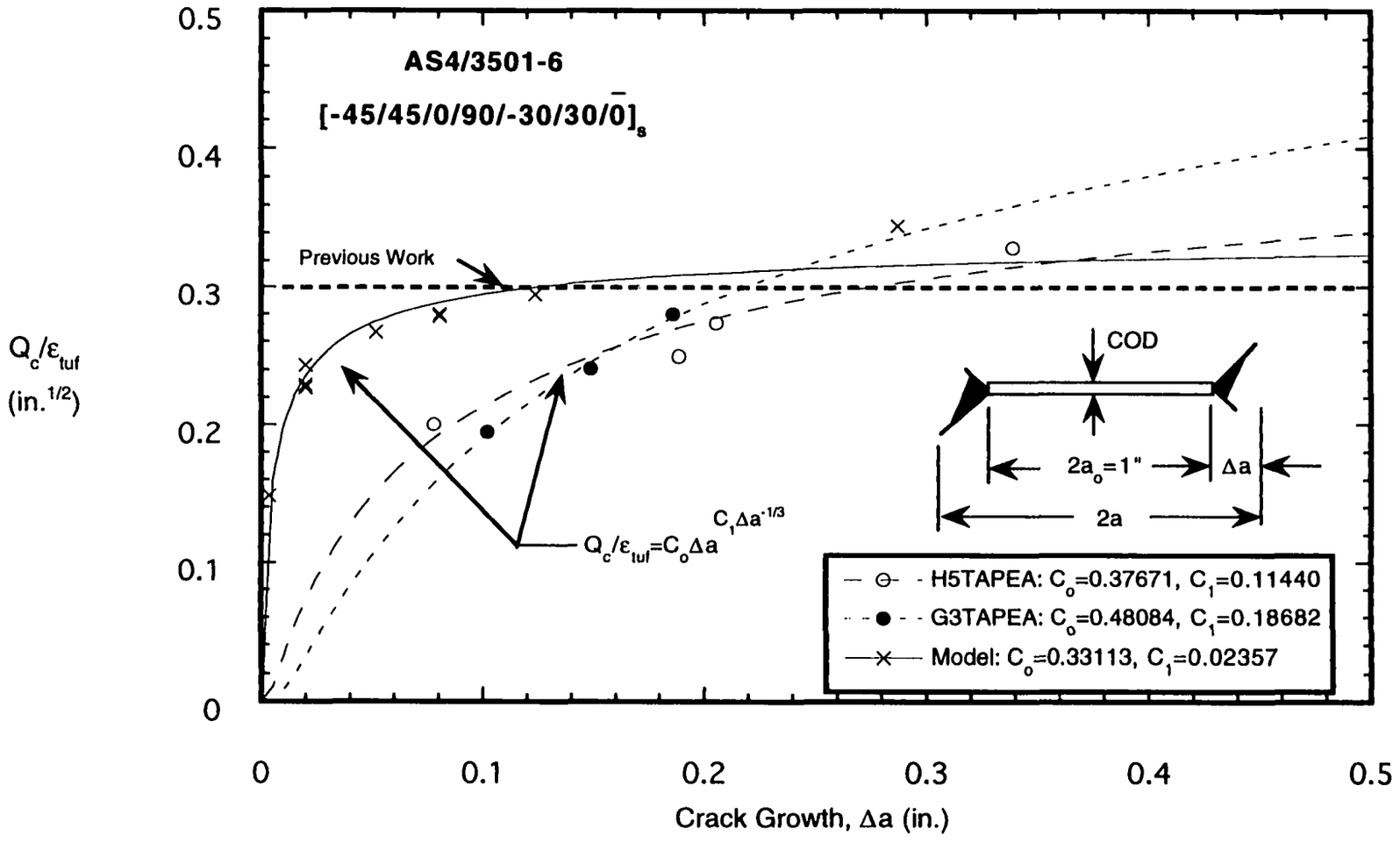

Figure D-10 - Experimental and Model Generated R-Curves Using Δa Measured from X-Ray Radiographs.

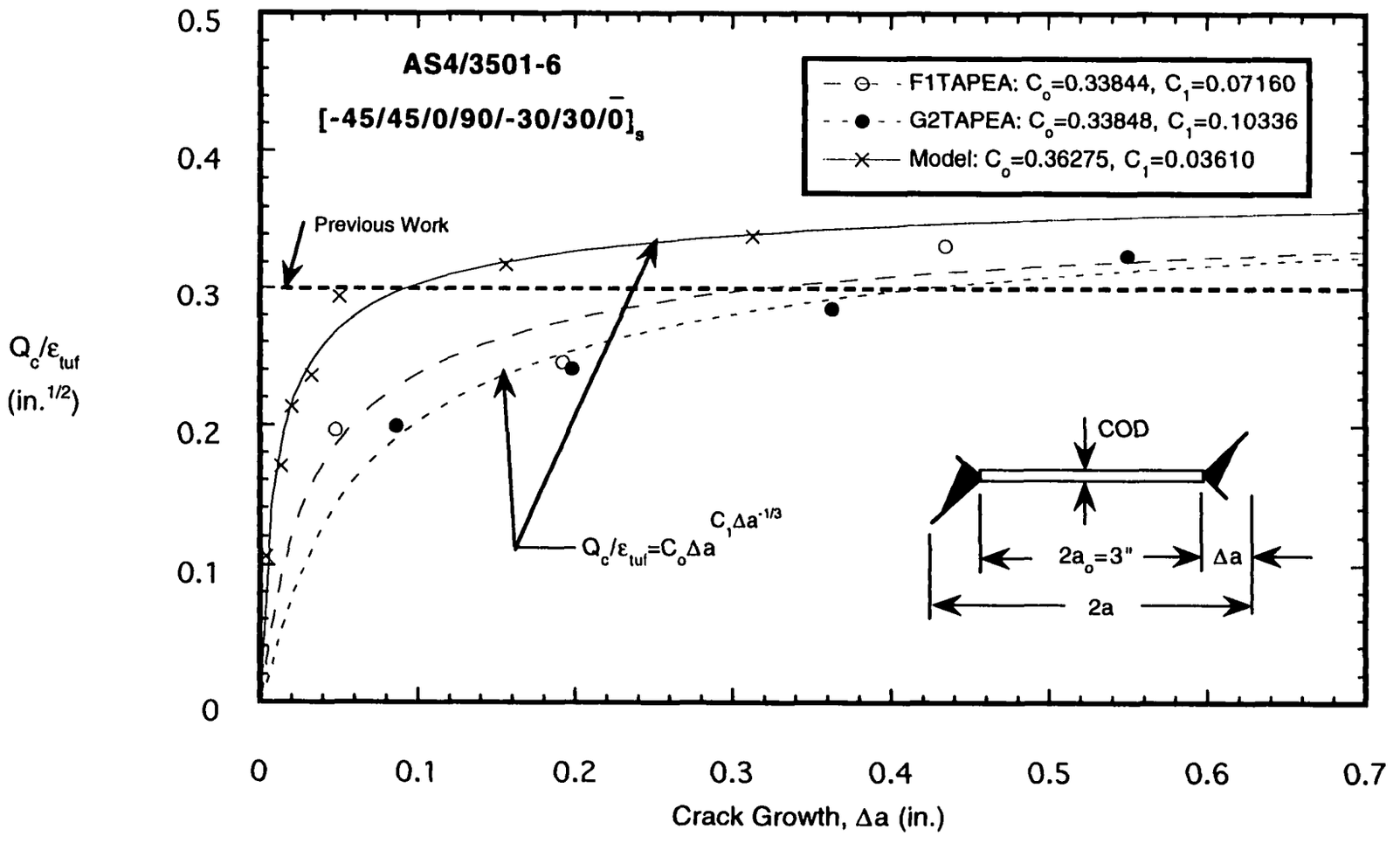

Figure D-11 - Experimental and Model Generated R-Curves Using Δa Measured from X-Ray Radiographs.